Universite Louis Pasteur – Strasbourg I
Faculte de Chimie

Thèse présentée pour obtenir le grade de
Docteur de l'Université Louis Pasteur de Strasbourg I
Discipline : chimie-physique

Supecritical Fluid Extraction: Spectroscopic Study of Interactions Comparison to Solvent Extraction

par

Anne Rustenholtz Farawila

Soutenue publiquement le 8 juin 2005

Dirigée par Dr Isabelle BILLARD & Professor Chien M. WAI

Membres du jury :
Directeur de Thèse : Dr Isabelle BILLARD, HDR, IReS, Strasbourg
Co-directeur de Thèse : Prof. Chien M. WAI, Prof., Université de l'Idaho, USA
Rapporteur Interne : Prof. Georges WIPFF, Prof, Faculté de Chimie, Strasbourg
Rapporteur Externe : Dr Stéphane SARRADE, HDR, CEA, Pierrelatte
Rapporteur Externe Préalable : Dr Oleg EGOROV, Senior Scientist, Pacific Northwest National Laboratory, USA

to Hobbi

Remerciements - Acknowledgment

I thank, je remercie :

- Mes Parents pour leur aide et leur soutien tout au long de ma scolarité ainsi que le reste de ma famille.
- My husband, for his love and support. I would not have finished this project on time without him. I also thank him for being my first and best proof-reader and for his help with LaTeX and Gnuplot.
- Dr Isabelle Billard pour m'avoir enseignée les bases du travail de recherche scientifique et pour m'avoir mise en contact avec Professeur Chien M. Wai et de ce fait permis d'aller aux Etats Unis. Merci aussi pour ses conseils et les discussions intéressantes que nous avons partagées tant par email que de vive voix.
- The University of Idaho, and Professor Chien M. Wai for his kindness, his encouragement, and his help with his scientific knowledge and ideas as well as his financial support all along my Ph.D. research.
- Les membres du Jury : Professeur Wipff avec lequel j'ai eu de très intéressantes conversations lors de mes passages en France et Dr Stéphane Sarrade que j'ai eu le plaisir de rencontrer pour la première fois lors de ma soutenance. Dr Oleg Egorov for his great comments that helped me to improve this thesis and for his friendship.
- Pacific Northwest National Laboratories, and Mr. John Fulton for his kindness and for sharing his laboratory and his knowledge which were indispensable for the FTIR experiments.
- AREVA and Mr. Syd Koegler for allowing me to perform some practical research in one of Framatome-ANP laboratories in Richland, Washington.
- Dr Alexander Blumenfeld, for sharing his knowledge of RMN.
- Mr. Thomas Eichenberg, Dr Scott Franz, Miss Virginia Sliman and Dr Peter Halverson for their editing help and their comments that helped me to improve this thesis. Dr Michel Billaux pour ses commentaires et ses corrections dans la partie Fran caise.

- M. Antony Jean-Mertens pour son amitié et pour m'avoir ouvert l'esprit sur d'autres mondes et m'avoir fait découvrir les Etats-Unis. Mes autres amis alsaciens avec qui j'ai passé des moments inoubliables.

- Dr Mari Hannele Mannila for being my best "sac de sable" during unforgettable motorcycle trips in the wild North West of the United States. I owe her my biggest laughs and she is the best friend that someone should hope for. Kitos!

- My Idaho's friends: Abeer, Hatem, Mohammed et al. for their friendship and the good time that we spent together.

- M^{me} Béatrice Henrioulle pour s'être occupée de sa poupouille, afin que je puisse finir la rédaction de cette thèse ainsi que pour sa bonne humeur générale, son amitié et ses encouragements.

- Enfin mon fils, Mohamed Yousef III, pour m'avoir laissée un peu de temps pour écrire entre deux pleurs et deux gazouillis!

Contents

Remerciements - Acknowledgment **5**

Résumé **19**

Titre 19

Résumé Court 19

Mots Clefs 20

Introduction 20

0.1 Interactions entre Ethers Couronne et Eau 21

0.1.1 En Milieu Supercritique 21

0.1.2 Dans des Solvants Classiques 24

0.1.3 Rôle de l'eau dans l'équilibre établi lors de l'extraction du césium par les éthers couronne 25

0.2 Interaction entre le TBP, l'Eau et l'Acide Nitrique 26

0.2.1 Interaction entre le TBP et l'Eau 26

0.2.2 Interaction entre le TBP, l'Eau et l'Acide Nitrique 28

0.2.3 Mise en Pratique : Extraction de l'Uranium à l'Aide de Phosphate de Tributyle et d'Acide Nitrique 29

Conclusion 31

General Introduction **33**

1 Crown Ether-Water Interaction **49**

Introduction 49

1.1 Crown Ether-Water Interaction In Supercritical CO_2 53
Introduction 53
1.1.1 Experimental Work 58
1.1.2 Summary of the Results 61
1.1.3 Additional Description 62
Conclusion 66
1.2 Crown Ether-Water Interaction in Solvents 69
Introduction 69
1.2.1 Experimental Section 75
1.2.2 Summary of Results 77
1.2.3 Comparison to FT-IR Results in CO_2 77
Conclusion 80
1.3 Introduction to Cesium Extraction Equilibrium Using Crown Ethers . 84
Introduction 84
1.3.1 Experimental Work 86
1.3.2 Calculations 88
1.3.3 Results and Discussion 93
Conclusion 95
Conclusion 97

2 TriButyl Phosphate–Water–Nitric Acid Interaction 99

Introduction 99
2.1 Interaction of Tributyl Phosphate with Water 105
Introduction 105
2.1.1 Interaction of Tributyl Phosphate with Water in Supercritical CO_2 Analyzed by Fourier Transform Infra-Red Spectroscopy . 105
2.1.2 Interaction of Tributyl Phosphate with Water in Solvent Analyzed by Nuclear Magnetic Resonance Spectroscopy 118

Conclusion . . . 129
2.2 Interactions with Nitric Acid Analyzed by Nuclear Magnetic Resonance 131
Introduction . . . 131
2.2.1 Experimental Work . . . 131
2.2.2 Results and Discussion . . . 134
Conclusion . . . 143
2.3 Practical Application: Uranium Extraction
from Solid Matrices . . . 144
Introduction . . . 144
2.3.1 Experimental Work . . . 145
2.3.2 Extraction of UO_2 from Different Matrices . . . 152
2.3.3 Stripping of the Uranium from TBP Media to Water . . . 157
Conclusion . . . 162
Conclusion . . . 164

General Conclusions **167**

A Mass Yield of the Fission Element **171**

B Decay Series **173**

C Acronyms **177**

D Curriculum Vitae **179**
Address . . . 179
Academic History . . . 179
Master Publications and Conference Presentations . . . 180
Ph.D. Publications and Conference Presentations . . . 180

E Abstract **181**

F An FT-IR Study of Crown Ether-Water Complexation in Supercritical CO_2 183

G Partition Coefficients and Equilibrium Constants of Crown Ethers between Water and Organic Solvents Determined by Proton Nuclear Magnetic Resonance 191

H Characterization of a Tri-n-butyl Phosphate-Nitric Acid Complex: a CO_2-Soluble Extractant for Dissolution of Uranium Dioxide 197

List of Figures

1 Schéma expérimental de la spectroscopie infrarouge à transformée de Fourier. 22

2 Structure moléculaire des trois types de liaisons entre éthers couronne et eau. Conformations pontée (a), simple (b) et en sandwich (c). . . 23

3 Une des configurations possible pour les liaisons hydrogènes entre une molécule de TBP, d'acide nitrique et d'eau. 29

4 Schéma expérimental pour l'extraction d'UO_2. 30

5 World map of nuclear reactors from the International Nuclear Safety Center (INSC) web page.[1] 34

6 Gamma radiation map in the Chernobyl area, results of the May 29, 1986, Gamma Radiation Survey.[2] 37

7 Phase diagram for CO_2, the shaded areas are the subcritical and supercritical fluid regions. 41

8 Mass (g) of elements (150 days after discharge from a PWR) per ton (Mg) of uranium (freshly loaded in the reactor) versus the atomic number of the element.[3] 43

9 Representation of a crown ether (18-crown-6) and the TBP and nitric acid molecules. 46

1.1 Molecular structure of 12-Crown-4 (a); 15-Crown-5 (b); 18-Crown-6 (c); 24-Crown-8 (d). 51

1.2 Molecular structure of dicyclohexano-18-Crown-6 (a) and of dibenzo-18-Crown-6 (b). 52
1.3 Fourier Transform Infra-Red (FT-IR) spectrometer. 55
1.4 Fourier Transform Infra-Red (FT-IR) experimental setup. 59
1.5 Molecular structure of the water-crown ether interaction in the bridge form (a), the single configuration (b) and the sandwich form (c). . . 62
1.6 Molar fraction of crown ether bonded to water k versus density at constant pressure (20 MPa). Lines are guides for the eyes and do not have any theoretical or analytical value. 65
1.7 Molar fraction of crown ether bonded to water k versus density at constant temperature (40 °C). Lines are guides for the eyes and do not have any theoretical or analytical value. 66
1.8 Dependence of $\ln K$ on 1000/T at 20 MPa. 67
1.9 Dependence of free water [D_2O] on the equilibrium constant K. . . . 68
1.10 Potential energy of a nucleus with a spin state I=1/2 outside and inside a magnetic field. 71
1.11 Nuclear magnetic resonance experiment.[4] 73
1.12 Acquisition sequence for a nuclear magnetic resonance experiment. . 74
1.13 P-NMR spectrum of the ethanal molecule (CH_3CHO).[5] 81
1.14 coupling due to spin-spin interactions and relative intensities. 82
1.15 Typical PNMR spectra of 18-crown-6 in the $CDCl_3$ phase. The concentrations of 18-crown-6 after equilibrium with water are 0.00, 0.002, 0.075 and 0.153 mol·L^{-1} (from top to bottom) and the water peaks are at 1.565, 1.874, 2.393 and 2.668 ppm, respectively. 83
1.16 Molecular structure of dicyclohexano-18-Crown-6 (a) and of Cesium picrate (b). 86
1.17 Typical PNMR spectrum for DCH18C6 (at 0.4 mol·L^{-1}) with water and cesium picrate (at 30 mmol·L^{-1}) in the $CDCl_3$ phase). 87

1.18 Typical PNMR spectrum for DCH18C6 (at 0.05 mol·L^{-1}) with water and cesium picrate (at 8 mmol·L^{-1}) in the $CDCl_3$ phase). 88
1.19 Total cesium picrate concentration versus water concentration in the organic phase for different initial ligand (L = DCH18C6) concentrations (from 0.05 to 0.4 mol·L^{-1}). 93
1.20 Total water concentration versus total ligand concentration in the organic phase. 94

2.1 One of the possible configurations of hydrogen bonds between a TBP, a nitric acid and a water molecule. 101
2.2 Principal steps of the Purex process. 104
2.3 FT-IR spectra of free and bonded D_2O at different TBP concentrations (0-0.16 mol·L^{-1}) and at one fixed D_2O concentration (0.054 mol·L^{-1}) in supercritical CO_2 (40 °C, 20 MPa). 107
2.4 Possible configurations of the hydrogen bond between a D_2O and a TBP molecule. 107
2.5 Possible configurations of the hydrogen bond between a D_2O and two TBP molecules. 108
2.6 Density effect on the equilibrium constant K at constant temperature (▲, 40 °C) and at constant pressure (▼, 20 MPa). 110
2.7 Molar fraction of TBP bonded to water k versus density at constant temperature (▲, 40 °C) and at constant pressure (▼, 20 MPa). . . . 111
2.8 Concentration of free D_2O versus temperature at 20 MPa. 112
2.9 Free D_2O concentration versus density for at constant temperature (▲, 40 °C) and at constant pressure (▼, 20 MPa). 112
2.10 Dependence of $\ln K$ on $1000/T$ (T in K) at 20 MPa. 113
2.11 Dependence of the free water concentration, $[D_2O]$, on the equilibrium constant K. 114

2.12 linear regression of the molar solubility of water[6,7] in CO_2 versus the temperature at constant pressure (20 (▲) and 40 (▼) MPa). 116

2.13 Volume of water droplets when 500μL of water saturated TBP is mixed with CO_2 in a 10 mL cell versus the temperature at constant pressure (20 MPa). 117

2.14 300MHz ^{1}H-NMR spectra of TBP·H_2O in $CDCl_3$. 119

2.15 Enlargement of a 500MHz ^{1}H-NMR spectra of TBP·HNO_3·H_2O in $CDCl_3$. 123

2.16 Possible configuration for the TBP hydrate. 124

2.17 Chemical shift observed of water in $CDCl_3$ and in TBP, versus the molecular fractions of free water (▼) and of bonded water (▲). The dashed lines corresponds to their linear regression fits. 125

2.18 Chemical shift observed (black points) and calculated (thin line) of water in $CDCl_3$ and in TBP versus total water concentration in the organic phase. 126

2.19 Chemical shift observed of $CHCl_3$ in TBP and in $CDCl_3$ versus the TBP concentration in the organic phase. 127

2.20 Total water ($[H_2O]^0_{org}$) versus total TBP ($[TBP]^0_{org}$) in the organic phase. 128

2.21 Chemical shift of nitric acid observed from the droplets (▼) and from nitric acid solutions in water (▲) and calculated (dashed line) using equation (2.29) versus total nitric acid concentration. 132

2.22 A typical proton NMR spectrum of TBP·$(HNO_3)_x$·$(H_2O)_y$ with a benzene-d6 insert. The sample was prepared by mixing 1.0 mL of 15.5M HNO_3 with 4.0 mL of 98% TBP. 133

2.23 Chemical shift observed of nitric acid and water in TBP versus the mole ratio of nitric acid on TBP in the organic phase. 136

2.24 Number of moles of HNO_3 in the TBP phase at equilibrium (or x) versus the initial volume ratio of HNO_3 (at 15.5 mol·L^{-1} in water) on TBP. 138

2.25 Mole ratio of HNO_3/H2O in the TBP phase at equilibrium (or x/y) versus the initial volume ratio of HNO_3 (at 15.5 mol·L^{-1} in water) on TBP. 138

2.26 Proton NMR spectrum of TBP·$(HNO_3)_x$·$(H_2O)_y$ in $CDCl_3$. The complex was prepared by mixing 4 mL of TBP and 1 mL of 15.5 mol·L^{-1} HNO_3; volume ratio of TBP·$(HNO_3)_x$·$(H_2O)_y$ to $CDCl_3$ = 1:1. 139

2.27 Proton NMR spectrum of TBP·$(HNO_3)_x$·$(H_2O)_y$ in $CDCl_3$. The complex was prepared by mixing 2 mL of TBP and 2 mL of 15.5 mol·L^{-1} HNO_3; volume ratio of TBP·$(HNO_3)_x$·$(H_2O)_y$ to $CDCl_3$ = 1:1. 139

2.28 Chemical shift of the nitric acid and the water versus total water and nitric acid concentration in the organic phase. 141

2.29 Concentration of nitric acid in the aqueous phase versus initial TBP concentration in the organic phase. 142

2.30 Total water and nitric acid concentration in $CDCl_3$ versus initial TBP concentration. 142

2.31 UO_2 extraction: experimental setup. 147

2.32 Gamma spectra of the background, and of uranyl ion enriched at 3.1% in ^{235}U and at 8.7 g·L^{-1} of uranium in water, and of the UO_2^{2+} ion (2.9% ^{235}U) at 24 g·L^{-1} in TBP. 150

2.33 Calibration curves for UO_2^{2+} ion in water (▼, 3.1% ^{235}U) and in TBP (▲, 2.9% in ^{235}U). 151

2.34 gamma spectra of the background and of the three kind of matrices (R, L and Y) used for extraction. 154

2.35 gamma spectra of the background and of the uranyl ion (2.9% U) in the TBP stripped solution at and in the aqueous solution. 158

2.36 Total mass of uranium stripped versus total volume of water used. The line is a guide for the eyes and does not have any theoretical or analytical value. 159

2.37 Partition of HNO_3 between the organic and the aqueous phases at 50 °C, 20 MPa and with a TBP:water volume ratio of 1:1.9. 160

2.38 Partition of uranium between the organic and the aqueous phases for different initial nitric acid concentrations. The experiment was performed at 50 °C, 20 MPa and with a TBP:water volume ratio of 1:1.9. Lines are guides for the eyes and do not have any theoretical or analytical value. 162

2.39 Lost of efficiency when the volume ratio is 1:1 between the two phases (▼) and when the temperature is 24 °C (▲). 163

List of Tables

1 Supercritical fluids critical values. 42

1.1 Equilibrium parameters for water-crown-ether interaction in supercritical fluids. 64

1.2 Values of I, the quantum spin number, for different nucleus. 70

1.3 Comparison of the values of the equilibrium constants K_1 and K_2 and of the molar fractions of ligand complexed to water k_1 and k_2. 78

1.4 Comparison of water solubilities in solvents and in CO_2. 79

2.1 Equilibrium parameters for water-TBP interaction in supercritical CO_2. 110

2.2 Antisolvent effect for a water saturated TBP mixed with CO_2 at different densities. 116

2.3 intensities and coupling constants of the TBP multiplets. 122

2.4 Composition of TBP·$(HNO_3)_x$·$(H_2O)_y$ complexes. 137

2.5 Composition of the different matrices used for extraction determined by mass spectroscopy. 146

2.6 Optimal parameters for the supercritical CO_2 extraction. 157

2.7 Optimum uranium recovery efficiencies. 157

2.8 Results of the stripping experiments at 50°C, 20 MPa, and with a 1:1.9 TBP to water volume ratio.[a] 161

A.1 Mass (g) and radioactivity (Ci) of elements (150 days after discharge from a PWR) per ton (Mg) of uranium (freshly loaded in the reactor) for all elements. 172

B.1 Main decay energies for 238-Uranium. 174
B.2 Main decay energies for 235-Uranium. 175

Résumé

Titre

Extraction en Milieu Supercritique : Etude Spectroscopique des Interactions – Comparaison avec des Solvants Classiques

Résumé Court

Le dioxyde de carbone supercritique (SF-CO_2) a été choisi afin d'étudier l'extraction en milieu supercritique d'ions métalliques tels que le césium et l'uranium. Un intérêt particulier a été porté au rôle de l'eau lors de ces extractions ainsi qu'à son interaction avec des agents chélateurs (AC). En première partie, les éthers couronne ont été choisis comme AC du césium et leur interaction avec l'eau a été étudiée dans le SF-CO_2 en utilisant la spectroscopie InfraRouge à Transformée de Fourier (IR-TF). Une configuration sandwich entre deux éthers couronne et une molécule d'eau a été observée dans le SF-CO_2. Pour les configurations simple et pontée, l'équilibre a été défini et l'enthalpie de formation de la liaison hydrogène a été calculée. Ces résultats ont ensuite été comparés à ceux obtenus dans des mélanges de $CHCl_3$ et de CCl_4 en utilisant la spectroscopie à Résonance Magnétique Nucléaire (RMN). Pour conclure cette première partie, le rôle de l'eau a été étudié lors de l'extraction du picrate de césium par le DCH18C6 et les constantes d'équilibre ont été déterminées.

Dans une deuxième partie, l'extraction de l'uranium a été étudiée dans le SF-CO_2. Des complexes de Phosphate de TriButyle (TBP), d'eau et d'acide nitrique ont été utilisés comme AC et oxydants. L'IR-TF a été utilisée pour étudier l'interaction

entre le TBP et l'eau dans le SF-CO_2. Ces résultats ont été comparés à ceux trouvés dans le $CHCl_3$ en utilisant la RMN. Cette même spectroscopie a été utilisée pour comprendre les interactions entre l'acide nitrique, le TBP et l'eau, seuls puis dissous dans du $CHCl_3$. La formation de microgouttelettes d'acide et d'eau dues à l'effet anti-solvant a été observée et quantifiée. Pour conclure ce travail de thèse j'ai réussi à optimiser l'extraction et la récupération d'uranium enrichi provenant de cendres d'incinération de déchets de fabrication de combustible nucléaire. Un complexe de TBP, d'eau et d'acide nitrique dissous dans du SF-CO_2 a été utilisé à cette fin.

Mots Clefs

RMN – IR – Extraction – Fluides supercritiques – CO_2 – Dioxyde de carbone – Solvants – Acide nitrique – Uranium – Césium – Eau – Ethers couronne – TBP – Uranyle – Retraitement – Déchets nucléaires – Liaison hydrogène – Effet anti-solvant

Introduction

Mon travail de thèse est basé sur l'extraction de cations métalliques à l'aide de dioxide de carbone supercritique. L'uranium et le césium ont été spécialement choisis pour leur abondance dans les déchets nucléaires d'origines diverses. L'eau fait partie intégrante de ces systèmes et j'ai concentré une partie de mon travail de recherche sur le rôle de l'eau dans ces extractions. Mais avant de discuter en détails ce travail, je vais décrire brièvement les caractéristiques de l'extraction à l'aide de fluides supercritiques.

Les fluides supercritiques, du fait de leurs propriétés uniques, sont de plus en plus utilisés pour l'extraction d'ions métalliques provenant de matériaux liquides ou solides. Le fluide le plus souvent utilisé dans ces procédés est le dioxyde de carbone (CO_2). Il a de nombreux avantages : il est peu toxique, bon marché et relativement bénin pour l'environnement, ses constantes critiques sont modérées (T_c = 31,0 °C et P_c = 7,38 MPa) et son pouvoir de solvatation peut être modifié par simple changement

de température et/ou de pression.

Néanmoins, le dioxyde de carbone est un solvant apolaire et nécessite souvent l'adjonction d'agents chélateurs pour faciliter l'extraction d'ions métalliques. Afin d'améliorer qualitativement et quantitativement l'extraction, ces agents doivent avoir des propriétés spécifiques : ils doivent être solubles dans le CO_2 et sélectifs de l'ion métallique que l'on veut extraire. Durant mon travail de thèse, deux types d'agents chélateurs ont été étudiés : les éthers couronne et le phosphate de tributyle.

0.1 Interactions entre Ethers Couronne et Eau

Les éthers couronne sont des macrocycles pouvant abriter au centre de leur cavité des cations de différentes tailles. Ils sont souvent utilisés pour extraire des ions alcalins tel que le lithium, le potassium ou le césium. La taille de la cavité dépend de l'éther couronne utilisé, le rendant généralement spécifique à un cation donné. Les éthers couronne sont relativement solubles dans le dioxyde de carbone et dans de nombreux solvants. Ils sont donc indiqués en tant qu'agents chélateurs dans le traitement de déchets contenant des cations métalliques. Ils peuvent être utilisés, par exemple, pour le traitement de déchets nucléaires contenant du césium 137. Ce traitement peut être réalisé à l'aide de dioxyde de carbone supercritique.

De tels déchets sont souvent extraits de matrices contenant de l'eau. L'eau fait partie intégrante du procédé d'extraction. Il est donc nécessaire de connaître les interactions entre l'eau et les éthers couronne dans différents solvants.

0.1.1 En Milieu Supercritique

Pour cette étude, la spectroscopie infrarouge à transformée de Fourier (IR-TF) a été utilisée comme méthode d'analyse (Figure 1). Cette méthode permet de distinguer trois types de liaisons entre les éthers couronne (18-couronne-6 pour cette étude) et l'eau. Le D_2O a été préféré à l'H_2O afin d'éviter la superposition des raies intenses provenant du dioxyde de carbone, entre 3500 cm^{-1} et 3800 cm^{-1}, et celles de l'eau.

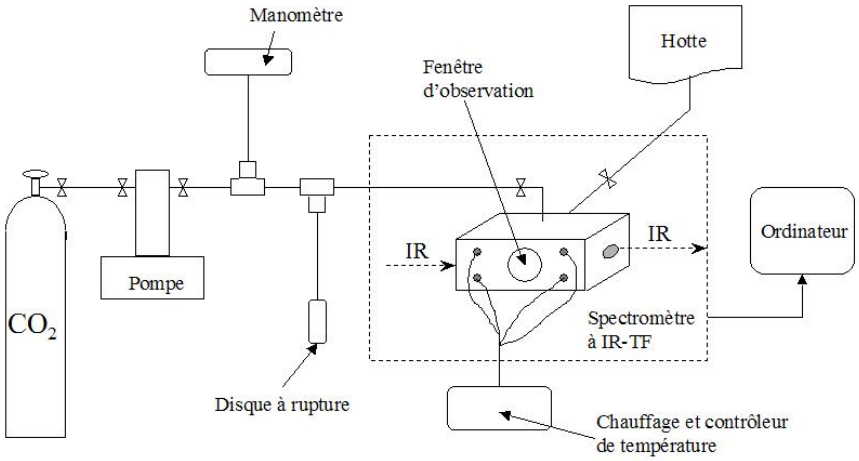

Figure 1: Schéma expérimental de la spectroscopie infrarouge à transformée de Fourier.

Le premier type de configuration n'est observé qu'à haut rapport de concentration entre les éthers couronne et le D_2O; il s'agit d'un "sandwich" composé de deux molécules de 18-couronne-6 entourant une molécule d'eau (Figure 2 c.). A faibles rapports de concentrations, une molécule d'eau peut être liée à un seul éther couronne de deux manières différentes (Figure 2 a. et b.). Le premier type de configuration est dit ponté et consiste en deux liaisons hydrogène entre le D_2O et deux atomes d'oxygène provenant de la cavité de 18-couronne-6. Le deuxième type de configuration est dit simple, le D_2O forme une seule liaison hydrogène avec un atome d'oxygène provenant de la cavité de l'éther couronne.

Les constantes d'équilibre de ces deux types de configurations ont été calculées et varient entre 16(4) et 9(2) $L{\cdot}mol^{-1}$ pour la configuration simple et entre 10(3) et 5(2) $L{\cdot}mol^{-1}$ pour la configuration pontée lorsque la densité du dioxyde de carbone

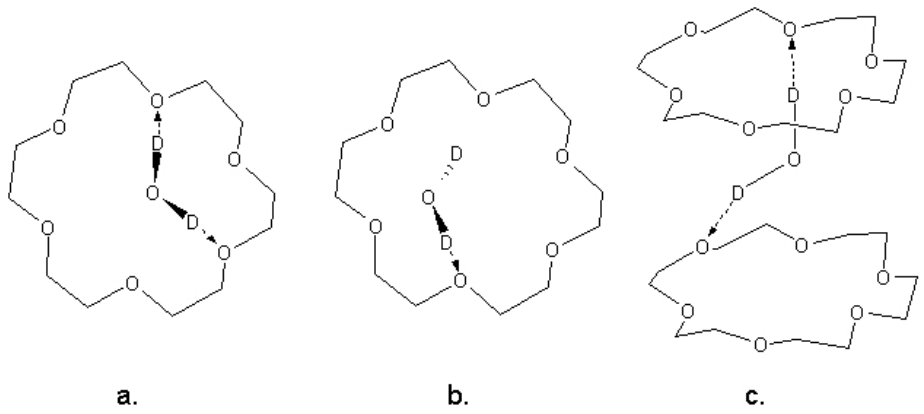

Figure 2: Structure moléculaire des trois types de liaisons entre éthers couronne et eau. Conformations pontée (a), simple (b) et en sandwich (c).

augmente de 850 à 960 g·L^{-1}. La mesure des constantes d'équilibre à différentes températures et à pression constante a permis de calculer l'enthalpie de formation des deux complexes considérés. Elle vaut -12(2) kJ·mol^{-1} pour le complexe simple et -38(3) kJ·mol^{-1} pour le complexe ponté. Ces valeurs sont en accord avec celles reportées pour des solvants classiques.

L'équilibre entre la forme pontée et la forme simple est décrit comme suit :

$$2\ 18C6 + 2\ D_2O \rightleftharpoons 18C6{\cdot}D_2O^{\text{simple}} + 18C6{\cdot}D_2O^{\text{pontée}} \tag{1}$$

A partir de cet équilibre, la constante d'équilibre K est donnée par:

$$K = \frac{[18C6{\cdot}D_2O^{\text{simple}}][18C6{\cdot}D_2O^{\text{pontée}}]}{[D_2O]^2[18C6]^2} = K_s \cdot K_p \tag{2}$$

avec

$$K_s = \frac{[18C6{\cdot}D_2O^{\text{simple}}]}{[D_2O][18C6]} \qquad \text{et} \qquad K_p = \frac{[18C6{\cdot}D_2O^{\text{pontée}}]}{[D_2O][18C6]} \tag{3}$$

Ceci m'a permis de comparer ces résultats à ceux obtenus par la spectroscopie RMN (Résonance Magnétique Nucléaire), cette dernière ne permettant pas de distinguer la forme pontée de la forme simple. La constante d'équilibre, K, varie entre 34(4) et 300(30) L^2·mol^{-2} lorsque la densité du CO_2 augmente à pression constante

(∼20 MPa). Dans les même conditions, la fraction molaire, k d'éther couronne liée à l'eau varie entre 33(3) et 54(5)%.

0.1.2 Dans des Solvants Classiques

L'interaction éthers couronne/eau dans des mélanges de chloroforme ($CHCl_3$) et de tétrachlorure de carbone (CCl_4) a également été étudiée afin de déterminer l'influence du solvant sur cette interaction. Pour cette étude, la RMN a été utilisée comme méthode d'analyse.

La RMN ne permet pas de distinguer les deux types de configurations possibles (simple et pontée) entre un éther couronne et une molécule d'eau. De ce fait, les différentes configurations ne peuvent pas être précisées par cette méthode. Il faut aussi noter que les concentrations choisies sont suffisamment faibles pour que la configuration "sandwich" entre deux molécules d'éther couronne et une molécule d'eau ne puisse pas être observée. L'équilibre est donc décrit par la formation d'un complexe 1:1 entre une molécule d'eau et un éther couronne en rapide échange avec des molécules non complexées d'eau et de ligand.

La fraction molaire, k d'éther couronne complexé avec une molécule d'eau a été calculée pour différents éthers couronne. Si k augmente avec la taille de la cavité de 15(1)% pour 12-couronne-4 à 97(5)% pour 18-couronne-6, l'addition de tétrachlorure de carbone abaisse la valeur de k pour tous les éthers couronne en équilibre avec l'eau et la constante est proche de zéro dans le CCl_4 pur. Au contraire, le coefficient de partage des éthers couronne entre la phase organique et la phase aqueuse augmente exponentiellement avec le pourcentage de CCl_4 dans cette phase.

Cette étude montre que l'interaction entre l'eau et les éthers couronne dépend fortement de la nature du solvant utilisé. Il a été démontré qu'un solvant à faible constante diélectrique, comme le CCl_4 n'est pas favorable à la formation d'un complexe entre l'éther couronne et l'eau. Ceci a aussi été démontré pour le dioxyde de carbone à haute pression et température. Lorsque la valeur de la constante diélectrique

augmente en utilisant le $CHCl_3$ comme solvant ou lorsque le CO_2 est utilisé à basse pression et température, les éthers couronne sont plus enclins à former un complexe avec l'eau. Ces résultats sont importants car l'eau joue un rôle primordial dans l'extraction d'ions métalliques utilisant des éthers couronne comme extractant.

0.1.3 Rôle de l'eau dans l'équilibre établi lors de l'extraction du césium par les éthers couronne

La RMN, comme précédemment, a été utilisée en tant que méthode d'analyse pour cette étude. L'introduction de césium (sous la forme de picrate de césium) dans l'équilibre induit de nouvelles relations d'équilibre dans la phase organique. Elle sont décrites comme suit :

$$\mathrm{CsP} + \mathrm{L} \rightleftharpoons \mathrm{CsPL} \quad \text{avec} \quad K_1 = \frac{[\mathrm{CsPL}]}{[\mathrm{CsP}][\mathrm{L}]} \tag{4}$$

$$\mathrm{CsPL} + \mathrm{L} \rightleftharpoons \mathrm{CsPL_2} \quad \text{avec} \quad K_2 = \frac{[\mathrm{CsPL_2}]}{[\mathrm{CsP}][\mathrm{L}]} \tag{5}$$

$$\mathrm{L} + \mathrm{H_2O} \rightleftharpoons \mathrm{L{\cdot}H_2O} \quad \text{avec} \quad K_a = \frac{[\mathrm{L{\cdot}H_2O}]}{[\mathrm{L}][\mathrm{H_2O}]} \tag{6}$$

$$\mathrm{CsPL} + \mathrm{H_2O} \rightleftharpoons \mathrm{CsPL{\cdot}H_2O} \quad \text{avec} \quad K_b = \frac{[\mathrm{CsPL{\cdot}H_2O}]}{[\mathrm{CsPL}][\mathrm{H_2O}]} \tag{7}$$

$$\mathrm{CsPL_2} + \mathrm{H_2O} \rightleftharpoons \mathrm{CsPL_2{\cdot}H_2O} \quad \text{avec} \quad K_c = \frac{[\mathrm{CsPL_2{\cdot}H_2O}]}{[\mathrm{CsPL_2}][\mathrm{H_2O}]} \tag{8}$$

avec P pour picrate et L pour ligand (dicyclohexane18-couronne-6 ou DCH18-couronne-6).

Les résultats de l'interaction entre DCH18-couronne-6 et l'eau sont similaires à ceux trouvés précédemment sans addition de césium. En effet, la fraction molaire, k, d'éther couronne lié à l'eau vaut 73(8)% et la constante d'équilibre K_a vaut 38(13) $\mathrm{L{\cdot}mol^{-1}}$. Il a également été montré que la constante K_c est nulle. Il n'y a donc pas de formation de sandwich entre deux éthers couronne, un picrate de césium et une molécule d'eau. La constante K_2 est égale à 47(15) $\mathrm{L{\cdot}mol^{-1}}$ ce qui implique qu'en l'absence d'eau, le sandwich entre deux éthers couronne et un picrate de césium

est préféré au complexe simple ne comprenant qu'un éther couronne et un picrate de césium. Quant à la constante K_b, elle vaut 27(7) L·mol^{-1} ce qui indique une préférence pour le complexe hydraté CsPL·H_2O sur celui non hydraté. Ces résultats montrent l'importance de l'eau dans l'extraction d'ions métalliques à l'aide de polyéthers macrocycliques.

0.2 Interaction entre le TBP, l'Eau et l'Acide Nitrique

Le phosphate de tributyle (TBP) est employé depuis des années dans le système PUREX (Plutonium URanium EXtraction) pour extraire et séparer l'uranium. Le CO_2 peut remplacer avantageusement le dodécane ou le kérosène habituellement utilisés dans de tels procédés. Ce solvant a en effet deux avantages sur les solvants classiques : il est beaucoup moins toxique pour l'environnement et, du fait de sa supercriticalité, il peut pénétrer plus en profondeur des matrices solides comme des cendres ou de la terre. L'acide nitrique et le TBP forment un complexe relativement soluble dans le CO_2 et permettent d'oxyder et d'extraire l'uranium.

0.2.1 Interaction entre le TBP et l'Eau

En Milieu Supercritique

Une étude similaire à celle faite dans le cas des éthers couronne et de l'eau a été conduite pour étudier l'interaction entre le TBP et l'eau dans le CO_2.

Comme pour le cas des éthers couronne, à haute concentration en TBP, la configuration comprenant deux molécules de TBP liées à une seule molécule d'eau est observée. La partie quantitative de cette étude a été réalisée à faible concentration en TBP; dans ces conditions, il y a formation d'un complexe 1:1 entre le TBP et l'eau en rapide échange avec du TBP et de l'eau non liés. L'enthalpie de formation de ce complexe est égale à -9(2) kJ·mol^{-1} alors que sa constante de formation varie entre 12(3) et 9(2) L·mol^{-1} lorsque la pression de CO_2 augmente de 20 à 40 MPa à

constante température (40 °C).

La fraction molaire, k, de TBP complexé avec une molécule d'eau varie entre 18(1) et 22(1)% avec l'augmentation de la densité du dioxyde de carbone. En l'absence de solvant, la fraction molaire k est de 100% car une solution de TBP saturée en eau a un rapport molaire de 1:1. Cette différence fait que, lorsqu'une solution de TBP saturée en eau est dissoute dans un solvant, il y a formation instantanée de micro-gouttelettes d'eau. Lors de cette formation, un nuage est d'abord observé puis les micelles s'agglomèrent pour former de plus grosses gouttelettes qui finalement se collent aux parois du récipient. Ce phénomène existe aussi lorsque de l'acide nitrique est ajouté au mélange TBP-eau. Connaissant la solubilité de l'eau dans le CO_2 aux conditions expérimentales utilisées, la quantité des micro-goutelettes a été déterminée après équilibre. Lorsque 0,5 mL de TBP saturé en eau (rapport molaire 1:1 entre le TBP et l'eau) est mélangé au CO_2 dans une cellule de 10 mL, la quantité de micro-gouttelettes formées varie de 0 à 11(2) μL lorsque la température diminue de 70 à 25 °C à pression constante ($\sim$20 MPa).

Dans des Solvants Classiques

Une étude similaire a été réalisée en utilisant la RMN et en remplaçant le dioxyde de carbone par du chloroforme afin d'explorer l'effet du solvant sur l'équilibre. Les concentrations choisies sont telles que seul le complexe 1:1 entre le TBP et l'eau est observé. Différentes quantités de TBP ont été dissoutes dans du chloroforme. Ces solutions ont ensuite été mélangées avec le même volume d'eau et, après équilibre, la phase organique a été analysée par RMN.

A partir des mesures du déplacement chimique de l'eau dans le TBP et le $CDCl_3$, les déplacements chimiques δ_0 et δ_1 de l'eau dans du chloroforme pur et dans du TBP pur ont été calculés. δ_0 = 1,51(0,04) ppm et δ_1 = 3,51(0,04) ppm. Le déplacement chimique du chloroforme en fonction de sa concentration dans le TBP a également été calculé.

L'analyse de ces données m'a également permis de calculer la constante de formation (K = 2,7(0,2) L·mol^{-1}) du complexe TBP-eau et la fraction molaire, k, de TBP complexée avec une molécule d'eau (k = 15(1)%). Cette valeur est inférieure à celle trouvée pour le CO_2 montrant qu'il y a moins de complexes TBP-eau formés dans le chloroforme que dans le CO_2. La concentration de l'eau libre, c'est à dire non complexée au TBP, dans le chloroforme a également été calculée ($[H_2O]_{org}$ = 0,07(0,02) mol·L^{-1}), cette valeur correspond aux valeurs trouvées dans la littérature. Enfin, la quantité de micro-gouttelettes a été calculée. Elle vaut 14(1) μL dans les mêmes conditions que précédemment (lorsque le CO_2 a été utilisé comme solvant). Cette valeur est supérieure de 3 μL à la valeur maximale trouvée pour le CO_2 (11(1) μL à 20 MPa et 25 °C).

0.2.2 Interaction entre le TBP, l'Eau et l'Acide Nitrique

Le phosphate de tributyle forme des liaisons hydrogène avec l'acide nitrique et l'eau, donnant un complexe, TBP·$(HNO_3)_x$·$(H_2O)_y$, très soluble dans le dioxyde de carbone supercritique (Figure 3). Le nombre de molécules d'acide nitrique par molécule de TBP, x, peut prendre des valeurs comprises entre 0 et 2,5. D'un autre coté, le nombre de molécules d'eau par molécule de TBP, y, varie entre 0,4 et 0,8. Lorsqu'un tel complexe est dissous dans un solvant il y a formation instantanée de micro-gouttelettes d'acide nitrique. Ces gouttelettes ont été détectées par RMN. Il a été prouvé que la concentration en acide des micro-gouttelettes augmente lorsque le nombre de molécules d'acide par molecule d'eau, x/y, dans le complexe de TBP, augmente. La quantité et l'acidité des micro-gouttelettes ainsi formées peut jouer un rôle important dans la dissolution et l'oxydation de dioxyde d'uranium lors de l'extraction de tels composés avec du dioxyde de carbone.

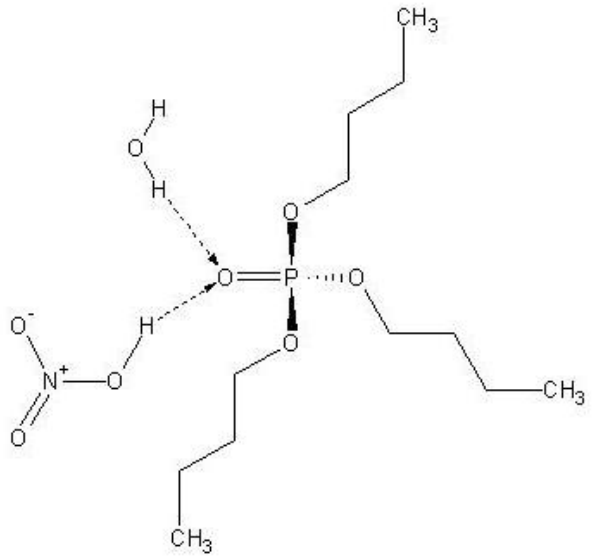

Figure 3: Une des configurations possible pour les liaisons hydrogènes entre une molécule de TBP, d'acide nitrique et d'eau.

0.2.3 Mise en Pratique : Extraction de l'Uranium à l'Aide de Phosphate de Tributyle et d'Acide Nitrique

La société AREVA (à Richland, Etat de Washington, USA) m'a permis d'utiliser la technique d'extraction supercritique afin de récupérer l'uranium enrichi contenu dans différentes matrices. Certaines de ces matrices sont des cendres venant de l'incinération de déchets secondaires à la fabrication du combustible nucléaire. Ces cendres contiennent de 5 à 10% d'uranium enrichi à 2-3%.

L'extraction se déroule en deux étapes. Premièrement, l'oxyde d'uranium, UO_2, contenu dans la matrice est oxydé avec de l'acide nitrique et le nitrate d'uranyle résultant est extrait avec du TBP et du CO_2. Pour cette première étape, un complexe $TBP{\cdot}(HNO_3)_x{\cdot}(H_2O)_y$ est dissous dans le dioxyde de carbone. Deuxièmement, l'ion uranyle est récupéré dans de l'eau pour être recyclé. Ces deux étapes sont présentées en détails sur la Figure 4.

Les conditions optimales de l'extraction sont les suivantes : (i) le complexe utilisé est $TBP{\cdot}(HNO_3)_{1.8}{\cdot}(H_2O)_{0.4}$, (ii) la température et la pression d'extraction sont re-

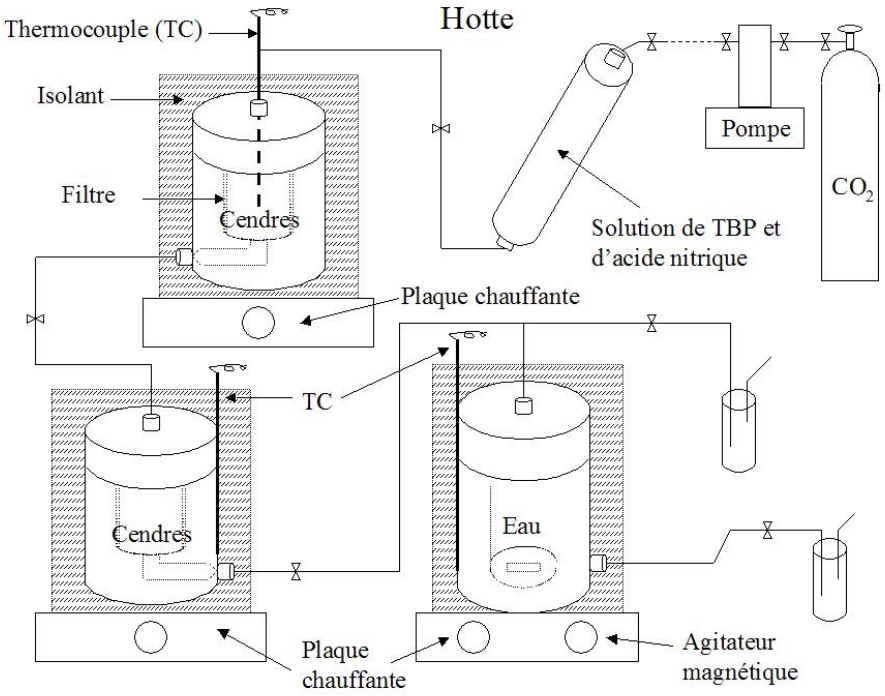

Figure 4: Schéma expérimental pour l'extraction d'UO_2.

spectivement de 60 °C et de 20 MPa, (iii) pour chaque gramme de cendre, 2 mL du complexe de TBP sont nécessaires, (iv) le temps de l'extraction statique est d'une heure et le débit est inférieur à 0.5 mL/min.

L'uranium a été récupéré de la phase organique de deux manières. Premièrement, la phase organique avait une concentration en acide de 5 mol·L^{-1} et l'uranium (à 535 g·L^{-1}) a été extrait avec de l'eau à 50 °C. Seulement 15(1)% de l'uranium a été récupéré de cette manière. Deuxièmement, l'uranium a été récupéré sous pression et en ligne avec l'extraction. Les conditions optimum sont : 20 MPa et 50 °C , avec 1,9 mL d'eau par mL de TBP. Le rendement de la récupération sous pression est bien meilleur que celui de la récupération à pression atmosphérique. Ce rendement diminue lorsque la concentration en acide augmente ou lorsque la concentration en uranium diminue. Lorsque les conditions ont été modifiées (température réduite à 24 °C ou volume d'eau réduit à 1 mL par mL de TBP), une perte allant jusqu'à

68% dans l'efficacité de la récupération de l'uranium a été observée. Cette perte est moindre à basse concentration en acide nitrique.

Conclusion

Durant ce travail de thèse, deux types d'extractants d'ions métalliques ont été étudiés. Les premiers, appelés éthers couronne, sont utilisés pour extraire des cations alcalins comme le césium. Leurs interactions avec l'eau ont été étudiées à l'aide de deux méthodes d'analyse différentes. La première méthode utilisée est la spectroscopie IR-TF. Cette méthode manque de précision, mais permet de distinguer les différentes configurations possibles. L'autre méthode utilisée est la RMN. Cette méthode est plus précise quantitativement, mais ne permet pas de discerner les configurations simples et pontées entre les éthers couronne et l'eau. Elle permet néanmoins d'étudier, sans interférences, des systèmes plus compliqués tel que le système éther couronne, eau et picrate de césium. Il n'a malheureusement pas été possible de l'utiliser dans les fluides supercritiques, l'équipement à disposition ne le permettant pas.

L'autre type d'extractant utilisé est le TBP. Cet extractant peut former un complexe en se mélangeant à l'acide nitrique. Ce complexe a été caractérisé et étudié dans différents solvants. Lorsqu'il est dilué dans le dioxyde de carbone, la formation de micro-gouttelettes d'acide facilite l'oxydation de l'UO_2 et l'extraction de l'UO_2^{2+}. Il a été prouvé que ce principe peut être utilisé pour extraire l'uranium de milieux tels que des cendres provenant de l'incinération de déchets secondaires à la fabricaton du combustible nucléaire. De nombreux progrès peuvent être faits dans la mise en application à grande échelle de ce procédé écologique d'extraction, notamment en ce qui concerne la récupération de l'uranium.

General Introduction

My thesis work is focused on the supercritical fluid extraction of uranium and cesium. These elements are present in nuclear waste, such as nuclear manufacturing byproducts or Spent Nuclear Fuel (SNF). Uranium is the main element constituting the fuel and Cesium-137 is an abundant fission product with a relatively long half-life that contributes largely to the heat production in SNF. The processing of uranium and cesium is of particular importance for waste management.

Water is often present in such waste and it plays an important role in the extraction process, which I studied as part of this research. I used different spectroscopic methods for analyzing the relevant chemical interaction in supercritical fluids and in solvents such as chloroform and carbon tetrachloride. In this introduction, I will first describe the origins and the diversity of nuclear waste and current practical methods of managing them, as well as the futuristic waste management processes envisioned by scientists. I will then describe the industry standard reprocessing technique which is solvent extraction. Supercritical fluids, especially carbon dioxide, are good alternatives to organic solvents in this process. I will therefore describe their characteristics. Thereafter I will relate the special characteristics of uranium and cesium as well as the chelating agents I used to extract them. Last, the spectroscopic techniques that I used will be briefly described.

Nuclear Wastes and Nuclear Waste Management

Nuclear byproducts and waste have been a serious issue from the dawn of the nuclear age. The first use of nuclear energy for military purposes during the world war II was

accompanied by the generation of large quantities of waste that continued to grow during the arms race between the United States and the Soviet Union as well as other countries with nuclear arms. The peaceful applications of nuclear energy, particularly for generating electric power, are also responsible for producing large quantities of heavy metal and radioactive waste through different steps of the fuel cycle. Hundreds of nuclear power plants are operating today in many countries (Figure 5). There are many other industrial applications of nuclear materials and they are used routinely in hospitals for medical diagnosis and treatments.

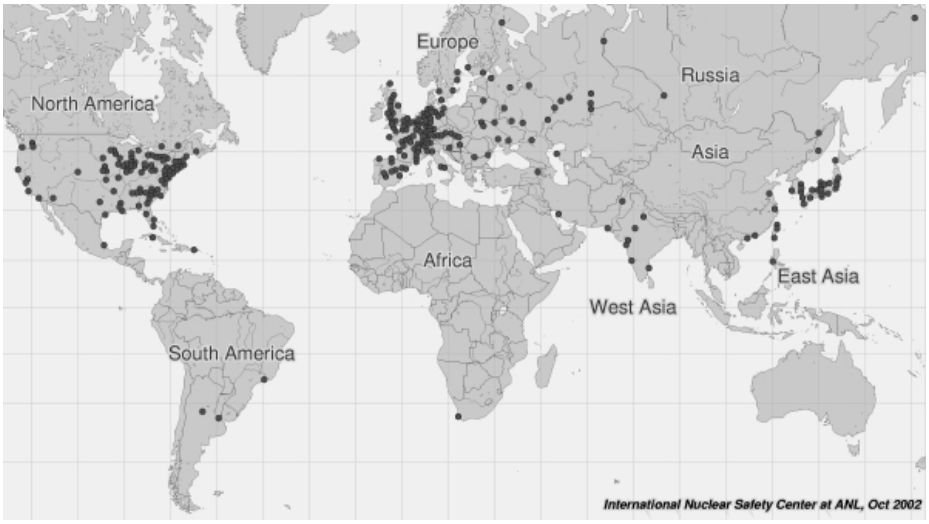

Figure 5: World map of nuclear reactors from the International Nuclear Safety Center (INSC) web page.[1]

Nuclear waste management is not only a problem in the present, but also will be in the future. Indeed, the fuel industry declining, the oil supply is going down and developing countries like India and China have a huge demand for power which is a basic need and is required for economic growth. Furthermore, to reverse the global warming effect, the emission of greenhouse gases from industry, transportation and power plants needs to be reduced. The solution to this problem is electricity produced from plants that do not generate greenhouse effect gases. The electricity can be for industrial use, home use or public transportation. Natural gas is cleaner than coal

because it does not produce as many particles and byproducts as coal or oil, but 4% of natural gas is lost during transport. The contribution of methane to global warming is 25% worse than that of CO_2, which is also produced by these plants. On the other hand, renewable energy (i.e. hydroelectric, windpower, solar, etc.) has now reached a plateau. There are not many large dams that can still be built on the world's rivers; wind-mills are expensive, inefficient and consume too much space; solar energy lacks power and is expensive. The only obvious way to overcome the energy crisis that is building is to increase the number of nuclear power plants.

For the same amount of energy produced, one can find more uranium in the filters and waste of a coal power plant than in a nuclear power plant. Furthermore, the Industrial Accident Safety Rate (IASR), based on the number of accidents per hour and per worker, in American nuclear power plants is well below the IASR for manufacturing industries and is at the same level as the IASR for banks or real estate agencies. For these reasons, the approval rate for new nuclear power plants in general opinion polls in America increased up to 60% recently. This approval rate is even greater in places where a nuclear power plant is already in place.

The majority of nuclear waste is associated with the uranium fuel cycle. The front end of the fuel cycle, the so called pre-fission stage, which includes mining, and enrichment and fuel fabrication activities, generates uranium-containing byproducts and waste. The back end of the fuel cycle, the stage after the fuel is irradiated in the reactors, generates large quantities of radioactive waste products. While these fission products are intentionally generated in production reactors for the purpose of processing to extract weapons grade plutonium, they are considered waste products when generated by power reactors. Most of the nuclear waste generated today comes from power plants and is stored without reprocessing, particularly in the United States. European countries and Japan continue to make progress in reprocessing, which can reduce the volume of highly radioactive waste and allow the recycling of useful isotopes. Regardless of the sources of nuclear waste – power plants, the legacy

of cold war nuclear weapons, hospital waste, food irradiation, etc. – improvements in the technology of handling and reprocessing are necessary for the economics of the respective application as well as for environmental protection. These reprocessing techniques are basically chemical in nature, and this thesis is a contribution in this direction.

Nuclear waste can be divided into four categories depending on its toxicity[8]:
(i) Low-Level Waste (LLW): The level of radioactivity and the half-life of the radioactive isotopes in low-level waste are both relatively small and LLW does not require shielding during handling and transport. To reduce its volume, it is often compacted or incinerated before disposal. Storing the waste for a period of 10 to 50 years will allow most of the radioactive isotopes in low-level waste to decay, at which point the waste is not considered radioactive and can be disposed as normal waste. This kind of waste, for example, is generated by hospitals and industries.
(ii) Intermediate-Level Waste (ILW) contains higher amounts of radioactivity and some requires shielding. This waste, for example, is made of contaminated materials from the manufacture of nuclear fuel, e.g., gloves, shielding outfits, plastic containers, papers, etc. In such cases, the contaminated material can be incinerated to lower the amount of waste and the resulting ash can be treated and then discarded as LLW.
(iii) High-Level Waste (HLW) comes mostly from the core of nuclear reactors and from nuclear weapons processing. HLW contains fission products, including uranium and plutonium, generated in the reactor core. HLW is highly radioactive and some isotopes have extremely long half-lives (some longer than 100,000 years). Therefore, HLW will take a long time to return to safe levels of radioactivity.
(iv) Transuranic Wastes have atomic numbers greater than uranium. They come mainly from weapons production and consist of clothing, tools, rags, residues, debris and other such items contaminated with small amounts of radioactive elements, mostly plutonium. Because of the long half-lives of these elements, this waste is not disposed of as either low-level or intermediate-level waste. It does not have the very

high radioactivity of high-level waste, nor its high heat generation.

In addition to the problems arising from the management of accumulating waste, there is another concern: the pollution generated by the Chernobyl incident, which quickly covered a large area (Figure 6). This disaster turned a localized problem into a major environmental one. Unless another solution is found, the population in the area affected by such pollution must wait for the intensity of radioactivity to decay and disperse sufficiently in order to return and pursue farming. However, certain places, e.g., proximal to a source of drinking water, will need real decontamination efforts.

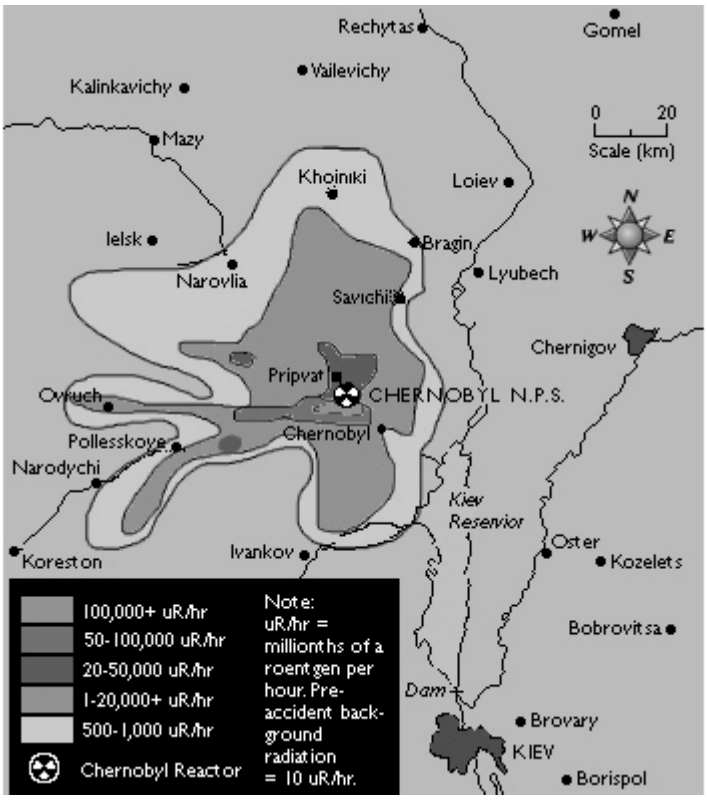

Figure 6: Gamma radiation map in the Chernobyl area, results of the May 29, 1986, Gamma Radiation Survey.[2]

Different ways of disposing of nuclear waste have been under investigation and trial.[8] First, short-term storage can be used. It decreases the radioactivity of HLW up to 100 times in 10 years. Unfortunately, the decay of radioactive material is not

linear but exponential, which limits the usefulness of passive storage. Short-term storage is a necessity for HLW because these materials cannot be shipped or handled easily when they are just coming out of the core of a reactor. It is important to know that short-term storage is not a final option; it only lowers the danger level of the waste but does not eliminate it. The waste will still need to be processed or stored in another way afterward. It is important to make sure that the storage area is stable and well protected from accidents or natural disaster. The spread of such radioactive material in drinking water or on agricultural and hunting lands would be a catastrophe.

As a follow-up or as a second option, long-term storage can be used for HLW or ILW. HLW and long-lived waste from ILW (from fuel reprocessing) are generally buried deep underground whereas ILW's short-lived waste (mainly from reactors) is generally buried in shallow repositories. Forgetting them underground until the danger is no longer present seems to be a good idea, but it does not take into account the fact that some waste has a very long half-life and nobody can assure that humanity will remember it after several thousand years. We are still discovering artifacts that are less than five thousand years old, for instance, in Egypt. Even the ancient Egyptian language and alphabet were forgotten. Will the archaeologist of the future dig with a Geiger counter? Besides, the earth is moving all the time in an unpredictable manner. Nobody can assure that the waste will remain stable and not be dispersed with underground water or seismic activity.

The toxicity of the waste beyond its radioactivity is another aspect to consider. Indeed, some of this waste contains plutonium, one of the most toxic of all elements. Some people consider sending such waste into space, but the cost would be enormous and unethical.

Nevertheless, there is a way of minimizing the consequences of leaks or other problems that might cause the waste to be scattered; it is the vitrification process before storage. With this method, radioactive waste is mixed with silica and melted

into glass beads. This process should prevent radioactive elements from going into the atmosphere or the groundwater, even if they are in direct contact with it.

In the United States, the Nuclear Regulatory Commission (NRC) uses the funds collected from nuclear power plant taxes to develop waste disposal programs. There is a long-term underground storage currently under development at Yucca Mountain, Nevada.[9]

Another way to get rid of such waste is to process it.[10] One way of processing nuclear waste is to transmute the unstable isotopes to stable ones in the same way alchemists would transform or transmute lead into gold. There have been some attempts to use photons in the x-ray range in a high-powered electron linear accelerator. The use of a laser to remove neutrons from a radioactive isotope also has been investigated. If the use of this technology were possible, Cesium-137 could be transmuted to Cesium-136 with a half-life of 13.1 days instead of 30.2 years. Unfortunately, this seems to be only an alchemist's dream. A more realistic way to use transmutation is to irradiate an isotope with neutrons in an accelerator to allow the isotope to absorb a neutron. With this process, iodine-129 can be transmuted to stable xenon with neutron absorption. The Accelerator Transmutation of Waste (ATW) system is currently being developed at Los Alamos National Laboratory in New Mexico.[11,12] The downside of ATW is that long-lived radioisotopes should be isolated for them to be transmuted without interferences and without transmuting good radioisotopes into bad ones. For example, Uranium-238, which is the main constituent of Spent Nuclear Fuel (SNF) can be transmuted into Plutonium-239. ^{239}Pu is not as manageable as ^{238}U and has a half-life of 25 thousand years.

Solvent Extraction

Solvent extraction has already been proven to be a good method to separate radioisotopes from SNF. One of the most famous solvent extraction processes is the PUREX (Plutonium Uranium Recovery by Extraction) process. The principle of this pro-

cess is to separate uranium and plutonium from the fission products and from one another. First the pellets are prepared for the dissolution (i.e. decladded). Then the SNF is dissolved in a solution of nitric acid in which the tetravalent uranium is oxidized to uranium(VI). Second, the uranium(VI) and plutonium(IV) nitrates are extracted from the nitric acid solution with a mixture of kerosene and Tri-n-Butyl Phosphate (TBP) (at 70% and 30% respectively), while the fission products remain in the aqueous nitric phase.[13] The plutonium is then reduced to an oxidation state III. In the trivalent state, the plutonium is insoluble in the organic phase and is therefore easily stripped out with water. Finally, the remaining uranium nitrate is stripped out of the organic solution with heated water. Uranium(VI) and plutonium(III) can also be purified and converted to uranium trioxide (UO_3) and plutonium dioxide (PuO_2). Despite this, solvent extraction has a big downside: its secondary waste production. If the organic solvents used in a Purex-like process could be exchanged for a volatile solvent that is harmless to the environment, the functioning cost would be reduced. That is exactly what Supercritical Fluid Extraction (SFE) does by using carbon dioxide.

Supercritical Fluids

A fluid is called supercritical when both its temperature and pressure exceed their critical values (T_c for the critical temperature and P_c for the critical pressure). See Figure 7. A phase diagram for CO_2 is shown in Figure 7 with a representation of the supercritical and the subcritical region. When a substance is at a pressure and temperature that is near the supercritical area, its state is called subcritical.

Supercritical fluid density depends on pressure and temperature. The density generally increases with a pressure increase and decreases with a temperature increase. Near the critical point, it is not unusual to observe inconsistency in density or other physical properties. The system can be greatly disturbed by a small difference in temperature or pressure or by adding a substance or an impurity to the fluid. It

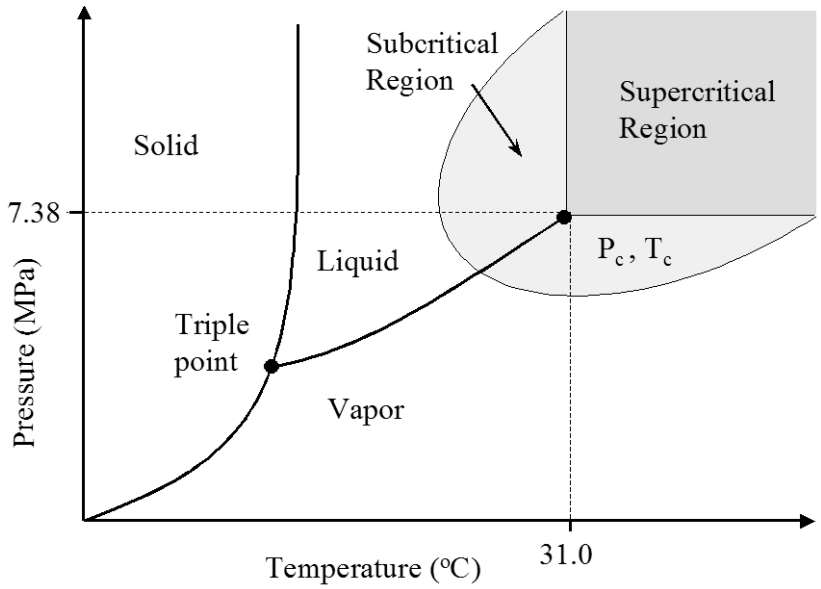

Figure 7: Phase diagram for CO_2, the shaded areas are the subcritical and supercritical fluid regions.

is then important to pursue quantitative measurements in the neighborhood of the critical values.

Different fluids such as water, methanol, ammonia, etc. can be in the supercritical state, see Table 1. Supercritical CO_2 offers numerous advantages over the other fluids: it has moderate critical values and it is inert, nontoxic, nonflammable, inexpensive and widely available in purified form. Furthermore, it is a gas at normal temperature and pressure, allowing an easy recovery of the extracted species without generation of secondary wastes that are very hard to discard or reprocess.

The solubility of a substance in Supercritical CO_2 is related to its density and temperature. Solubility increases with an increase in density at constant temperature and decreases with increasing temperature at constant pressure.[7,14] With regard to the above factors, we can see that supercritical CO_2 is more economic in the long run. Besides the fact that supercritical CO_2 requires less energy to reach its critical parameters, its density can be easily raised to improve solubility.

Table 1: Supercritical fluids critical values.

Name	Symbol	T_c (°C)	P_c (MPa)	ρ_c^a (g·L^{-1})
Methanol	CH_3-OH	240 ± 1	8.1 ± 0.1	273
Methane	CH_4	-82.6 ± 0.3	4.61 ± 0.03	162
Carbon dioxide	CO_2	31.03 ± 0.04	7.380 ± 0.015	467
Ammonia	NH_3	132.3 ± 0.01	11.300 ± 0.005	225
Water	H_2O	374 ± 2	22.064 ± 0.005	322
Nitrogen	N_2	-273.0248 ± 0.0005	12.619 ± 0.001	952

Source: The National Institute of Standards and Technology (NIST) Chemistry WebBook, http://webbook.nist.gov/
[a] uncertainty on densities ≤ 2 (g·L^{-1})

CO_2 is the most widely used substance for supercritical fluid applications. For many years, it has been used on a large scale to remove caffeine from coffee and tea. CO_2 is also used to extract other lipophylic substances such as nicotine. The extraction of metallic ions is more challenging because they are generally insoluble in CO_2 . To circumvent this problem, neutral chelating agents are chosen[15–17] and I will describe in details their action later in this general introduction.

During my thesis work, I studied supercritical fluid extraction (SFE), directly or indirectly with the use of organic solvents such as chloroform or carbon tetrachloride. I focused on the extraction of two elements present in nuclear waste and nuclear contamination sites. The first one, cesium-137, is a man-made isotope produced by the fission of uranium-235. Its half-life is 30.17 years. Cesium-137 is present in a radio-contaminated environment such as the Chernobyl area, but it is more of an issue in nuclear power plant waste. The second, uranium, is the main isotope present in Spent Nuclear Fuel (SNF) and is also found in nuclear weapons and in ILW.

Cesium and Uranium Elements

Cesium-137 is a relatively long-lived isotope with a large contribution to the heat production in SNF. As shown on Figure 8 and appendix A, cesium is one of the

most abundant fission products in SNF from Pressurized Water Reactors (PWR) 150 days after its discharge. The amount of cesium produced per ton of uranium in the fresh fuel load is even greater in Liquid Metal Fast Breeder Reactors (LMFBR) such as Super-Phenix in France. Recovering the cesium from waste is a very interesting project because it lowers the radioactivity of the matrices from where it is extracted, allowing the remaining material to be more easily handled and discarded. After separation from the waste, ^{137}Cs is a good candidate for long-term storage because of its moderate half-life. Cesium-137 can also be recycled and used for radiotherapy, for example.

Cesium-137 is also a concern in cesium-contaminated areas such as the Chernobyl area. It is accumulated in the human body, mimicking potassium, which disturbs the transmission of nerve messages. Extracting cesium from cesium-contaminated areas, along with other isotope cleaning, can effectively reduce the waiting period (∼300 years for ^{137}Cs) required to return the land to the people.

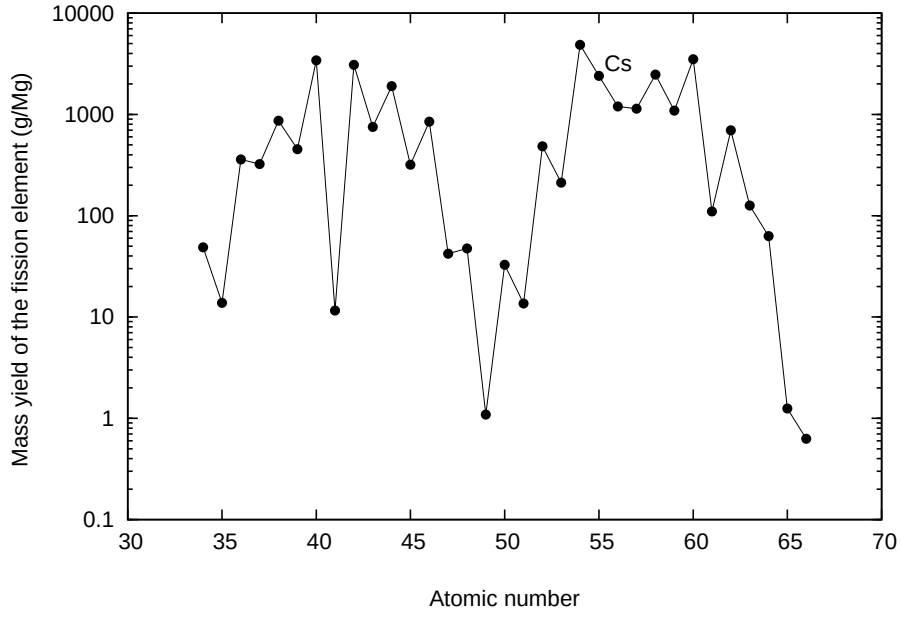

Figure 8: Mass (g) of elements (150 days after discharge from a PWR) per ton (Mg) of uranium (freshly loaded in the reactor) versus the atomic number of the element.[3]

The other element in which I was interested, is uranium. The uranium in nuclear waste generally contains a higher uranium-235 isotope fraction than it does in natural form, which makes it attractive to recover and recycle for use as fuel in power reactors. This recycling strategy would reduce the energy needed and reduce the pollution generated to enrich uranium. Recycling uranium from waste is particularly relevant considering that the natural abundance of the uranium-235 isotope is only 0.72% while recovered uranium (from fuel manufacturing waste for example) contains up to $\sim$4% ^{235}U.

Chelating Agents

Because supercritical CO_2 is a nonpolar solvent, there is a weak solute-solvent interaction in the Supercritical Fluid Extraction (SFE) of metal ions. Consequently, supercritical CO_2 needs the presence of a chelating agent,[14–17] also called ligand, to enhance its ability to extract metal ions and their counter ions into a hydrophilic liquid.

The role of a chelating agent is to bind with the metal ion to form a metal chelate that is soluble in CO_2. Furthermore, a good chelating agent needs to have the following properties: it has to be soluble in CO_2, selective for the species that needs to be extracted, and relatively harmless for the environment, or easily recyclable.

Metal chelates can be formed in CO_2 using two methods. First, the chelating agent is dissolved in CO_2, which is then directed into the sample containing the metal ions. In the second method, the ligand is introduced into the sample before the SFE is initiated.

Most matrices, from which metal ions are extracted, contain water. During the extraction, chelating agents change the hydration sphere of the ions. Some water can be solubilized in the organic phase with or without the help of the chelating agent. Consequently, the presence of water has a great effect on the efficiency of the extraction.[16,18] Therefore, the understanding of the water interaction with ligands

and metal ions has a significant impact on the understanding of the thermodynamics of the extraction. The understanding of these interactions might lead to the discovery of new ways to enhance the extraction efficiency.

Crown ethers have been intensively studied for their selectivity in the solvent extraction of cations and, especially, alkaline-earth-metal cations.[18–23] See Figure 9 for a representation of 18-crown-6. Furthermore, crown ethers have relatively high solubility in sub- and supercritical CO_2.[14] These properties make crown ethers highly attractive for Supercritical Fluid Extraction (SFE) of cesium. A study[24] used crown ethers to extract sodium and potassium cations in supercritical CO_2 with perfluorocarboxylic acid as a counter ion. Another study performed by Wai et al.[25] showed a successful extraction of cesium with crown ethers and fluorinated compounds. Nevertheless, the role of water and the interactions involved in the chelating process were not detailed in these publications. I paid special attention to these important properties in my work.

On the other hand, the TBP-nitric acid efficiency in the Purex process has been proven.[13] See Figure 9 for the representation of TBP and nitric acid, respectively. TBP is highly soluble in supercritical CO_2[14,26] and forms an adduct with nitric acid. This adduct can be used to dissolve uranium oxides.[27–29] The resulting metal chelate, $2TBP{\cdot}UO_2(NO_3)_2{\cdot}2H_2O$, is known to have very high solubility in CO_2.[30,31] Consequently, TBP-nitric acid adducts were chosen as chelating agents for the extraction of uranium.

Spectroscopic Methods Used

For this research work, two experimental devices were used : Proton Nuclear Magnetic Resonance (NMR) and Fourier Transform Infra-Red spectroscopy (FT-IR). NMR is a precise analytical tool for the quantitative understanding of water interactions in organic solvents.[32,33] The crown ether-water interactions with and without cesium picrate and the TBP-nitric acid-water interactions in solvents were determined using

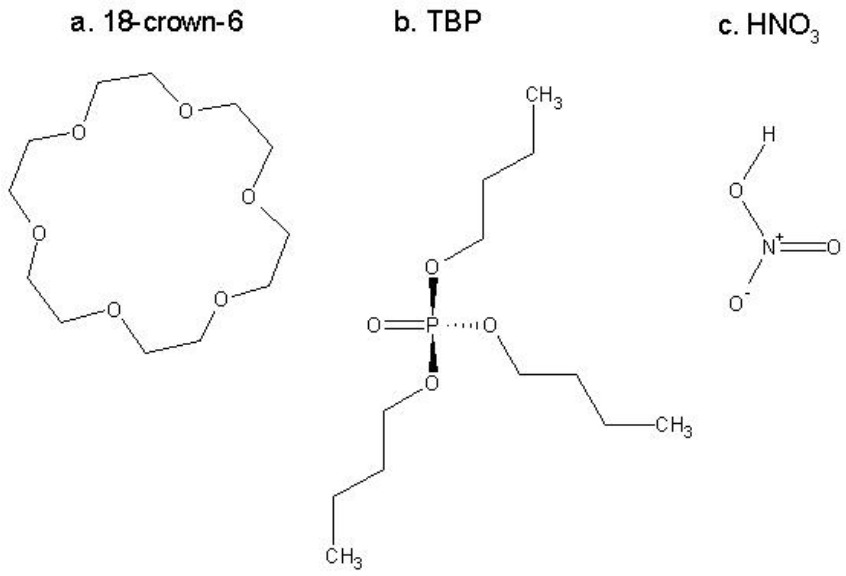

Figure 9: Representation of a crown ether (18-crown-6) and the TBP and nitric acid molecules.

this analytical technique. Unfortunately, I was unable to use it with supercritical fluids in spite of numerous attempts. I tried to use capillaries, but they were not suitable for my system where many compounds were dissolved in CO_2. I also tried to use a PEEK (TM)[1] polymer high-pressure cell[34] in collaboration with C. Yonker (Pacific Northwest National Laboratory, Richland, Washington), but the results obtained were random and not reproducible. The reasons for this failure might be the inability to have a lock on the NMR spectroscope or a consistent standard for concentration determination.

I was not able to use the NMR for quantitative measurement in supercritical fluids with the materials that I tried. Nevertheless, as an alternative technique, I used FT-IR spectroscopy with the help of John Fulton and his lab equipment[35] in the Fundamental Science Directorate of the Pacific Northwest National Laboratory in Richland, Washington. FT-IR is not as accurate as NMR, and the overlapping of rays from different species can be a problem. However, if the system is kept simple with a limited number of compounds, it can be used for quantitative measurements with

[1]Manufactured by Victrex plc.

an acceptable accuracy. Indeed, it has been used successfully in the past few years to study hydrogen bonding in supercritical CO_2.[36–40] I used FT-IR successfully to understand crown ether-water and TBP-water interactions in super- and subcritical CO_2. Furthermore, I was able to distinguish different crown ether-water configurations where the NMR was showing only an average of all configurations.

Finally, I used gamma spectroscopy to monitor the enhancement of the uranium extraction from ash with supercritical CO_2. This gamma spectroscopy technique lacks accuracy but gives fast and inexpensive approximate measurements of uranium, which is used to estimate the extraction efficiency. Key samples were analyzed by Inductively Coupled Plasma Mass Spectroscopy (ICP-MS) for higher accuracy.

Overview of the Thesis Structure

My thesis is divided into two chapters. The first one focuses on cesium extraction with crown ethers and the second one on uranium extraction with a TBP/nitric acid complex.

In the first chapter, I describe the crown-ether water interaction because the water plays an important role in solvent extraction. To pursue this goal, I first used the FT-IR spectroscopy in supercritical CO_2 and then the NMR technique in organic solvents for comparison. To finalize this part of my research, I show the results of the addition of cesium picrate to the system in order to understand the whole picture of the recovery of cesium.

In the second chapter, I describe the antisolvent effect of the TBP-water and the TBP-water-nitric acid systems in supercritical CO_2 and in solvents using FT-IR and NMR. To conclude this part, I demonstrate the efficiency of supercritical fluid extraction for a pilot plant where the uranium is extracted from the incineration ash of the byproduct of the nuclear fuel production. For this work, I used the TBP-nitric acid solutions described in supercritical CO_2. Lastly, I will summarize the conclusions of this research thesis.

Chapter 1

Crown Ether-Water Interaction

Introduction

The scope of work presented in this chapter covers the various mechanisms of the cesium extraction in supercritical fluids and solvents using crown ethers as ligands. Special attention is focused on the role of water. The interaction in sub- and supercritical CO_2 were studied in detail. This was complemented and compared with a parallel study using solvents, specifically chloroform and carbon tetrachloride mixtures. Different spectroscopic tools, Fourier Transformed Infra-Red (FT-IR) and Nuclear Magnetic Resonance (NMR) were used for the analysis thus yielding detailed information about the molecule structure and the interaction equilibria as these techniques complement each other. To conclude the work of this chapter, the role of water was studied in the cesium extraction equilibrium using crown ethers.

I will first describe the crown ethers properties. Crown ethers are macrocycles formed of a succession of ether molecules (-H_2C-O-CH_2- named methoxymethane or methyl methyl ether) bonded together through the carbon atoms to form a ring. The carbon atoms are positioned outside of the ring whereas the oxygen atoms are inside the cavity and therefore form a powerful attractor for positively charged atoms or molecules. Furthermore, the number of ether molecules forming the ring determines the size of the internal cavity and is therefore very selective of the cation extracted. Representations of different crown ethers are shown in Figure 1.1. When unsub-

stituted, their nomenclature depend on the number of chemical bonds and oxygen atoms in their cycle. For example, a macrocycle composed of 12 chemical bonds and 4 oxygen atoms is called 12-crown-4 or 12C4 and a macrocycle composed of 18 bonds and 6 oxygen atoms is called 18-crown-6 or 18C6. Unsubstituted, crown ethers can be in various conformations. The most represented conformation for 18-crown-6 is D_{3d} (Figure 1.1) but other conformations are possible where the crown is more or less closed on itself like a jaw. Different substitutes can take the place of the hydrogen atoms outside the ring. Some substitutes such as the cyclohexane or benzene molecules are very commonly used and are represented in Figure 1.2. When these substitutes are used with 18-crown-6, they force the crown ether to be in a "plane" or D_{3d} conformation.

Solvent extraction technique is commonly applied for the removal of metal, organic molecules or ions from soil or aqueous solutions using many acidic, anionic or neutral extractants.[41–46] Crown ethers have been intensively used as extractants for their selectivity and efficiency to extract cations and especially alkaline-earth-metallic cations from aqueous solutions, making them ideal for the extraction of cesium.[41,47,48] Furthermore, crown ethers are soluble in a large variety of solvents like carbon tetrachloride, chloroform or supercritical carbon dioxide, making them suitable for environmentally friendly processes using supercritical CO_2.

In such extractions, the organic or the CO_2 phase contains often water and its interaction in the solvent needs to be taken in account especially since Dietz et al.[18] showed that the efficiency of a solvent extraction depends on the solubility of water in the organic phase.

Most published research on solvent extraction do not discuss the role of water in sufficient detail.[18,36,49–53] For example, Dietz et al.[18] studied the extraction of cesium from acidic nitrate media using crown ethers as extractant in various organic solvents. An increase in the efficiency of the extraction was observed when the water solubility in the organic phase increased. The enhanced extraction efficiency was

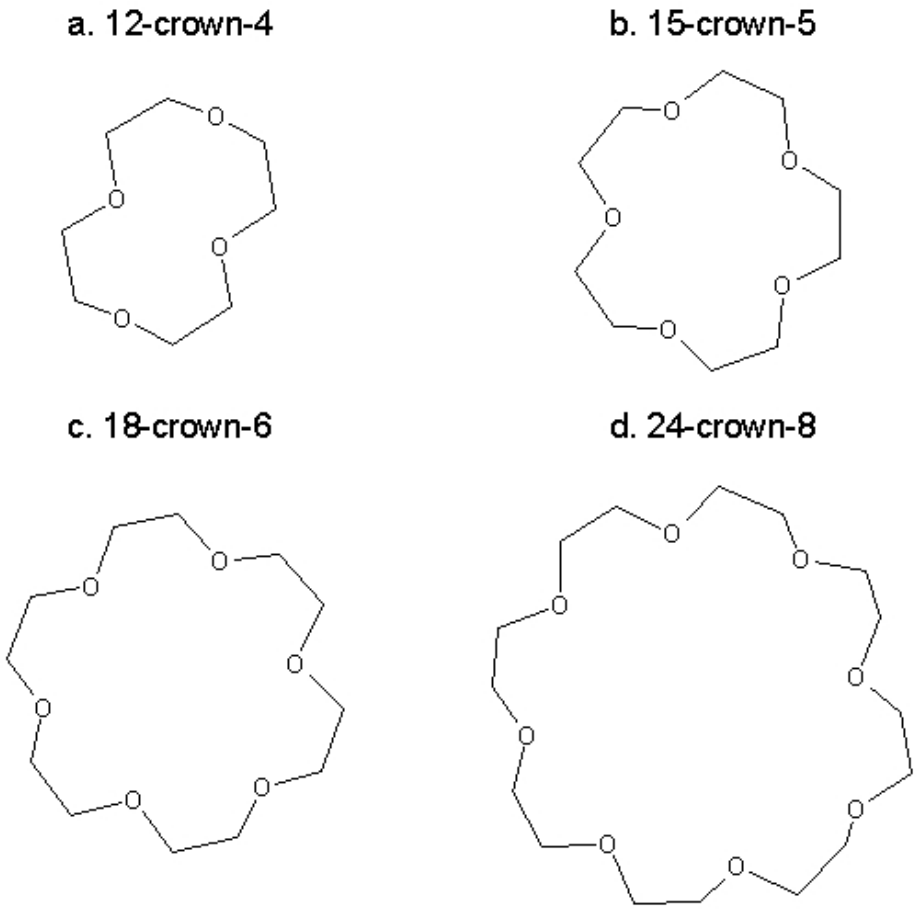

Figure 1.1: Molecular structure of 12-Crown-4 (a); 15-Crown-5 (b); 18-Crown-6 (c); 24-Crown-8 (d).

partly attributed to the water-saturated organic phase. Another study[52] states that the role of the water must be taken into account in the description of the equilibria of the extraction from water since the organic phase is water saturated. Some molecular dynamics studies[54] showed that the water is mainly bridge-bonded to the crown ether in a D_{3d} conformation. In addition, Moyer et al.[36] used FT-IR to describe the general equilibrium between water and 18-crown-6 in carbon tetrachloride. This study neither discusses the effect of the solvent nor describes the ligand partition between the two phases. Moreover, no published work described the water-crown ether interaction in supercritical fluids.

It was therefore important as a first step in this work to analyze the crown ether-

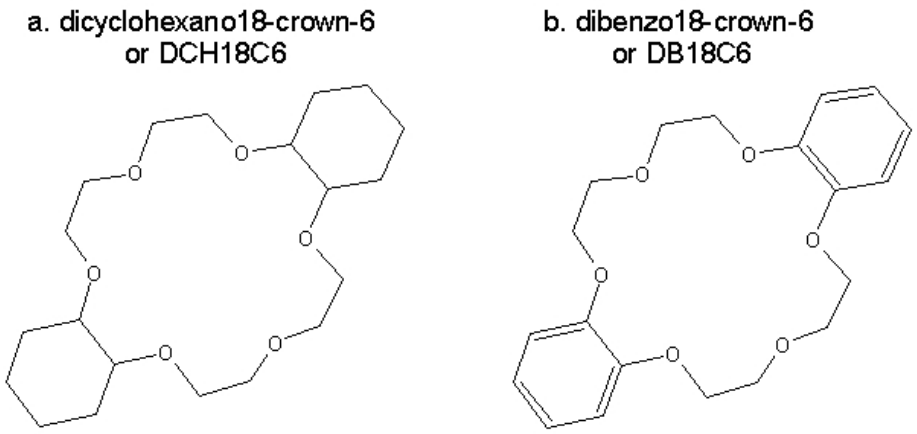

Figure 1.2: Molecular structure of dicyclohexano-18-Crown-6 (a) and of dibenzo-18-Crown-6 (b).

water interaction in supercritical and liquid CO_2. Thereafter, I used Nuclear Magnetic Resonance (NMR) to study the role of the solvent in this interaction. Solvents such as chloroform and carbon tetrachloride were used. I finally worked on constructing a more complete picture of the cesium extraction by introducing some cesium picrate to the water-crown ether equilibrium.

1.1 Crown Ether-Water Interaction In Supercritical CO_2

Introduction

The purpose of this section is to provide in-depth understanding of the interaction between water and crown ethers in supercritical fluids. The description of this interaction is important to give an insight into cesium extraction using crown ethers. This interaction was studied in supercritical CO_2 using the Fourier Transform Infra-Red (FT-IR) spectroscopy. I will therefore describe this analytical tool in more details because of the impact on the specific adaptations necessary for my experiments.

The FT-IR spectroscopy is the spectroscopic technique most widely used to analyze molecular structures. It is a fast and sensitive method for most chemical systems. Furthermore, it is an economically attractive device that is easy to use. Essentially, FT-IR is used for the understanding of the chemical bonds. Chemical bonds have frequencies of vibration that are mostly in the infra-red domain. These frequencies depend on the nature and on the environment of chemical bonds. Thus, if a molecule is irradiated with a range of waves within the infra-red region, it will absorb all the waves that have the same frequency as the frequency of vibration of the bonds of the molecule. Therefore the absorption spectra can be represented by the plot of the intensity of the transmitted beam versus the frequency of vibration. The analysis of such spectra can give the molecular structure of the molecule irradiated. At a fundamental level, the vibration between two atoms can be explained with the classical mechanics model of the harmonic oscillator composed of two masses attached to the opposite ends of a spring. According to this model, the frequency of the oscillations (ω) in rad/s is obtained from

$$\omega = \sqrt{k_s / \mu} \tag{1.1}$$

where k_s is a constant related to the strength of the chemical bond analogous to the spring constant which is the ratio between the spring force and the displacement. The

reduced mass, μ, is defined as

$$\mu = \frac{m_1 m_2}{m_1 + m_2} \tag{1.2}$$

where m_1 and m_2 are the masses of the atoms 1 and 2 respectively. The frequency of oscillation, ω in rad/s, is related to the frequency (ν) in Hertz according to

$$\omega = 2\pi\nu, \tag{1.3}$$

and to the wavenumber ($\bar{\nu}$) in cm^{-1} is obtained from

$$\bar{\nu} = \frac{\nu}{100\,c} \tag{1.4}$$

where c is the speed of light in m/s. Combining the above equations, the wave number is:

$$\bar{\nu} = \frac{\sqrt{k_s}}{200\pi c}\sqrt{\frac{m_1 + m_2}{m_1 m_2}} \tag{1.5}$$

which demonstrates that the wave number (proportional to the frequency of vibration) clearly depends on the mass of the atoms, i.e. the isotopes used.

Utilizing the previous equations, the O–H bond in the water molecule can be approximated as a diatomic molecule. Thus, a significant shift in wave number should be expected by using deutered water instead of normal water. This is confirmed by the following calculations, where the constant k_s for the O–D and the O–H bond was assumed to be the same as an approximation. The two frequencies are related according to

$$\bar{\nu}_{\text{O-D}} = \bar{\nu}_{\text{O-H}}\sqrt{\frac{\mu_{\text{O-H}}}{\mu_{\text{O-D}}}} = \bar{\nu}_{\text{O-H}}\sqrt{\frac{16\times 1}{16+1}\Big/\frac{16\times 2}{16+2}} = 0.73 \times \bar{\nu}_{\text{O-H}}. \tag{1.6}$$

This approximation is very good given that the symmetric stretching vibration wave numbers for O–H and O–D are known to be 3652 and 2666 cm^{-1} respectively.[55] the ratio of the measured frequencies is 2666/3652 = 0.73, confirming the accuracy of equation 1.6. In the work presented in this section, I used this property to avoid the overlapping of intense CO_2 absorption bands between 3500 and 3800 cm^{-1} with water bands by using D_2O instead of H_2O.

Most of the IR spectrometers are Fourier transformed. Their principle of operation is described here with reference to Figure 1.3. A laser source of infra-red radiation is used to generate the main beam. This beam travels from the source to a half-transparent mirror (beam-splitter) positioned at 135 degrees, which splits the beam in two. The first beam (11) is reflected at 90 degrees and hit a mirror that is fixed and perpendicular to the beam. The second beam (22) is transmitted and bounces off a mirror that is perpendicular to the beam. This mirror can be moved to change the length of the optical path. Both beams return to the beam-splitter where half of all the photons travel toward the source and are lost, and the other half are reflected (2) or transmitted (1) to the sample with a phase difference due to their different path-lengths. The combined beam transmitted through the sample finally arrives at a detector placed at the other side of the test sample and the resulting signal will be analyzed.

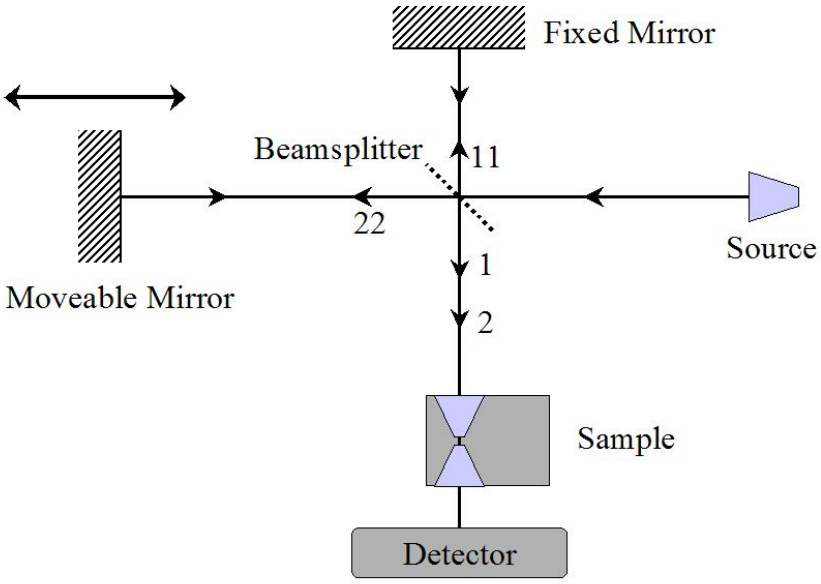

Figure 1.3: Fourier Transform Infra-Red (FT-IR) spectrometer.

Due to the difference in optical path (δ), the two beams with two different phases will go through the sample. It will therefore produce some interferences that are either constructive or destructive resulting in intensity changes depending on the value of δ. As a result the graph of the intensity as function of δ can be plotted. To obtain the spectrum, which is a plot of intensity versus frequency, a mathematical tool is needed. This tool is called the Fourier transformation and it is generally done by a computer connected to the spectrometer.

The resulting spectrum is composed of peaks of varying width. As explained before, the position of those peaks depends on the bond energy and therefore depends on the nature of the bond and on its chemical environment. On the other hand, at relatively low concentration, the intensity (I) of a peak at a given wave number can be used to calculate the concentration of the molecule responsible for the peak using the Beer Lambert law:

$$I = I_0 e^{-\epsilon\, l\, C} \tag{1.7}$$

where I_0 is the initial intensity (before the sample), l is the light path-length in the sample, C is the concentration of the molecule responsible for the signal and ϵ is the wavelength dependent molar absorptivity coefficient. The coefficient ϵ needs to be calculated from the spectra of the molecule at known concentrations. Generally the computer connected to the spectrometer transforms the intensities values in absorbance, (A), which is defined from

$$A = -\ln \frac{I}{I_0} \tag{1.8}$$

The absorbance is therefore directly proportional to the concentration, C, and according to the Beer-Lambert law,

$$A = \epsilon\, l\, C\cdot \tag{1.9}$$

To minimize the interference of the background noise, and thus improve accuracy, one can sum up the absorbances for the entire width of the peak. In such case the

Beer-Lambert law would be written as:

$$\int_{\bar{\nu}_1}^{\bar{\nu}_2} A\, d\nu = \int_{\bar{\nu}_1}^{\bar{\nu}_2} \epsilon\, l\, C\, d\nu = l\, C \int_{\bar{\nu}_1}^{\bar{\nu}_2} \epsilon\, d\nu \tag{1.10}$$

where ν_1 and ν_2 are the wavenumbers for which the peak begins and ends.

This spectroscopic technique can be used in supercritical fluids and it has been used successfully in the past few years to study hydrogen bonding in CO_2.[37–40] I used FT-IR to understand crown ether-water and TBP-water interactions in super- and subcritical CO_2. Because FT-IR actually measures the bond energy between atoms and molecules, it provides structural information and good understanding of how the species are bonded in a solution. Furthermore, there are vast databases of spectra available which is helpful for the recognition of most of the bonds in very different molecules. The main problem with FT-IR is its low accuracy for quantitative measurements. The spectral peaks are generally broad and the determination of the intensities generally lacks precision. FT-IR can be easily overloaded with a system that contains too many different species causing the overlapping of peaks. In such cases the intensity and therefore the concentration determination will be even less accurate. Nevertheless, with a system kept as simple as possible and with the use of innovative techniques to avoid overlapping, as I did with substituting deuterium for hydrogen, FT-IR can be used effectively for quantitative analysis. Moreover, with the use of a specially designed high pressure cell, it can be easily used for measurement in supercritical fluids.

In this section, I will present the experimental setup and a summary of the results that are detailed in the paper "An FT-IR study of crown ether-water complexation in supercritical CO_2," which I published with other colleagues. This paper is reproduced here as appendix F. Generalization and more details beyond the published work will be presented.

1.1.1 Experimental Work

Chemicals.

D_2O (100% D, 99.96% pure), 18-Crown-6 (99.5% pure), dicyclohexano-18-crown-6 (98% pure), methanol-d (99.5+ atom % D) and carbon tetrachloride (99.9% pure) were purchased from Aldrich Chemicals Company and used without further purification. Carbon dioxide was obtained as Supercritical Fluid Chromatography (SFC) grade (purity $\geq$ 99.99%) from Scott Specialty Gases Inc.

Experimental Setup.

The experimental setup is shown in Figure (1.4). It consists of a syringe pump (ISCO, model 100DX) that pressurizes, regulates and delivers CO_2 to a specially designed high pressure cell. A detailed description of the high pressure cell will be presented later. The pressure is measured with an electronic transducer (Precise Sensor Inc., model D451-10) with a $\pm$ 0.1 MPa accuracy. To avoid any incident caused by over pressurization, a rupture disc was installed on the line between the cell and the syringe pump. The cell is heated with four electric cartridge heaters and the temperature is monitored by a controller (Watlow company) with a $\pm$ 1 °C accuracy. For safety reasons, the controller was set up to shut down the heater if the temperature exceeds 80 °C. The different solutions inside the cell were analyzed using a Bruker IFS 66V FT-IR spectrometer with a Mercury-Cadmium-Telluride (MCT) detector (Kolmar Technologies). A 5 min acquisition time and an 80 kHz scanner velocity for a 4 cm^{-1} wavenumber resolution were used to optimize the spectrum quality and signal-to-noise ratio. Spectrum analysis and corrections, including curve fitting and spectrum subtraction, were performed with the OPUS (Bruker Optics) software. At the end of each experiment, the solutions were released to a hood.

The stainless steel cell is rated up to 50 MPa and has an internal volume of 9.2 mL. It has an observation window made of sapphire which allows visual determination of the number of phases present inside the cell. This kind of information is important for

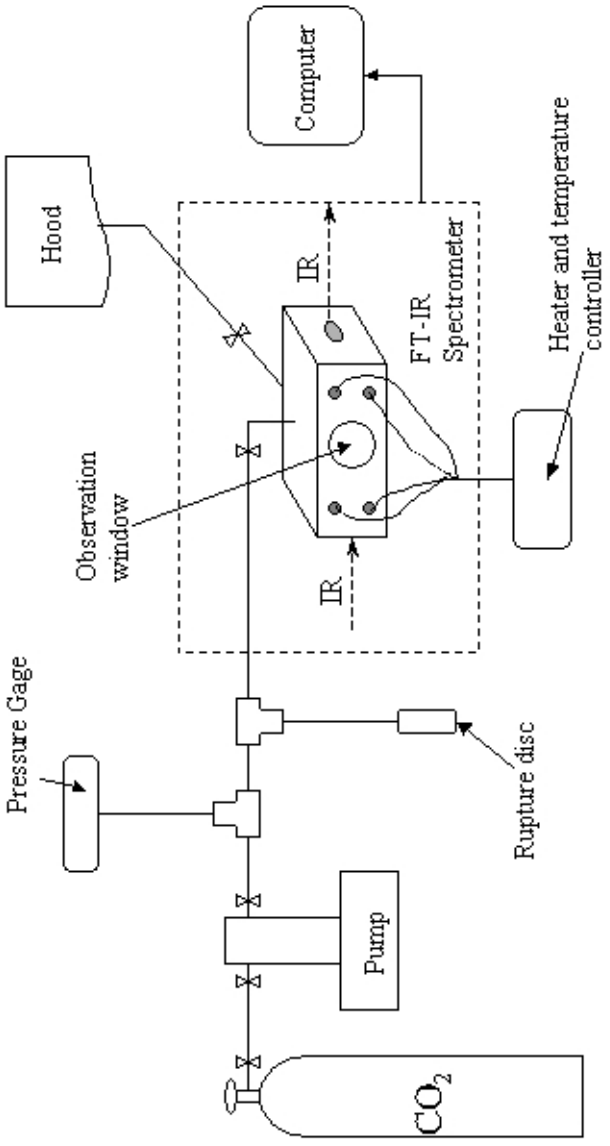

Figure 1.4: Fourier Transform Infra-Red (FT-IR) experimental setup.

quantitative analysis, as some water droplets can potentially form in the path of the beam, which would alter the measured spectral data. The infrared beam is focused along two conical holes and passes through two small diamond windows providing a path-length of 100 μm. The stirring of the solution during the whole experiment was done using a Teflon-coated magnetic stirring bar.

Water contamination from the atmosphere or from previous cleaning can change equilibrium parameters and lead to erroneous results. Such contamination of the cell and its content must be avoided. Thus, for each experiment, the cell was purged with nitrogen, and chemicals were introduced to the cell under a glove box. The cell was then connected to the line and the CO_2 was introduced. The solutions were stirred for 20 to 30 minutes to reach equilibrium after each change of experimental conditions such as chemicals, concentration of species, pressure, and temperature. Longer experimental times were tested without any significant change in the IR spectra.

Heavy water (D_2O) was used instead of H_2O to avoid the overlapping of water peaks and strong CO_2 absorption bands between the wave numbers of 3500 and 3800 cm^{-1}. The pure CO_2 density was varied from 660 to 1040 $g{\cdot}L^{-1}$ by adjusting the temperature between 25 and 70 °C and the pressure between 20 and 40 MPa. The pure CO_2 density was determined using a reported table from the National Institute of Standards and Technology (NIST) Chemistry WebBook.[56]

It is important to contain the chemicals inside the cell to maintain accuracy for quantitative analysis and to avoid any back flow to the pump. Therefore, any decrease in density was prevented in successive experiments that did not require new chemicals but simply required increasing pressure and/or decreasing temperature. After each set of experiments, the cell was cleaned several times with CO_2 and acetone and dried using nitrogen. A blank spectrum was taken to be certain that there is no contamination. It was also used to subtract the empty cell spectrum, including the signal from the diamond windows, from the spectrum of each sample. Another background correction was performed because of the overlapping of weak 18-crown-6 bands (C-H

stretch) and D_2O bands. The spectrum of pure 18-crown-6 at the same pressure and temperature as the sample was also subtracted.

To study the nature of crown-water hydrogen bonding in liquid and supercritical CO_2, a series of mixtures composed of a fixed D_2O concentration (0.049 mol·L^{-1}) and variable 18-crown-6 concentrations (up to 0.25 mol·L^{-1}) were introduced in the cell with a syringe before the CO_2 was added.

1.1.2 Summary of the Results

FT-IR spectroscopy was used as an analytical method for the understanding of crown ethers-water interaction. The chosen crown ether for this study was 18-Crown-6 and D_2O was used instead of water to avoid overlapping of CO_2 intense signal and water peaks in the wave number range between 3500 and 3800 cm^{-1}.

Three types of bonding were observed between the crown ether and the water. The first one (Figure 1.5(c)) can only be observed at high crown to D_2O concentration ratio. The configuration is a "sandwich" formed with two 18-crown-6 molecules surrounding one water molecule. The sandwich configuration is one possible configuration among many, examples of other configurations being the "offset" or the "perpendicular." This configuration is characterized by a broad peak at 2590 cm^{-1}. At low crown to D_2O concentration ratio, a water molecule can bond with a crown ether molecule in two different ways. The first type is a bridge configuration (Figure 1.5(a)) formed by hydrogen bonds between D_2O and two oxygen atoms that belong to the crown cavity. The bonds involved in this configuration have the same nature as the one in the sandwich configuration, thus their respective FT-IR peaks are overlapping. The second type is a single configuration (Figure 1.5(b)) where D_2O makes a single hydrogen bond with an oxygen atom belonging to the crown ether cavity. It is characterized by two peaks at 2679 and 2733 cm^{-1} assigned respectively to the hydrogen-bonded O–D stretching and the unbonded O–D stretching.

The equilibrium constants of formation, K_s and K_b for the single and the bridge

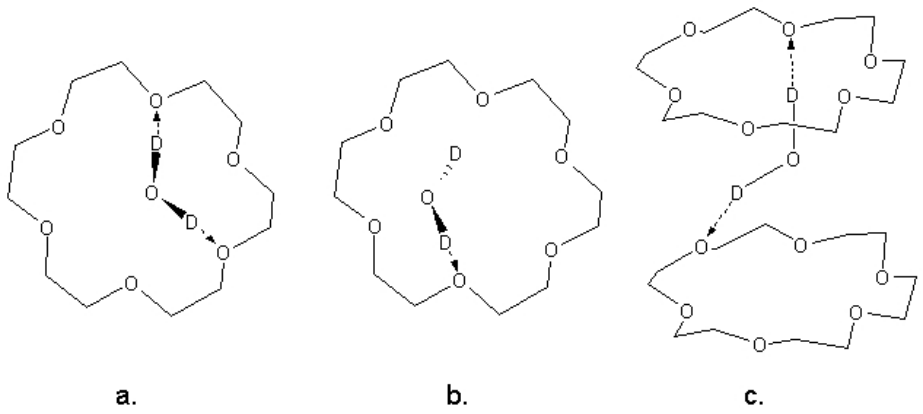

Figure 1.5: Molecular structure of the water-crown ether interaction in the bridge form (a), the single configuration (b) and the sandwich form (c).

configurations, were calculated with the CO_2 density increased at several step from 850 to 960 g·L^{-1}. For the single configuration, K_s was found to vary between 16 ± 4 and 9 ± 2 L·mol^{-1}. For the bridge configuration K_b was found to vary between 10 ± 3 and 5 ± 2 L·mol^{-1} in the range of CO_2 densities considered. Different equilibrium constant measurements at constant pressure and variable temperature allow the calculation of the enthalpy of the hydrogen bond for the two complexes. Their values were calculated to be -12 ± 2 kJ·mol^{-1} for the single complex, and -38 ± 3 kJ·mol^{-1} for the bridge one. These values are in agreement with hydrogen bond enthalpy values found in the literature for other solvents.[57]

1.1.3 Additional Description

The equilibrium parameters of crown ether-water interaction in supercritical CO_2 found by FT-IR need to be compared with the equilibrium parameters in solvents analyzed by NMR. The later is described in section 1.2. NMR is an analytical technique that does not allow the differentiation of the two configurations being bridge or single. Thus, the equilibrium parameters of both the single and the bridge configurations need to be calculated from the FT-IR study in supercritical fluids. For this purpose, the equilibrium is described next in the section covering the theoretical

analysis.

Theoretical Calculations

The equilibrium relation is given as

$$2\ 18C6 + 2\ D_2O \rightleftharpoons 18C6{\cdot}D_2O^{\text{single}} + 18C6{\cdot}D_2O^{\text{bridge}} \tag{1.11}$$

From this equilibrium, the constant K can be defined as

$$K = \frac{[18C6{\cdot}D_2O^{\text{single}}][18C6{\cdot}D_2O^{\text{bridge}}]}{[D_2O]^2[18C6]^2} = K_s \cdot K_b \tag{1.12}$$

where

$$K_s = \frac{[18C6{\cdot}D_2O^{\text{single}}]}{[D_2O][18C6]} \qquad \text{and} \qquad K_b = \frac{[18C6{\cdot}D_2O^{\text{bridge}}]}{[D_2O][18C6]} \tag{1.13}$$

and the molar fraction, k, of crown ether bonded to water is given as

$$k = \frac{[18C6{\cdot}D_2O^{\text{single}}] + [18C6{\cdot}D_2O^{\text{bridge}}]}{[18C6{\cdot}D_2O^{\text{single}}] + [18C6{\cdot}D_2O^{\text{bridge}}] + [18C6]}. \tag{1.14}$$

The molar enthalpy (ΔH) of the hydrogen bond, at constant pressure can be determined from the equilibrium constant (equation 1.12) using the well-known thermodynamic relations (equation 1.15, 1.16 and 1.17):

$$\left(\frac{\partial \Delta G}{\partial T}\right)_P = -\Delta S = \frac{\Delta G - \Delta H}{T}, \tag{1.15}$$

$$\Delta G^0 = -RT \ln K, \tag{1.16}$$

and

$$\left(\frac{\partial \ln K}{\partial (1/T)}\right)_P = -\frac{\Delta H}{R}, \tag{1.17}$$

where T is the absolute temperature in K, ΔS is the entropy in $J{\cdot}mol^{-1}{\cdot}K^{-1}$, ΔG is the Gibbs free energy in $J{\cdot}mol^{-1}$, and R is the molar gas constant in $J{\cdot}K^{-1}{\cdot}mol^{-1}$.

Table 1.1: Equilibrium parameters for water-crown-ether interaction in supercritical fluids.

Pressure MPa	temp °C	density g.cm^{-3}	$K = K_s \times K_b$ L^2·mol^{-2}	k %	$[D_2O]$ mol·L^{-1}
20.2	60	0.724	34	33	0.035
20.2	50	0.784	62	35	0.034
20.2	40	0.840	161	45	0.031
20.1	35	0.866	108	40	0.032
20.0	33	0.876	174	45	0.030
20.0	31	0.886	242	47	0.029
20.0	25	0.913	298	54	0.028
20.2	40	0.840	161	45	0.031
30.3	40	0.910	53	34	0.035
35.4	40	0.935	61	35	0.034
40.5	40	0.956	64	35	0.034
40.5	25	1.004	178	44	0.030

Typical Statistical errors are: Pressure ± 0.1 MPa, Temperature ± 1 °C, K± 10% and k± 10%

Results and Discussion

The variation of the constant of formation, K, and the molar fraction of crown ether bonded to water, k, with pressure and temperature are shown in Table 1.1. The constant of formation K varies from 34 ± 4 to 300 ± 30 L^2·mol^{-2} when the temperature decreases from 60 to 25 °C at constant pressure (of ∼20 MPa). At constant temperature (40 °C), K tends to decrease with pressure increase (from 20 to 40 MPa).

The same trend is observed for the molar fraction k of crown ether bonded to water. Figure 1.6 shows this trend at constant pressure (20 MPa). When the density increases (i.e. the temperature decreases) the value of k increases from 33 ± 4% to 54 ± 6%. Therefore, there is more water molecules bonded to the crown at low temperature or at high density for a constant pressure of 20 MPa.

The variations of k at constant temperature (40 °C) versus density is shown in

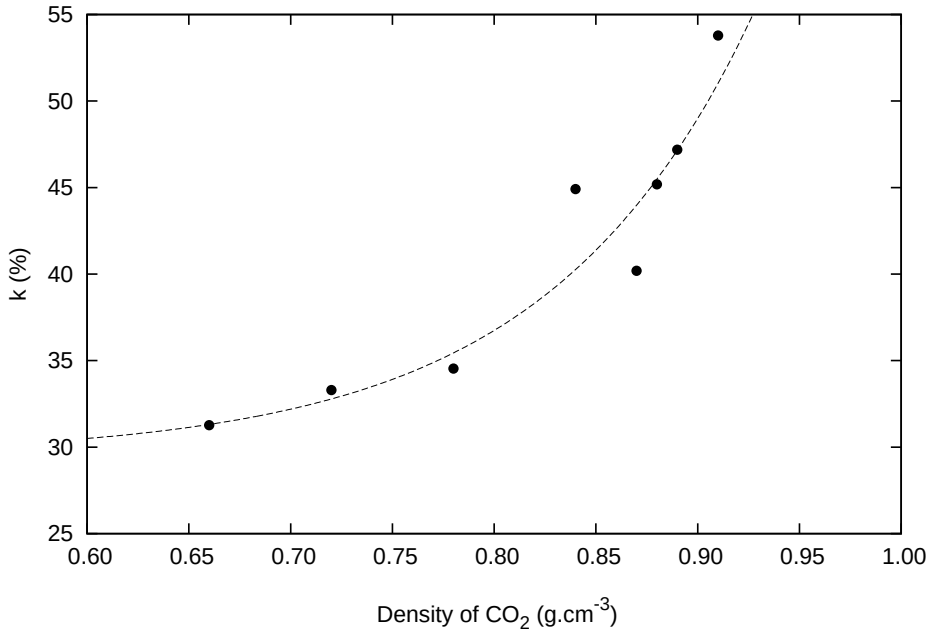

Figure 1.6: Molar fraction of crown ether bonded to water k versus density at constant pressure (20 MPa). Lines are guides for the eyes and do not have any theoretical or analytical value.

Figure 1.7. When the density increases (i.e. pressure increases), the value of k decreases rapidly at first and then reaches a plateau at approximately 35% when the density exceeds 900 g·L^{-1}. At lower pressure values, there is more water bonded to the crown ether. However, pressure does not appear to influence the amount of bonded water for pressures higher than 30 MPa.

Equation 1.17 shows that the plot of $\ln K$ versus $1/T$ at constant temperature (Figure 1.8) can give the value of the molar enthalpy, ΔH, of the hydrogen bond between water and 18C6. To demonstrate this, linear regression of the plotted data is needed and the resulting slope multiplied by the inverse of the molar gas constant (R = 8.3144 J·K^{-1}·mol^{-1}) gives directly the value of ΔH. At 20 MPa, ΔH was found equal to -51 ± 6 kJ·mol^{-1}.

Consequently, the complexation process is exothermic and since the species are more entropically ordered it explains the decrease of the K values with the increase of temperature. In other respects, it is important to remember that for this calculation

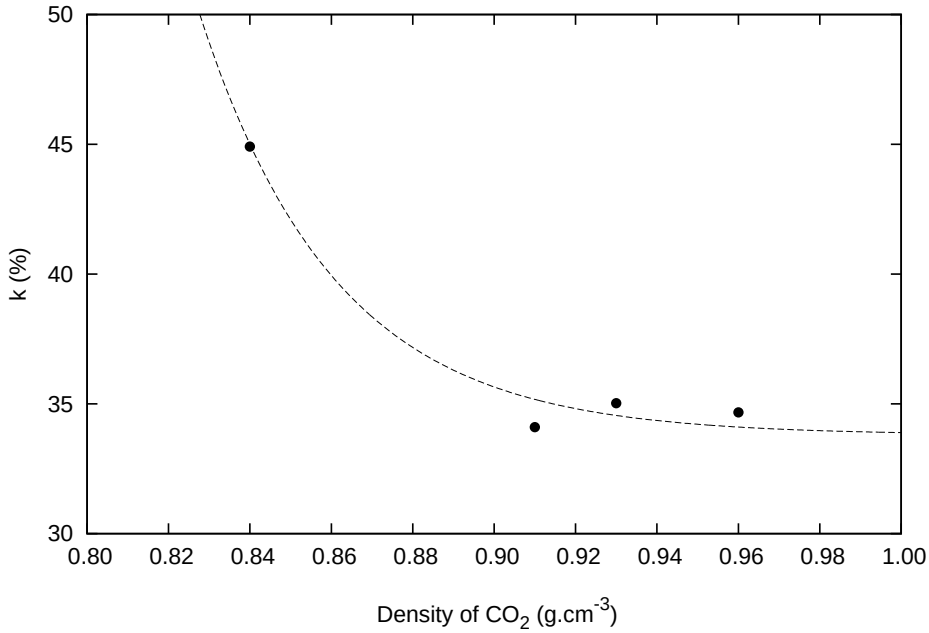

Figure 1.7: Molar fraction of crown ether bonded to water k versus density at constant temperature (40 °C). Lines are guides for the eyes and do not have any theoretical or analytical value.

I needed to assume that ΔH is independent of density. This result is in accordance with the values for hydrogen bonding in the literature.[57]

Figure 1.9 shows the dependence of $[D_2O]$ on the global equilibrium constant K. The amount of free water in CO_2 decreases when K increases. This dependence appears to be linear simply because the range of the water concentration data is too narrow to clearly display any curvature as expected from equation 1.12.

Conclusion

This section was devoted to the study of water-crown ether interaction in sub- and supercritical CO_2 using FT-IR. This analytical technique allows us to see the different configurations, including bridge, single, and sandwich forms between water and crown ethers. The equilibrium constant, the molar fraction of crown ether bonded to water, and the amount of free water were determined for the bridge and single configurations at different pressures and temperatures. From these data, the enthalpy of the hydro-

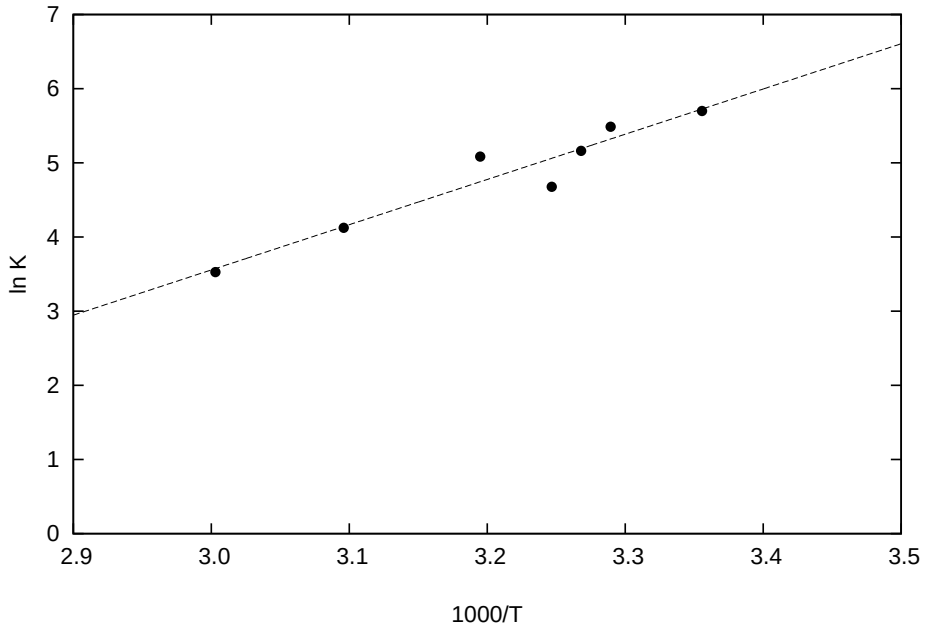

Figure 1.8: Dependence of $\ln K$ on 1000/T at 20 MPa.

gen bond was found to be -12 ± 2 kJ·mol^{-1} and -38 ± 3 kJ·mol^{-1} for the single and the bridge configurations respectively. These results correspond to a total enthalpy of -51 kJ·mol^{-1}for the two hydrogen bond configurations as found in the global study that lumps together the equilibra of the bridge and the single configuration in one equilibrium. This last group of results will be compared in the next section, section 1.2.3, to the one in organic solvent using NMR (Nuclear Magnetic Resonance) as a method of analysis.

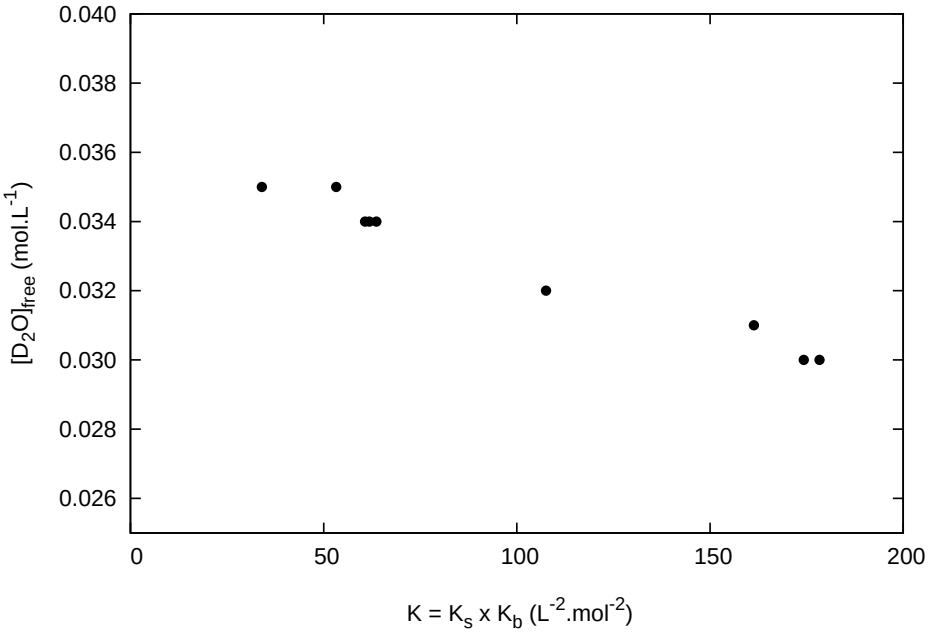

Figure 1.9: Dependence of free water $[D_2O]$ on the equilibrium constant K.

1.2 Crown Ether-Water Interaction in Solvents

Introduction

The main objective of the work describe in this section is to understand the role of the solvent in the interaction between water and crown ethers. This interaction will be compared to the one in supercritical CO_2 described in the previous section. The description of this interaction will lead to a better understanding of cesium extraction using crown ethers. This interaction was studied with Nuclear Magnetic Resonance (NMR) spectroscopy. I will therefore describe this analytical tool before discussing the water-crown ether interaction in more detail.

The history of NMR started in the late thirties with the discovery by Rabi of the magnetic moment. In 1946, two different research groups observed for the first time an NMR signal. Bloch, Hanse, and Packard from Stanford University detected the signal ^{1}H of water; while Purcell, Torrey, and Pound from Harvard University detected it in paraffin wax. Bloch and Purcell shared the Nobel prize of Physics in 1952 for this discovery. Since then, numerous improvements have been made and NMR is nowadays the most important and most used technique to determine chemical structures or to perform Magnetic Resonance Imaging (MRI).

Basically, the NMR spectroscopic technique is based on measuring the absorption of Radio Frequency (RF) radiation from the nucleus in a strong magnetic field. After the absorption of the radiation, the spin of the nucleus will go to its highest energy state. Thereafter, the nucleus will return to its initial state by emitting RF radiation, which is recorded versus time for the spectrum.

The principle of the NMR operation is described in more details as follows. The nucleus of some atoms has an angular moment $\vec{M}$; these nuclei are therefore similar to an electric charge in rotation. As a result, the nucleus has a nuclear magnetic moment $\vec{\mu}$ that is directly proportional to the angular moment. The constant of proportionality, γ, is called magnetogyric ratio and it is a characteristic of each particular

nucleus. When a nucleus with a magnetic moment is placed in a magnetic field $\vec{H_0}$, it gains an excess of potential energy, E_s, where

$$E_s = -\vec{\mu} \cdot \vec{H_0} = -\gamma \vec{M} \cdot \vec{H_0} \tag{1.18}$$

The projection of $\vec{M}$ over $\vec{H_0}$ is quantified in the sense that it can only take integral or half integral multiples of $\hbar$, which is the Plank constant ($h = 6.6261 \times 10^{-34} J \cdot s$) divided by 2π. Hence, this projection, M_z, can take 2I+1 values:

$$M_z \in \{I\hbar, (I-1)\hbar, \ldots, (1-I)\hbar, -\hbar\} \tag{1.19}$$

where I is the nuclear spin quantum number. The spin quantum number, I, can take different values ($0, 1/2, 1, 3/2, 2 \ldots$, cf. Table 1.2) depending on the nucleus.

Table 1.2: Values of I, the quantum spin number, for different nucleus.

^{1}H	^{2}H	^{12}C	^{13}C	^{14}N	^{15}N	^{19}F	^{31}P	^{16}O	^{17}O	^{133}Cs	^{137}Cs
1/2	1	0	1/2	1	1/2	1/2	1/2	0	5/2	7/2	7/2

Nuclei with a nuclear spin quantum number equal to zero do not have a nuclear magnetic moment and therefore can not be seen by NMR. The analysis of the spin state $I = 1/2$ is very straightforward because of its spherical charge distribution with no electric quadrupole moment. This is why NMR is intensively used to analyze hydrogen nuclei and, to less extent, carbon 13, fluorine 19 and phosphorous 31 nuclei. Therefore, for the rest of this presentation, I will consider only the properties of the $I = 1/2$ spin state.

According to equations 1.18 and 1.19, with a spin state of I=1/2, $M_z = 1/2\hbar$ or $-1/2\hbar$ and $E_s = -1/2\hbar\gamma H_0$ or $+1/2\hbar\gamma H_0$. Therefore, a nucleus which has a potential energy E in the absence of magnetic field, will have two different possible energies when placed in a magnetic field $\vec{H_0}$ (Figure 1.10. The difference between these two energies ΔE is equal to $\gamma\hbar H_0$.

The number of nuclei in each energy state follows the Boltzmann relation:

$$\frac{n_2}{n_1} = e^{-\Delta E/k_B T} = e^{-\gamma\hbar H_0/k_B T} \tag{1.20}$$

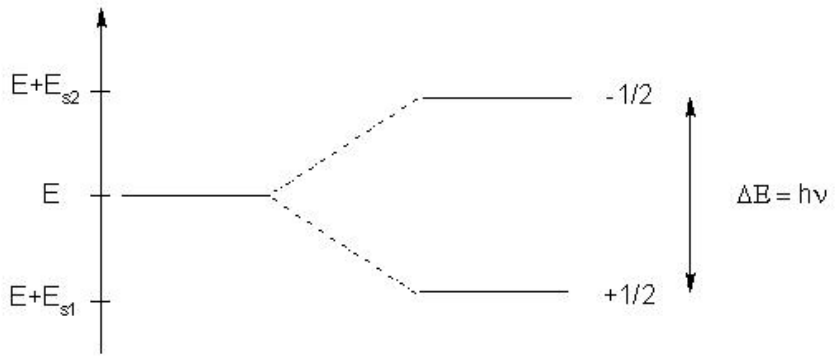

Figure 1.10: Potential energy of a nucleus with a spin state I=1/2 outside and inside a magnetic field.

where n_1 and n_2 are the number of nuclei in the state $E_1 = E + E_{s1}$ and $E_2 = E + E_{s2}$, k_B is the constant of Boltzmann ($k_B = 1.38066 \times 10^{-23} J \cdot K^{-1}$) and T is the temperature in K. Consequently more nuclei are in the state E_1 than in the state E_2. However nuclei can transit from state E_1 to E_2 under an adequate electromagnetic field. The frequency of this electromagnetic wave follows the Einstein equation,

$$h\nu = \Delta E = \gamma \hbar H_0 \tag{1.21}$$

which leads to defining the frequency

$$\nu = \frac{\gamma H_0}{2\pi} \tag{1.22}$$

which is generally in the radio frequency wavelength, i.e. from 20 to 900 MHz, for a magnetic field strength between 1 and 20 Tesla. For comparison, the earth magnetic field is approximately 10^{-4} T and the energy of a IR transition is a thousand times greater whereas the one of an electronic transition is nearly one million times greater.

NMR is a sensitive and non destructive analytical method but it has drawbacks. The equipment is very expensive because it needs to be able to observe a very little change in frequency or energy, and at the same time, it needs to be capable of producing a very strong magnetic field. A typical NMR experiment setup is represented as a simplified diagram in Figure 1.11. During the NMR experiment, represented in figure 1.12, the sample is placed in a tunable magnetic field and irradiated with RF

waves from a transmitter. The wave frequency is maxed out for the proton NMR (i.e. it is chosen close to 500 MHz when a 500 MHz spectrometer is used and close to 300 MHz with a 300 MHz spectrometer). The time during which the sample is irradiated is called pulse-width and lasts 1 to 30 μs depending on the system studied. The pulse-width can also be given in degrees which correspond to the angle that the spin has with the z-axes at the end of the pulse. During irradiation, waves having the same energy as the energy difference between the spin states of the nuclei are absorbed in the sample. This matching of energies (frequencies) is called the resonance. When the nuclei in the sample returns to its normal state, RF waves are emitted and acquired by the receiver. Wave intensities are then recorded as a function of time and the resulting graph is called the Free Induction Decay (FID). Acquisition lasts for several seconds and the process is performed several times to reduce the signal to noise ratio. In between pulses, the sample has to go back to equilibrium (relaxation) to avoid the overlapping of the signals, this is the relaxation delay that takes 5 to 20 seconds, depending on the sample. Therefore, the time between scans is equal to the pulse-width (which is relatively small and can be ignored) plus the acquisition time plus the relaxation delay. After the last scan, the FID is finally Fourier transformed to obtain the spectra of the intensities versus frequencies.

Proton NMR (PNMR) is the most commonly used NMR spectroscopy because of the abundance of hydrogen in organic molecules and because of the simplicity of its spectral interpretation. Each peak in such spectra offers three characteristics: location, intensity, and coupling.

First, the location of a peak is defined as the frequency at which the proton enters in resonance. This property depends on the electron(s) surrounding the nucleus. Electrons are responsible for bonds between atoms and as charged particles they are responsive to the external magnetic field. When electrons are put in a magnetic field H_0, they would move to compensate for the effect of H_0 and therefore shield the nucleus that will enter in resonance at a higher frequency. As a consequence, one can

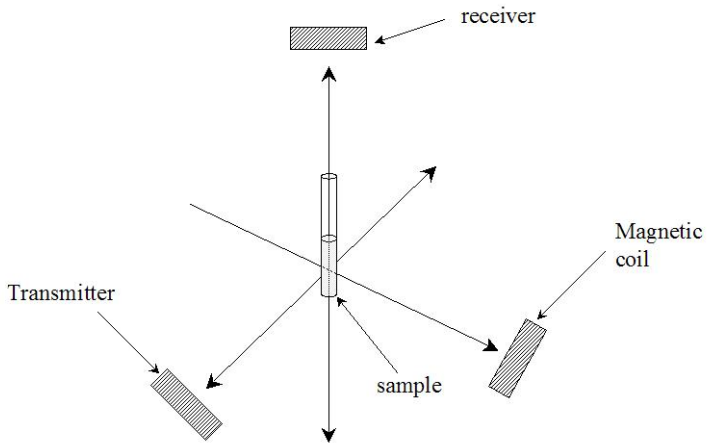

Figure 1.11: Nuclear magnetic resonance experiment.[4]

have an idea of the surrounding of the atom observed depending on the location of a peak. The downside is that this location will differ from one spectrometer to another, indeed the location of a peak is dependent on both the RF and the strength of the magnetic field and the later can not be standardized due to magnet differences. To go around this problem, most scientist use as a reference a compound that is chemically nonreactive, gives a single sharp peak, and does not interfere with the resonances of the species in the sample studied. The compound that meets all these specifications is TetraMethylSilane, $(CH_3)_4Si$ or TMS. The frequency of a peak, δ, is called a chemical shift (from that of the TMS, taken as a reference). Nevertheless, there is another problem with the spacing between the peaks being still not standardized. The way to solve his problem is to divide the frequency observed of the peak by the frequency of the spectrometer (i.e. 100 or 500 MHz). Since the number obtained is very small (Hz divided by MHz), the result is multiplied by one million and the part per million unit (ppm)is used.

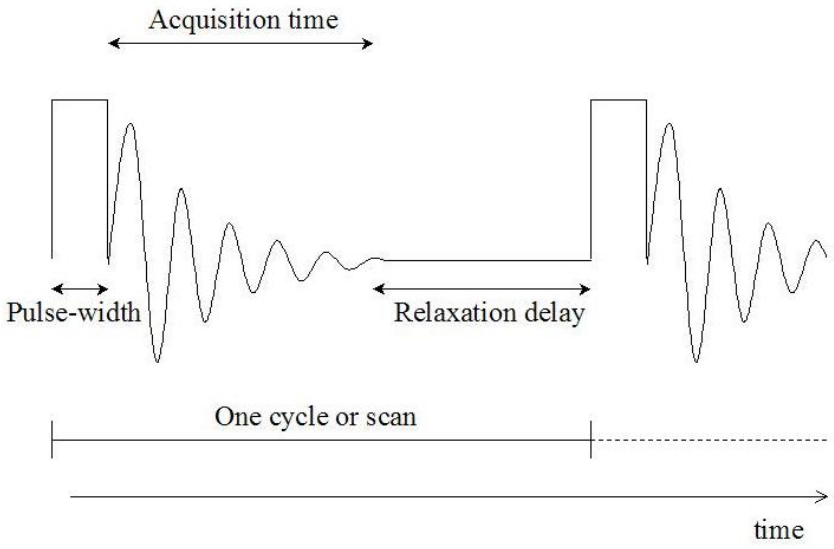

Figure 1.12: Acquisition sequence for a nuclear magnetic resonance experiment.

The second characteristic of a PNMR spectrum is intensity. The intensity of a peak for a nucleus type is directly proportional to the number of nuclei having exactly the same electronic surroundings. These nuclei are called isochronous because they show at the same chemical shift. For example, the peak of the three protons of a methyl group will show at the same chemical shift, and the peak will have an intensity three times greater than the one of an alcohol group.

Coupling is the third major property of a PNMR spectrum. When different sets of hydrogen atoms are close together in a molecule (i.e. when there is generally three bonds or less in between them), there is a spin-spin interaction and their nuclei are coupled. For example, the spectrum of ethanal (CH_3CHO, Figure 1.13) can be looked at . In this molecule, a proton from the methyl can "see" the proton from the aldehyde group, they are coupled. Therefore the methyl peak will be split in a doublet. In the same way, the proton from the aldehyde group can "see" the three protons from the methyl group and the proton peak from the aldehyde will split in a quartet (Figure 1.14 a.).

In all cases, the space between the coupled peaks is constant for a given multiplet and it is called coupling constant (J). J is independent of the magnetic field strength, and is the same for both groups of the same spin-spin interaction. Quantitatively, J value is generally between 2 and 10 Hz. In Figure 1.14, the ideal splitting patterns are shown with their intensities. A group will split in a doublet if it "sees" one proton, to a triplet if it "sees" two, in a quartet if it "sees" three, etc. The global intensity is the same as the one you would have with a single peak, but the relative intensity depends on the tree shown in Figure 1.14 b. It happens nevertheless that the chemical shifts are too close to one another and the pattern of the multiplets are distorted.

In this section I will present the experimental setup and a summary of the results that are detailed in the paper "Partition Coefficients and Equilibrium Constants of Crown Ethers between Water and Organic Solvents Determined by Proton Nuclear Magnetic Resonance," which I published with other colleagues. This paper is reproduced as appendix G. At last, I will compare the results from this section to the one using FT-IR in solvents.

1.2.1 Experimental Section

All chemicals were purchased from Aldrich Chemical Company and used without further purification. Chloroform was used in its deuterated form (99.5% $CDCl_3$) and the water phase contains 5% D_2O by volume.

The crown ethers were diluted in the $CDCl_3$ + CCl_4 mixtures with a concentration range of 0.02 to 0.2 mol·L^{-1}. These solutions were subsequently mixed with an equal volume of the D_2O-enriched water and the equilibrium was reached by shaking the two phases with a wrist-type shaker for 2 hours or more. The studies involving 15-crown-5, 18-crown-6 and dicyclohexano-18-crown-6 in solvents containing high percentages of CCl_4 required longer shaking time to get consistent data. After the shaking, the mixtures were centrifuged for one hour.

The remaining organic and aqueous phases were then analyzed by proton NMR

using a 500 MHz Bruker DRX500 spectrometer. To obtain quantitative results, 16 scans were taken and for each, the pulse interval was set to 11.3 sec (acquisition time 3.3 sec, relaxation delay 8 sec). The pulse-width was 30 degrees (corresponding to a 2 μs pulse) in all systems (organic, aqueous, with or without chelator agent). Chemical shifts in the organic phase were calibrated by setting the chloroform chemical shift to 7.24 ppm. For the solvent mixtures containing CCl_4, the chloroform resonance peak shifts upfield (lower ppm) as CCl_4 was added. The shift was measured by turning off the field lock; this operation allows the comparison of the solvent mixtures at constant field. A 0.14 ppm shift was observed when the solvent used is 25% $CHCl_3$ in CCl_4 instead of 100% $CHCl_3$. An upfield correction was then added for all mixed solvent samples run with a $CDCl_3$ field lock. The intensity (based on integrated area calculations for all data) of the water peaks in the Proton-NMR (PNMR) spectra was corrected for the 5% D_2O (by volume) present in the water phase. For the 100% CCl_4 mixture, an insert filled up with benzene-d6 has been used as a reference for the intensity and the chemical shift, which was set at 7.15 ppm.

Typical PNMR spectra for 18-crown-6 in the $CDCl_3$ phase are shown in Figure 1.15. A single resonance peak for the protons belonging to unsubstituted crown ethers is generally observed in the region between 3 and 4 ppm. The free water and the bonded water are in rapid exchange in solution due to the equilibrium. The observed water resonance peak consists then of an average of the resonance of the free water and the bonded water. Thus the resonance peak for the water shifts downfield as the concentration of the bonded water is increased which correspond to an increase in ligand concentration. The concentration of the ligand in the organic phase has been corrected for its solubility in the aqueous phase based on PNMR measurements of its partition between the two phases.

1.2.2 Summary of Results

The influence of solvent on water-crown ethers interaction was studied by NMR in chloroform and carbon tetrachloride mixtures. The two configurations (single or bridge) of 1:1 water-crown ether complex, that have been observed by Moyer et al.[36] in carbon tetrachloride using FTIR, cannot be distinguished by NMR analysis. Therefore only one complex, taking in account the two configurations, is used for the different calculations. The analysis of the data shows that water and crown ether form a 1:1 complex in rapid exchange with uncomplexed ligand and water. The crown ether concentrations used for this study are small enough to avoid the formation of a 1:2 complex or "sandwich" between one water and two crown ether molecules.

Different constants were determined in the course of this study. First the partition coefficient (D) for crown ether between the two phases was found to depend strongly on the solvent. Its value for 18-crown-6 varies from 0.25 ± 0.02 in a 100% $CDCl_3$ solution to 48 ± 3 in a 100% $CCl_4$3. Otherwise, D stays in the same order of magnitude for different crown ethers soluble in water. Second, the equilibrium constant (K) and the molar fraction (k) of crown ether complexed with water were measured. They were found to depend strongly on the cavity size. For example, k varies from $15 \pm 1\%$ for 12-crown-4 to $97 \pm 5\%$ for 18-crown-6 in chloroform. Moreover, the molar fraction k is reduced to 70% for DC18C6 in 100% $CDCl_3$ which shows the effect of a substituant like the cyclohexane. In the other hand, the molar fraction k varies from $97 \pm 5\%$ in 100% $CDCl_3$ to $61 \pm 3\%$ in 25% $CDCl_3$ in CCl_4 for 18-crown-6 which shows that k is also affected by the solvent used. Last, the chemical shifts of free and complexed water in the organic phase were determined for each solvent mixture and each crown ether.

1.2.3 Comparison to FT-IR Results in CO_2

Beside the difference in solvent and in the spectroscopic tool used, there is a third difference between the two experiments. In the first experiment (using FT-IR in CO_2)

the total amount of water in the organic phase is constant and completely dissolved in the organic phase. In the second experiment (using NMR in solvents), the amount of free water is constant, but the total amount of water is not constant, as there is a reservoir of water allowing water to go in the organic phase to be bonded to crown ether when the crown ether concentration increases. Therefore, the partition coefficient of water between the organic and the water phase was not determined in the first experiment. The only data that I can compare is the equilibrium constant (K) and the molar fraction of ligand complexed to water (k). In an effort to clarify this distinction in the rest of this section, these constants will be respectively called K_1 and k_1 for the first experiment using FT-IR in CO_2 and K_2 and k_2 for the second experiment using PNMR in solvents. The values of theses constants are detailed in Table 1.3.

Table 1.3: Comparison of the values of the equilibrium constants K_1 and K_2 and of the molar fractions of ligand complexed to water k_1 and k_2.

CO_2					$CDCl_3/CCl_4$ mixtures		
Pressure MPa	Temperature °C	Density $g{\cdot}L^{-1}$	K_1 $L^2{\cdot}mol^{-2}$	k_1 %	$CDCl_3$ % /vol	K_2 $L{\cdot}mol^{-1}$	k_2 %
20.2	60	724	34	33	25	141	61
20.2	40	840	161	45	50	97	63
20.0	25	913	298	54	75	102	79
20.2	40	840	161	45	50	97	63
40.5	40	956	64	35	100	545	97

In CO_2, at constant pressure, the values of K_1 and k_1 decrease with an increase in temperature and their values decrease as well at constant temperature with an increase in pressure. Whereas in $CDCl_3$ and CCl_4 mixtures the values of K_2 and k_2 decreases as the percentage of $CDCl_3$ in CCl_4 decreases. Therefore, at high pressure and temperature, regarding the equilibrium constants and the molar fraction of ligand bonded to the water, CO_2 behave more like CCl_4 which is a nonpolar solvent (its

dielectric constant $\epsilon = 2.24$ and its electric dipole moment in the gas phase μ is equal to zero[58]). On the other hand, when the temperature and pressure of CO_2 decreases its properties are closer to the one of $CDCl_3$ which is a polar solvent ($CHCl_3$ dielectric constant $\epsilon = 4.81$ and $CHCl_3$ electric dipole moment in the gas phase $\mu = 1.01$ D,[58] the isotopic effect is weak for these properties and their values should be closed to the one of $CDCl_3$).

The amount of free water in solvents can be compared to the one in CO_2. Numerous published studies have recorded the solubility of water in sub and supercritical CO_2.[59,60] Values obtained from Argonne National laboratory in collaboration with Michael J. Chen[61,62] are reproduced in Table 1.4 and are compared with the one from Fulton et al.[59] to the one in different mixtures of CCl_4 and $CDCl_3$. At constant temperature and at increased pressure, $[H_2O]$ increases to reach approximately the value of free water in $CDCl_3$ when the density exceeds 0.8 g.cm^{-3}. When the density is fixed at 900 g·L^{-1}, or the pressure is fixed at 34.5 MPa, the amount of free water increases rapidly when the temperature is increasing. Regarding water solubility, CO_2 behaves like CCl_4 at low pressure and temperature and shifts to a behavior resembling that of $CDCl_3$ when the temperature and/or the pressure increases.

Table 1.4: Comparison of water solubilities in solvents and in CO_2.

CO_2				$CDCl_3/CCl_4$ mixtures	
Pressure MPa	Temperature °C	Density g·L^{-1}	$[D_2O]$ mol·L^{-1}	$CDCl_3$ % /vol	$[H_2O]$ mol·L^{-1}
8.3[a]	35	576	0.032	0	0.00
17.6[a]	35	845	0.067	25	0.011
26.2[a]	35	909	0.074	50	0.017
36.2[a]	50	905	0.122	75	0.037
45.5[a]	65	901	0.183	100	0.060
34.5[b]	50	804	0.137		
34.5[b]	75	896	0.271		

a. Michael J. Chen,[61,62] b. Fulton et al.[59]

Conclusion

This study shows that interaction between water and crown ethers depends strongly on the crown ether used and on the nature of solvents. The main factor of this dependence is the polarity of the solvent. As the polarity increases (decrease of CCl_4 concentration in $CDCl_3$), the molar fraction (k) of crown ether complexed with water increases from 61 to 97% for 18-crown-6. These values can be compared to the ones in supercritical fluids, where regarding the values of k, CO_2 behaves more like $CDCl_3$ at low temperature and low pressure. These tendencies are the same regarding the equilibrium constant K in both systems whereas it is the opposite for the quantity of free water in the oil that is the same as the solubility of water in oil. This value increases with the polarity of the solvent and increases with increasing pressure and temperature. Therefore CO_2 is a tunable solvent that can behave like a polar or non polar solvent depending on the property observed and its pressure, temperature, and density.

These data are important for understanding and improvement of liquid-liquid extraction of metallic ions with crown ethers, where water plays an important role. Section 1.3 will show this importance for cesium extraction.

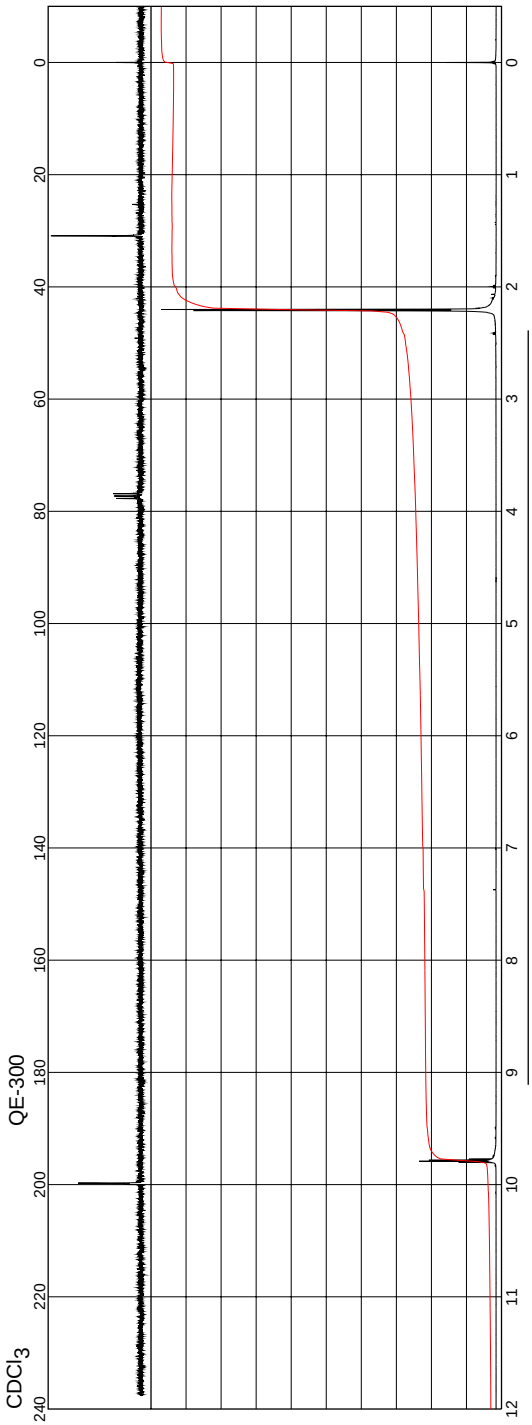

Figure 1.13: P-NMR spectrum of the ethanal molecule (CH_3CHO).[5]

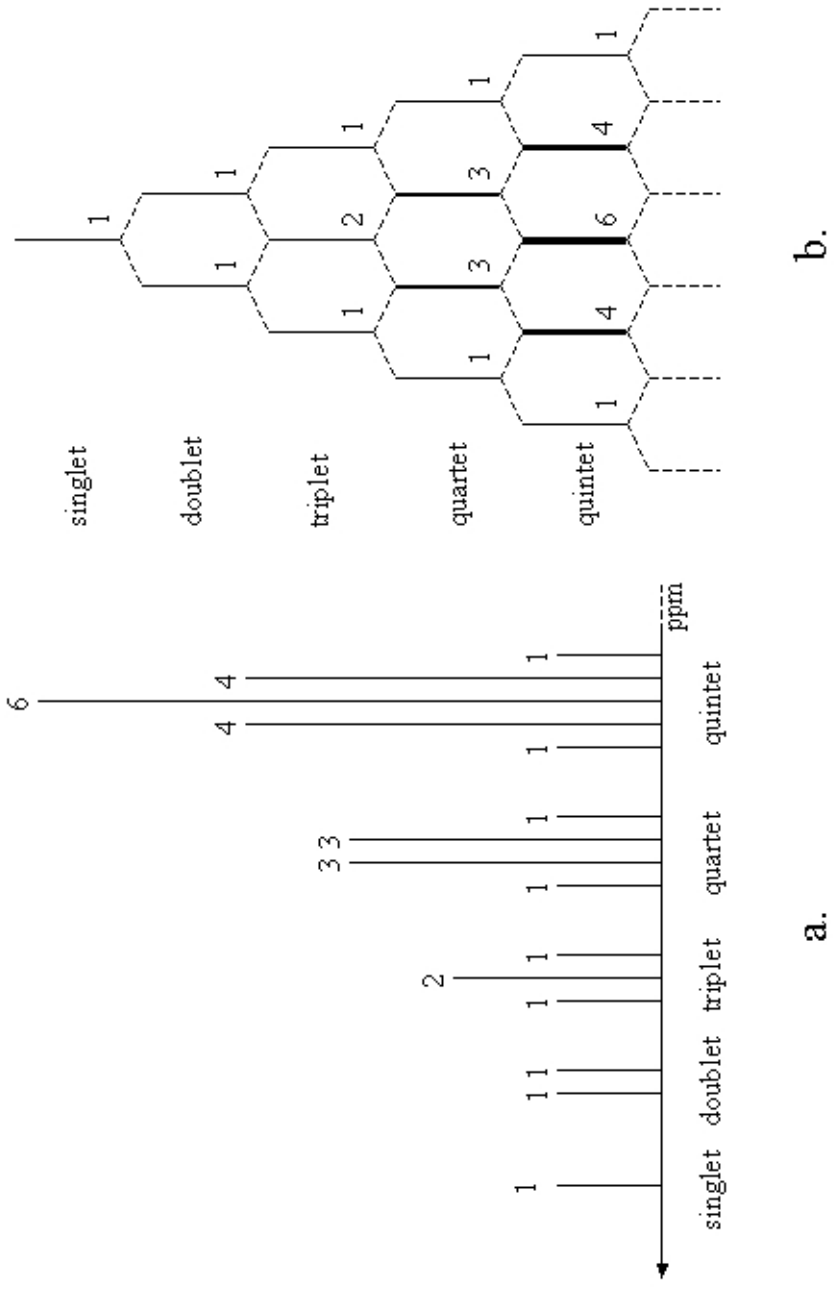

Figure 1.14: coupling due to spin-spin interactions and relative intensities.

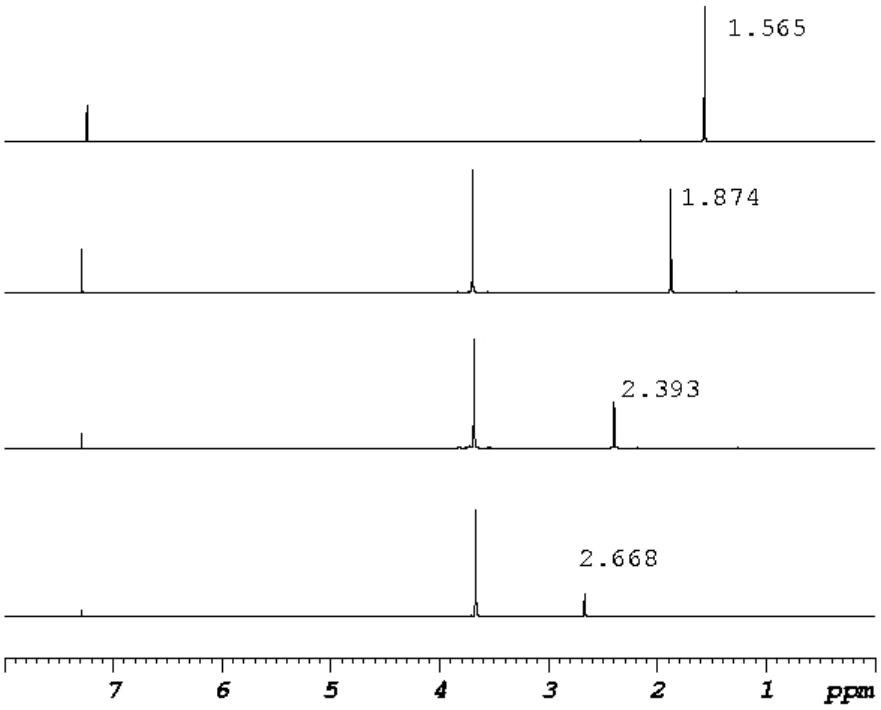

Figure 1.15: Typical PNMR spectra of 18-crown-6 in the $CDCl_3$ phase. The concentrations of 18-crown-6 after equilibrium with water are 0.00, 0.002, 0.075 and 0.153 mol·L^{-1} (from top to bottom) and the water peaks are at 1.565, 1.874, 2.393 and 2.668 ppm, respectively.

1.3 Introduction to Cesium Extraction Equilibrium Using Crown Ethers

Introduction

The purpose of this section is to show the importance of the water in the equilibrium describing the solvent extraction of cesium picrate using Dicyclohexano-18-crown-6 (DCH18C6) as a ligand. This section complements the previous presentation of the interaction between water and crown ethers in various solvents (section 1.2). I must first describe the origin and properties of cesium–137 before venturing into the details of its extraction equilibria.

Cesium–137 (^{137}Cs) is an isotope produced by the fission of uranium-235 which takes place in nuclear reactors or when an atomic bomb is detonated. It is radioactive with a physical half-life of 30.17 years. It can be found in the soil and is metabolized in plants and animals. Its concentration is particularly high in wild animals and in mushrooms because of the specificity of game way of eating and mushrooms accumulation mechanisms. Furthermore, those species are generally found in forests where the soil is protected from rain washing and wind dispersion causing a slow natural decrease in concentration.

Soil contamination is mainly the result of atmospheric nuclear weapon tests and of the Chernobyl reactor accident. The contamination is high in Ukraine and Russia and still a concern in western Europe. ^{137}Cs is dangerous for the human consumption because it is recognized by the body and accumulated mimicking potassium, which is important in the transmission of nerve messages. Like any radioactive material it also increases the risk of cancer when inhaled or ingested. ^{137}Cs contamination of land and foodstuffs in the territories around Chernobyl is a major problem, as thousands of square miles of land in Belarus, Russia and Ukraine cannot be used for agricultural production whereas in some areas the population had to be relocated. These social and economic consequences of ^{137}Cs contamination will remain for decades unless a

decontamination solution is found.

Nuclear waste from power plants is another source of ^{137}Cs. This isotope is abundant in Spent Nuclear Fuel (SNF) and is largely responsible for the heat produced in such waste. ^{137}Cs has a relatively long half-life (30.17 years) and therefore it survives the short-term storage period of 10 years commonly allocated for SNF. In order to recycle the uranium and the plutonium from nuclear waste, one should clean it up by removing other isotopes like strontium-90 and ^{137}Cs. Furthermore, ^{137}Cs can be recycled and used for radiotherapy at cancer medical centers.

Crown ethers, with their particular geometry, can be used to extract and separate alkali ions from soil, water or other media. Their cavity varies in size depending on the number of oxygen atoms forming it. They can thus be selective for one specific ion size like the cesium cation. In this section, I am presenting a new model allowing the calculation of the interaction between crown ether, water and cesium picrate in a two-phases medium. The crown ether chosen for this study is dicyclohexano-18-crown-6 (Figure 1.16 a.). Its cavity size is compatible with the extraction of the cesium ion. The two cyclohexane molecules attached to the crown ether force the cavity to be open in a "plane" conformation, which is more favorable for the extraction. Furthermore, the DCH18C6 is not soluble in water which simplifies the calculations and the understanding of the equilibrium. Because of the explosive nature of the picrate ion (Figure 1.16 b.) chosen as a counter ion, I could not analyze these interactions in supercritical fluid by FT-IR. I had to use, like in the previous section, NMR as an analytical instrument and chloroform as a solvent. The radioactive ^{137}Cs and the stable Cesium-133 isotopes have the same chemical properties, therefore I used ^{133}Cs isotope for the following experiments that describe crown ether–water–cesium picrate interactions that occur during the extraction of cesium from water with chloroform.

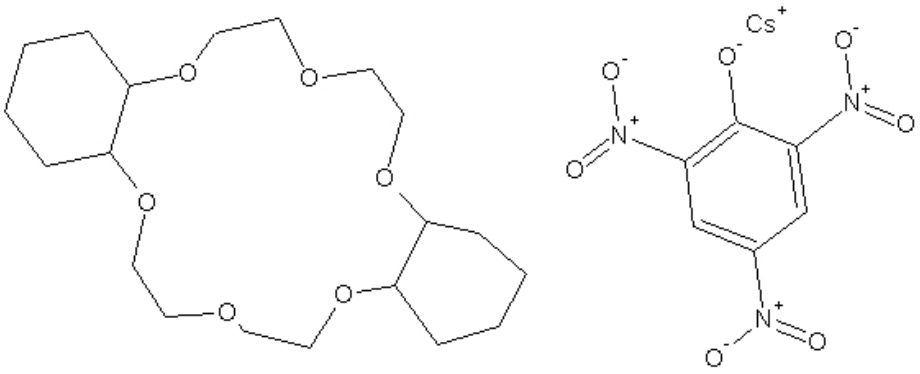

a. Dicyclohexano-18-crown-6 b. Cesium Picrate

Figure 1.16: Molecular structure of dicyclohexano-18-Crown-6 (a) and of Cesium picrate (b).

1.3.1 Experimental Work

Dicyclohexano-18-crown-6 (DCH18C6, 98% pur), chloroform-d (99.5% $CDCl_3$) were purchased from Aldrich Chemical Company and used with no further purification. Cesium picrate was synthesized from cesium chloride and picric acid and was recrystallized in water. Its purity is estimated to be over 95% because no impurity peak can be seen in the NMR spectra of the specie dissolved in water (5% D_2O).

The ligand was dissolved in chloroform-d (in the concentration range of 0.05–0.4 mol·L^{-1}) whereas the cesium picrate was dissolved in water (in the concentration range of 0.01–0.12 mol·L^{-1}). The two solutions were mixed in equal volume for 4 hours to reach equilibrium. Both phases were analyzed with a 500 MHz Brucker DRX500 spectrometer. The pulse interval was set to 9 sec (acquisition time 3 sec, relaxation delay 6 sec). DCH18C6 has a very low solubility in water and is not detectable in the water phase by NMR. Thus, its solubility in water was considered equal to zero and it was used as a standard for the peak integration in the organic phase.

Two typical PNMR spectra for DCH18C6 with water and cesium picrate in the $CDCl_3$ phase are shown in Figure 1.17 where the initial ligand concentration ([L]) is

0.4 mol·L^{-1} and the initial cesium picrate concentration ([CsPi]) is 30 mmol·L^{-1} and in Figure 1.18 where [L] = 0.05 mol·L^{-1} and [CsPi] = 8 mmol·L^{-1} . The chloroform chemical shift was set at 7.24 ppm and used for the calibration of all other chemical shifts in the organic phase. The group of peaks around 3.6 ppm is attributed to the 20 protons of the crown ether ring, whereas the 4 peaks for the protons of the cyclohexanes are between 1 and 2 ppm. The single resonance peak for the two equivalent protons of the picrate ion is found at 8.8 ppm. The free water and the bonded water are in rapid exchange in the solution due to their equilibrium. The observed water resonance peak consists of an average of the resonance of the free water and the bonded water in $CDCl_3$. Thus the resonance peak for the water shifts downfield as the ligand concentration is increased. In these spectra, the water resonance in $CDCl_3$ is found at 2.2 ppm (Figure 1.18) and 2.9 ppm (Figure 1.17). In this last figure, the concentrations are very low and the contamination of a water droplet can be seen at 4.7 ppm, which correspond to the chemical shift of water in water.

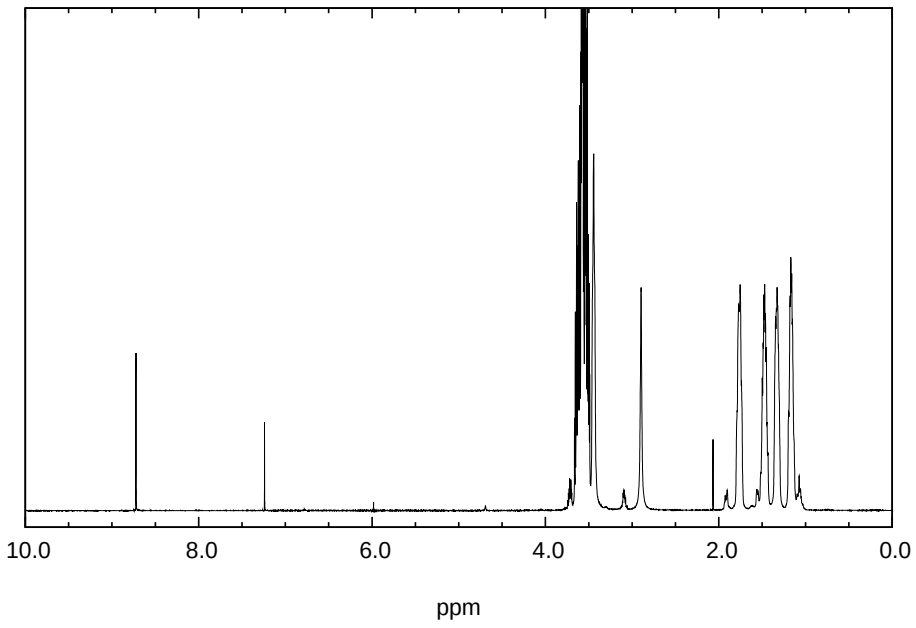

Figure 1.17: Typical PNMR spectrum for DCH18C6 (at 0.4 mol·L^{-1}) with water and cesium picrate (at 30 mmol·L^{-1}) in the $CDCl_3$ phase).

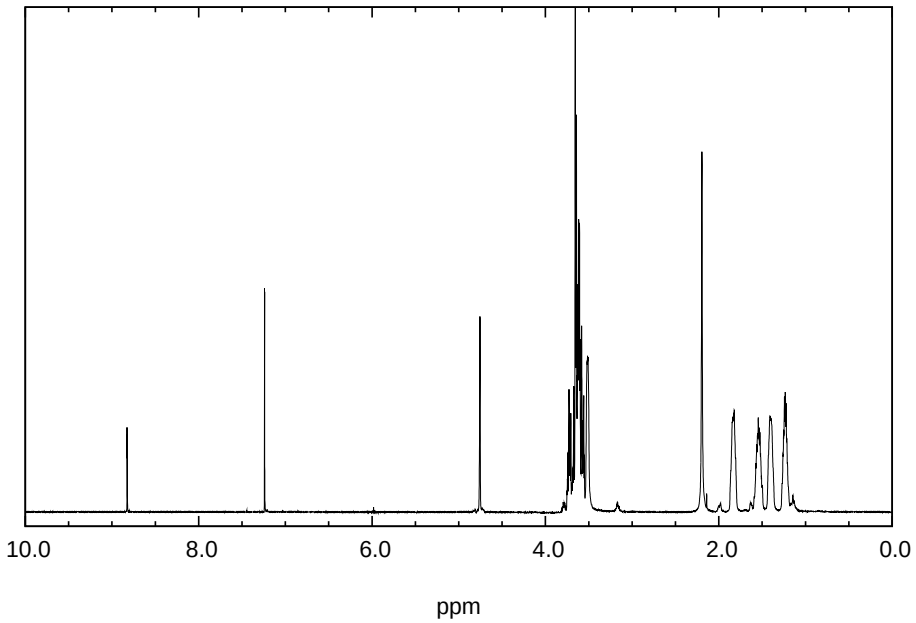

Figure 1.18: Typical PNMR spectrum for DCH18C6 (at 0.05 mol·L^{-1}) with water and cesium picrate (at 8 mmol·L^{-1}) in the $CDCl_3$ phase).

1.3.2 Calculations

NMR spectra give directly the total concentration of cesium picrate (CsPi), ligand (L) and water in the organic phase by an integration of the peaks belonging to the former species. In order to simplify the notation, the suffix "aq" was added to the species in the aqueous phase, whereas no suffix was added to the species in the organic phase.

Equilibrium Model Between the Two Phases

The partition of water, crown ether and cesium picrate between the organic and the aqueous phase is described as:

$$H_2O_{aq} \rightleftharpoons H_2O \tag{1.23}$$

$$L_{aq} \rightleftharpoons L \tag{1.24}$$

$$CsPi_{aq} \rightleftharpoons CsPi \tag{1.25}$$

Equilibrium Model in the Organic Phase

In the organic phase, the interaction between water, cesium picrate and DC18C6 follows the equilibrium reactions:

$$\mathrm{CsPi} + \mathrm{L} \rightleftharpoons \mathrm{CsPiL} \tag{1.26}$$

$$\mathrm{CsPiL} + \mathrm{L} \rightleftharpoons \mathrm{CsPiL_2} \tag{1.27}$$

$$\mathrm{L} + \mathrm{H_2O} \rightleftharpoons \mathrm{L{\cdot}H_2O} \tag{1.28}$$

$$\mathrm{CsPiL} + \mathrm{H_2O} \rightleftharpoons \mathrm{CsPiL{\cdot}H_2O} \tag{1.29}$$

$$\mathrm{CsPiL_2} + \mathrm{H_2O} \rightleftharpoons \mathrm{CsPiL_2{\cdot}H_2O} \tag{1.30}$$

Equilibrium Constants

Equilibrium constants corresponding to equations (1.26) through (1.30) are respectively defined as:

$$K_1 = \frac{[\mathrm{CsPiL}]}{[\mathrm{CsPi}][\mathrm{L}]} \tag{1.31}$$

$$K_2 = \frac{[\mathrm{CsPiL_2}]}{[\mathrm{CsPiL}][\mathrm{L}]} \tag{1.32}$$

$$K_a = \frac{[\mathrm{L{\cdot}H_2O}]}{[\mathrm{L}][\mathrm{H_2O}]} \tag{1.33}$$

$$K_b = \frac{[\mathrm{CsPiL{\cdot}H_2O}]}{[\mathrm{CsPiL}][\mathrm{H_2O}]} \tag{1.34}$$

$$K_c = \frac{[\mathrm{CsPiL_2{\cdot}H_2O}]}{[\mathrm{CsPiL_2}][\mathrm{H_2O}]} \tag{1.35}$$

Determining the Concentration of Different Species

The total unbonded water concentration $[H_2O]$ is constant at equilibrium, because of the equilibrium relation (1.23). To facilitate further calculation the following notation is employed for the former equilibrium constants.

$$k_x = [H_2O]K_x \tag{1.36}$$

with $x = a$, b or c.

Material balance at equilibrium leads to equations (1.38), (1.40) and (1.42) where the "org" suffix is used for the total concentration in the organic phase.

$$[L]_{org} = [L] + [L{\cdot}H_2O] + [CsPiL] + [CsPiL{\cdot}H_2O] + 2[CsPiL_2] + 2[CsPiL_2{\cdot}H_2O] \tag{1.37}$$

$$\Rightarrow [L]_{org} = (1 + k_a)[L] + (1 + k_b)[CsPiL] + 2(1 + k_c)[CsPiL_2] \tag{1.38}$$

$$[CsPi]_{org} = [CsPi] + [CsPiL] + [CsPiL{\cdot}H_2O] + [CsPiL_2] + [CsPiL_2{\cdot}H_2O] \tag{1.39}$$

Cesium picrate solubility in the organic phase is very low and considered as null.

$$\Rightarrow [CsPi]_{org} = 0[L] + (1 + k_b)[CsPiL] + (1 + k_c)[CsPiL_2] \tag{1.40}$$

$$[H_2O]_{org} = [H_2O] + [L{\cdot}H_2O] + [CsPiL{\cdot}H_2O] + [CsPiL_2{\cdot}H_2O] \tag{1.41}$$

$$\Rightarrow [H_2O]_{org} - [H_2O] = k_a[L] + k_b[CsPiL] + k_c[CsPiL_2] \tag{1.42}$$

Equations (1.38), (1.40) and (1.42) can be put in a matrix product as follows:

$$\begin{pmatrix} [L]_{org} \\ [CsPi]_{org} \\ [H_2O]_{org} - [H_2O] \end{pmatrix} = \mathbf{A} \begin{pmatrix} [L] \\ [CsPiL] \\ [CsPiL_2] \end{pmatrix} \tag{1.43}$$

where **A** is a 3×3 matrix defined as:

$$\mathbf{A} = \begin{pmatrix} 1+k_a & 1+k_b & 2(1+k_c) \\ 0 & 1+k_b & 1+k_c \\ k_a & k_b & k_c \end{pmatrix} \cdot \tag{1.44}$$

The resulting [L], [CsPiL] and [$CsPiL_2$] concentrations can then be found by solving equation (1.43) to get

$$\begin{pmatrix} [\mathrm{L}] \\ [\mathrm{CsPiL}] \\ [\mathrm{CsPiL_2}] \end{pmatrix} = \mathbf{A}^{-1} \begin{pmatrix} [\mathrm{L}]_{\mathrm{org}} \\ [\mathrm{CsPi}]_{\mathrm{org}} \\ [\mathrm{H_2O}]_{\mathrm{org}} - [\mathrm{H_2O}] \end{pmatrix} \tag{1.45}$$

where

$$\mathbf{A}^{-1} = \frac{1}{-D} \cdot \mathbf{B} \ , \tag{1.46}$$

$$\mathbf{B} = \begin{pmatrix} k_b - k_c & -k_b(k_c+2)+k_c & (1+k_b)(1+k_c) \\ -k_a(k_c+1) & k_a(k_c+2)-k_c & (1+k_a)(1+k_c) \\ k_a(k_b+1) & k_b - k_a & -(1+k_a)(1+k_b) \end{pmatrix} \ , \tag{1.47}$$

and

$$D = (1+k_a)(k_c - k_b) - k_a(1+k_b)(1+k_c). \tag{1.48}$$

The unbonded water concentration calculations are shown later on in this section. Other species concentration can be derived directly from the k_a, k_b and k_c values as shown by equations (1.33) through (1.36).

Determination of k_a and k

The molar fraction of water molecules bonded to the ligand, k, is defined by

$$k = \frac{[\mathrm{L{\cdot}H_2O}]}{[\mathrm{L}]+[\mathrm{L{\cdot}H_2O}]} \tag{1.49}$$

Because of equilibrium (1.23), the unbonded water concentration in the organic phase ($[H_2O]$) is independent of the other species dissolved and thus independent of the $[L{\cdot}H_2O]/[L]$ ratio and k.

When no cesium picrate is added to the solution, the material balance is

$$[H_2O]_{org} = [H_2O] + [L{\cdot}H_2O] \tag{1.50}$$

$$[L]_{org} = [L] + [L{\cdot}H_2O] \tag{1.51}$$

Combining the material balance relations (1.50) and (1.51) with equation (1.49), the linear relation

$$[H_2O]_{org} = k[L]_{org} + [H_2O] \tag{1.52}$$

can be derived. According to this equation, a linear plot of $[H_2O]_{org}$ versus $[L]_{org}$ should give the value of k as the slope, and the unbonded water concentration, that is constant and is independent of the other dissolved species, as the y-axes intercept. Replacing $[L{\cdot}H_2O]$ by $k_a[L]$ using equations (1.33) and (1.36) in equation (1.49) leads us to determine the relationship between k and k_a from

$$k = \frac{k_a}{1 + k_a} \tag{1.53}$$

or

$$k_a = \frac{k}{1 - k} \tag{1.54}$$

Determination of the Constants k_b and k_c

The constants, k_b and k_c, are respectively dependent on the concentrations of the CsPiL complex and on the $CsPiL_2$ "sandwich" which are used to calculate K_2. There-

fore, the correct values of k_b and k_c are the one for which K_2 is constant for a large set of data. As a consequence, values of the constants k_b and k_c, were calculated by minimizing the standard deviation on the equilibrium constant K_2 for different concentrations in ligand (from 0.05 to 0.40 mol·L^{-1}) and in cesium picrate (up to 0.12 mol·L^{-1}).

1.3.3 Results and Discussion

The total water versus cesium picrate concentration in the organic phase for different ligand concentrations is shown in Figure 1.19. Since unbonded cesium picrate is insoluble in the organic phase, all the cesium picrate in these experiments is bonded. As expected, the total water concentration in the organic phase decreases when the cesium picrate concentration increases. Indeed, the cesium picrate is captured inside the crown ether cavity instead of water. There is then less water than can be carried out from the water phase to the organic phase by crown ether.

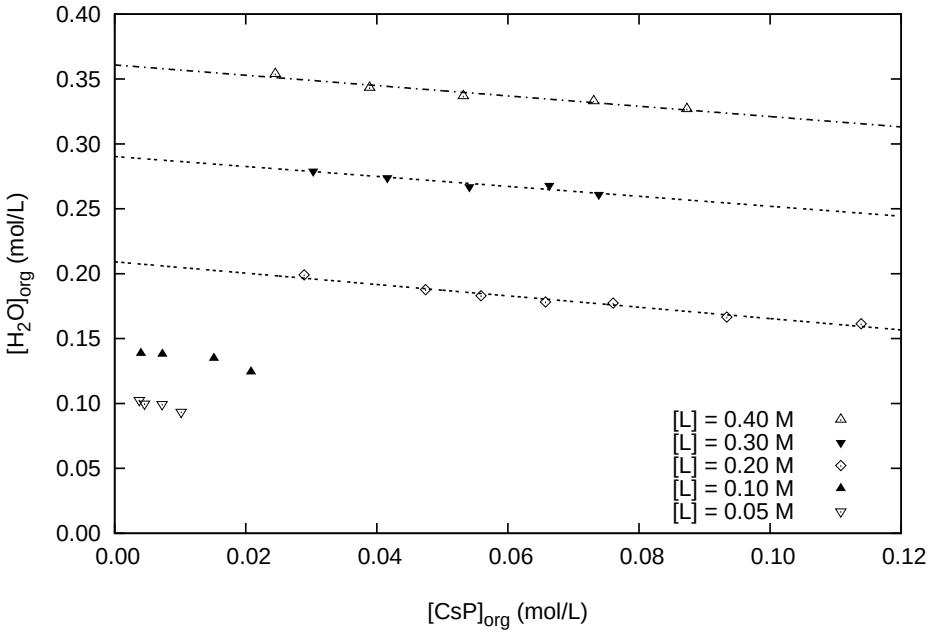

Figure 1.19: Total cesium picrate concentration versus water concentration in the organic phase for different initial ligand (L = DCH18C6) concentrations (from 0.05 to 0.4 mol·L^{-1}).

The y axis intercept value for each ligand concentration in Figure 1.19 gives the water concentration in the organic phase when no cesium picrate is added to the solution. A plot of this value versus the ligand concentration is shown on Figure 1.20.

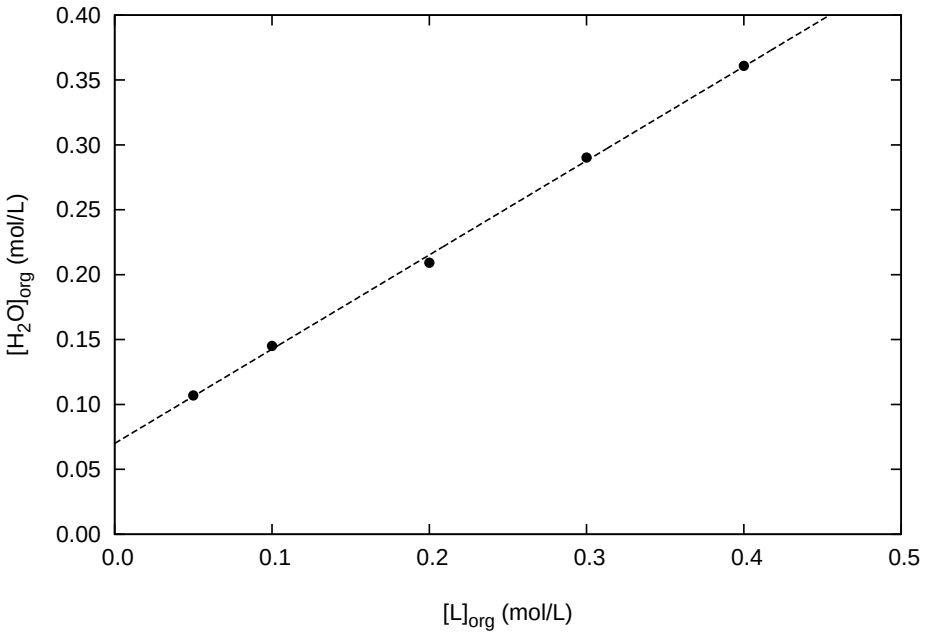

Figure 1.20: Total water concentration versus total ligand concentration in the organic phase.

The constant unbonded water concentration in the organic phase is found to be 0.07 ± 0.01 mol·L^{-1} using the linear regression on the data shown in Figure 1.20 and equation (1.52). This value is in good agreement with the experiment and with another calculation made in section (1.2.1) on page 75 that involved different crown ethers and water equilibrium in chloroform. The equation (1.52) also gives the molar fraction of water molecules bonded to the ligand (k). It is found to be 73 ± 4% and confirms the value found in section (1.2.2) for DC18C6 (70%). Therefore, about 30% of water in solution is not bonded to the crown.

The equilibrium constant K_a was found via equation (1.36) and (1.54) to be equal to 38 ± 13 L · mol^{-1}. This result is in accordance with the previous study in section (1.2.1) where K_a (named K in section (1.2.1)) was equal to 32 ± 3 L·mol^{-1}.

The equilibrium constant K_c was found to be equal to zero. Therefore, there is no sandwich between two crown ethers and one cesium picrate when the water is involved. The only sandwich forms in the organic phase are not complexed with water.

The equilibrium constant K_b was found to be equal to 21 ± 7 L $\cdot$ mol^{-1}. Thus the 1:1:1 complex between crown ether, water and cesium picrate is preferred to the one without water.

The equilibrium constant K_2 was found to be equal to 47 ± 15 L $\cdot$ mol^{-1}. This last result implies that when no water is involved in the complexion process, the sandwich form between two crown ethers and one cesium picrate is preferred than the 1:1 complex between one crown ether and one cesium picrate.

Conclusion

In this section, the cesium picrate-water-crown ether interactions were fully described using chloroform as a solvent. The importance of the role of water in the solvent extraction of cesium was demonstrated. The molar fraction of water bonded to the ligand (DCH18C6), k, was calculated from the measured data, and found to be $73 \pm 4\%$. This result confirms the value calculated in the study of the crown ether–water interaction in chloroform without cesium picrate (i.e. $70 \pm 4\%$ in section 1.2.2 page 77). This result implies that there is only 30% of the water that is not bonded in the organic phase.

Cesium extraction was described using four equilibrium reactions. The calculation of the equilibrium constants leads to three conclusions.

1. The sandwich configuration in between two crown ether and one cesium picrate is not possible if water is part of it.

2. The one–to–one complex of the cesium picrate with the crown ether is preferred with water than without.

3. the "sandwich" configuration is preferred to the one–to–one complex, when no water is involved.

It was also observed that the amount of water in the organic phase decreases with the increase of the cesium picrate concentration (Figure 1.19). It seems that the water is competing with crown ether to be carried out of the water phase. The efficiency of the extraction might be enhanced in a "water–free" extraction.

For future consideration, additional experiments need to be performed in supercritical CO_2 to find out if cesium extraction is efficient enough and confirm the feasibility of large scale plants to extract cesium from spent nuclear fuel (SNF) or clean large contaminated areas.

Conclusion

In this chapter, the interaction between water and crown ethers was studied in sub and supercritical CO_2 and in organic solvents that have physical properties comparable to the ones of CO_2. Two different spectroscopies were used to describe these interactions. First, the FT-IR spectroscopy used in CO_2, and second the NMR spectroscopy used in organic solvents. These two spectroscopies have their specific advantages and drawbacks. The FT-IR spectroscopy is a simple and affordable technique and most chemical laboratories possess a FT-IR spectrometer. The interpretation of a FT-IR spectrum can shed light on the bonds involved in a chemical system. On the other hand, NMR is very accurate in regard to the qualitative and quantitative analysis and its spectrum interpretation is straightforward. However it is an expensive device that is complex to operate and because of these reasons, it is not as easily usable as FT-IR in a non-conventional way. The versatility of the FT-IR technique allows the conduct of experiments in supercritical fluids that were not possible to perform with our NMR equipment.

First the crown ether–water interaction were studied in supercritical CO_2 and then in solvents that have a low dielectric constant and that are believed to have solubility parameters in the same magnitude as the one of CO_2. Carbon tetrachloride and chloroform were selected as solvents, and to investigate their properties, mixtures of these two solvents at different volume ratios were used. It was demonstrated that regarding the equilibrium constant K and the molar fraction of ligand complexed with water k, CO_2 acts like a solvent with high dielectric constant at low temperature and pressure and its behavior gets closer to the one of CCl_4 when temperature and pressure increase. On the other hand, with regards to the solubility of water in the CO_2 phase (amount of free water), it is the opposite. That is, the solubility increases with an increase in temperature and pressure in the same manner it increases as the dielectric constant of the solvent increases.

Finally, experiments were conducted with cesium, and the important role of water in the extraction process was demonstrated. No sandwich can be formed between two crown ethers and a cesium picrate with water bonded to it. Conversely, the 1:1 complex seems to be preferred with water. The amount of water tends to increase with an increase in the concentration of the ligand in the organic phase because the ligand carries water into the oil. It was also observed that the amount of water in oil decreases with the increase of the cesium picrate concentration. Therefore, the efficiency of the extraction might be enhanced if the water is removed from the sample. Indeed, water competes with cesium for space in the crown ether cavity in which they are carried into the organic phase.

More experiments need to be performed in supercritical CO_2 to ascertain whether cesium extraction is efficient enough to build a large scale plant to reprocess spent nuclear fuel (SNF) or to be able to clean large contaminated areas. For the SNF retreatment, a cesium extraction plant could be combined to a uranium extraction plant using a PUREX (Plutonium Uranium Recovery by Extraction) like process in supercritical CO_2. Using the fact that CO_2 is a tunable solvent, such a plant could also be used to extract and separate other radioactive elements, reducing the risk and the cost of having several extraction plants. The next chapter will describe the feasibility of supercritical CO_2 processes for the extraction of uranium.

Chapter 2

TriButyl Phosphate–Water–Nitric Acid Interaction

Introduction

This chapter is focused on the most important constituent of various nuclear waste, uranium. This study complements and benefits from the previous chapter, where the supercritical fluid extraction (SFE) of cesium was investigated and the role of the water in this extraction was detailed. Nitric acid and TriButyl Phosphate (TBP) complexes are used as oxidizing agent and ligand to extract uranium in supercritical CO_2. The antisolvent effect is observed when the TBP–water and the TBP–nitric acid–water adducts are dissolved in a solvent. This effect was investigated in order to have a better understanding of the mechanism of the extraction. I conclude this chapter by presenting a practical application: TBP–nitric acid–water adducts were used for the supercritical fluid extraction of uranium from incineration ash of the byproduct of the nuclear fuel production. However, before describing my research work in more detail, I will present a brief background on solvent extraction and especially on the PUREX (Plutonium Recovery by Extraction) process on which the supercritical extraction of uranium is based.

Numerous physical and chemical processes have been envisaged to separate, reprocess and recycle spent nuclear fuel and nuclear waste. Some thought to use neutrons absorption to transmute highly radioactive isotopes to stable or fast decaying ones,

but this costly method has not been proven viable yet and has many drawbacks. Others thought of chemical processes to separate radioisotopes that can be reprocessed and recycled. The first chemical process used in a large scale plant (1945, Hanford, Washington State, USA) was the bismuth phosphate process[10] which is designed to precipitate the plutonium with bismuth phosphate. This process was abandoned in the late forties, for solvent extraction processes, because it had too many steps, generated a large amount of waste and required a succession of dissolutions and precipitations that cannot be automated in a continuous way. Solvent extraction has the advantage of reprocessing both uranium and plutonium in a continuous way. The first large-scale plant that used solvent extraction was built by GE (General Electric company) at Hanford in 1951. This plant used the Redox process which consists of salting the aqueous solution containing the waste with aluminum nitrate and using 2-hexanone as an extractant for uranyl and plutonyl nitrate. This plant was replaced with a PUREX (Plutonium Recovery by Extraction) plant in 1956 after it was successfully used by the DuPont company in Savannah River (South Carolina State, USA) plutonium production plant. The Purex process uses nitric acid as a oxidizing agent and TBP (TriButyl Phosphate) and kerosene as an extractant. This process is still the most commonly used nowadays and I will describe it in more details later, but first I will describe the properties of TBP.

TBP is a molecule that has three butyl ether groups attached to the phosphorus atom which is also double-bonded to a single oxygen atom. Recent molecular dynamics studies shown that this single oxygen can be hydrogen bonded to water or nitric acid.[63,64] Indeed, the oxygen of the P=O bond in TBP is very electronegative, making TBP a Lewis base that can be engaged in hydrogen bonding with water or other lewis acids like nitric acid. Figure 2.1 shows one possible configuration of hydrogen bonds between a TBP, a nitric acid, and a water molecule. TBP is a colorless liquid at room temperature (boiling point is 289 °C at normal pressure[65]), it is almost non-volatile and it is non-miscible with water (solubility in water at 25 °C = 0.39

$g \cdot L^{-1}$). It does not react with nitric acid, it is stable under high level of radiation and it is miscible with common organic solvents such as kerosene, dodecane, alcohol, acetone, chloroform and carbon dioxide.[26]

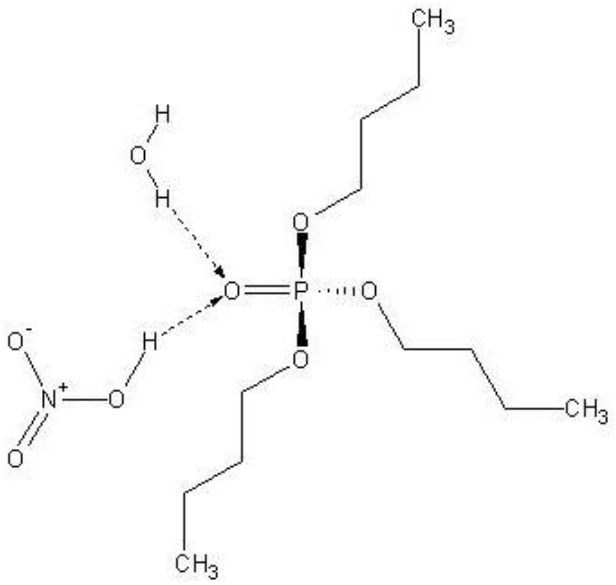

Figure 2.1: One of the possible configurations of hydrogen bonds between a TBP, a nitric acid and a water molecule.

Figure 2.2 (simplified from a schematic drawing in "Nuclear Chemical Engineering"[13]) describes the principal steps for the Purex process. First, the matrix containing the uranium and the plutonium, which can be spent nuclear fuel or other waste, needs to be prepared for the dissolution. This preparation, the so-called decladding, is used when the matrix is cladded which is common for spent nuclear fuel; it consists of opening the cladding with mechanical and chemical methods. This preparation will allow the dissolution of the matrix which is the second step. The matrix is dissolved in hot nitric acid. Nitric acid is used to oxidize the uranium to an oxidation state VI. Both of these steps produce radioactive gases, and mostly NO_x that can be converted to nitric acid and recycled. After the dissolution, the remaining cladding hulls are discarded and the acidity of the feed solution is adjusted to a desirable value. For the primary extraction, a mixture of TBP (30% by volume) and kerosene

is added to the nitric acid solution and the uranium and the plutonium are separated from the other water soluble contaminants. After the primary decontamination, the plutonium is separated from the uranium by reducing the plutonium(IV) to plutonium(III) which is not soluble in the organic phase. Both uranium and plutonium nitrates are thereafter purified separatly using a succession of solvent extractions. The aqueous solutions are finally evaporated and the uranium and the plutonium nitrates are converted to their oxide form by calcination.

The Purex process has numerous advantages; the volume of waste is low compared to preceding methods and the salting agent (HNO_3) can be removed by evaporation, TBP is less volatile and flammable than hexanone, and the cost of operation is low. Nevertheless, the process needs kerosene or dodecane in large volume. These solvents are flammable, toxic for the environment and cannot be easily recycled, therefore the use of carbon dioxide, which can be released in the atmosphere after the extraction, will add a real plus to the process. Furthermore, the physical properties of supercritical CO_2 can enhance the extraction efficiency, especially when the extractants are deeply bonded to the matrix and when the Purex process is not efficient. In this chapter, I will demonstrate the efficiency of uranium extraction for a pilot plant in which the uranium is extracted from ash (incineration of byproduct of the manufacture of UO_2 pellets) using a TBP-nitric acid solution in supercritical CO_2, but before that I needed to present a study of the TBP-water-nitric acid complex in supercritical CO_2 and in solvents using FT-IR and NMR.

Some compounds are more soluble in one solvent than in another, therefore, when a change of solvent occurs to a chemical system, the solute can precipitate out of the system. This phenomenon has been used for a long time, for example, to precipitate the soap after the saponification process and it is called the salting-out effect. The changes in the solvent can be induced by the addition of a poor solvent for the solute or by the addition of a salt very soluble in the solvent. When this technique is used in supercritical fluids it is called the antisolvent effect and it is induced by a change

of pressure or temperature and therefore a change in solubility of the fluid.

When the TBP-water complex is diluted in a solvent like CO_2 or $CDCl_3$, some water droplets appear immediately due to the anti-solvent effect. Some nitric acid droplets, at different concentrations, are also observed when the TBP-nitric acid complex is used. It is believed that these droplets improve the extraction of uranium with CO_2 over the traditional Purex process, by improving the dissolution and oxidation of uranium dioxide. In this chapter, this phenomenon is quantified by using FT-IR as an analytical device in super- and sub-critical CO_2. This study was then compared to the one using proton NMR spectroscopy in organic solvents. Last, I demonstrate the efficiency of uranium extraction for a pilot plant where the uranium is extracted from the ash, which is the product of the nuclear fuel fabrication waste, using a TBP-nitric acid solution in supercritical CO_2.

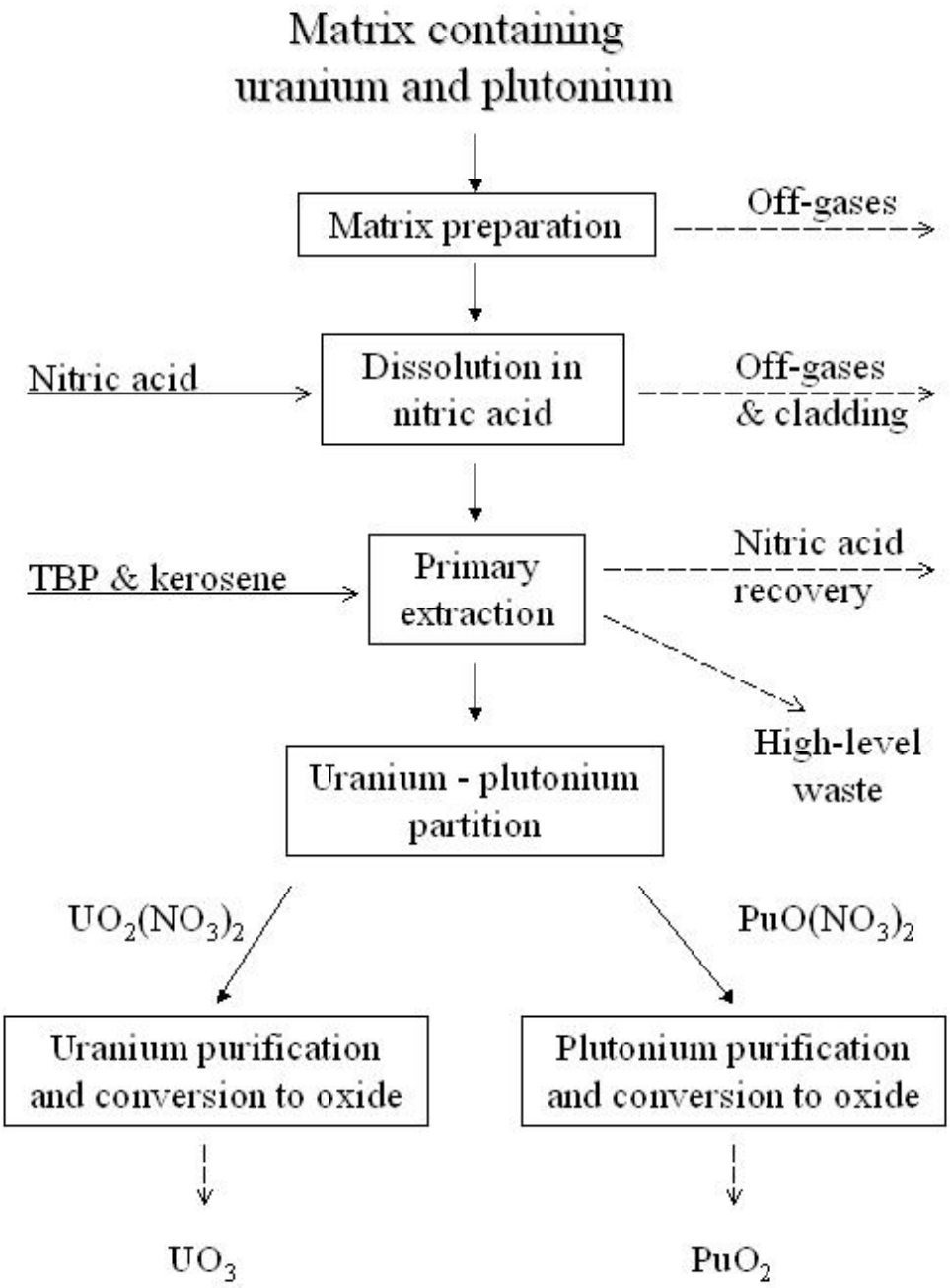

Figure 2.2: Principal steps of the Purex process.

2.1 Interaction of Tributyl Phosphate with Water

Introduction

In this section, an investigation of the interaction between TBP and water in different solvents is presented. The knowledge of this interaction is important as a first step to have a better understanding of the interaction between TBP, water and nitric acid in the uranium extraction process. For this process, TBP-nitric acid-water complexes are mixed with CO_2 to oxidize uranium(IV) to its hexavalent state and to extract it into the CO_2 phase. When one of these TBP complexes is mixed with a solvent having a low dielectric constant, some micro-droplets appear due to the antisolvent effect. The amount and acidity of these droplets are believed to play important role in the extraction of uranium with supercritical CO_2. This phenomenon is also observed when a TBP-water complex is diluted in an organic solvent such as chloroform or liquid and supercritical CO_2. To study this effect, the interaction of TBP and water was studied in supercritical and liquid CO_2 and in chloroform.

2.1.1 Interaction of Tributyl Phosphate with Water in Supercritical CO_2 Analyzed by Fourier Transform Infra-Red Spectroscopy

This first part of the section is devoted to describing the TBP-water interaction in sub- and supercritical CO_2. The FT-IR spectroscopy was used as an analytical tool.

Experimental Work

The experiment setup including the protocol, the cell, the spectrometer and the FT-IR settings are the same as described in chapter 1.1.1 on page 58. As mentioned previously, D_2O was used instead of H_2O because strong CO_2 absorption peaks between 3500 and 3800 cm^{-1} are overlapping the H_2O signal.

Tributyl Phosphate or TBP ($\geq$ 99% purity) and D_2O (100% D, 99.96% pure) were purchased from Aldrich Chemical Co. and used without further purification.

CO_2 (purity $\geq$ 99.99%) was obtained from Scott Speciality Gases Inc.

A series of mixtures composed of a fixed D_2O concentration (0.054 mol·L^{-1}) and variable TBP concentrations (from 0.04 to 0.16 mol·L^{-1}) were used to study the nature of TBP-water hydrogen bonding in liquid and supercritical CO_2. Each solution was introduced in the cell with a syringe before the addition of CO_2. The pressure and temperature of CO_2 were controlled in order to record the first spectrum at the lower density. The density was then increased by lowering the temperature (from 70 to 25 °C) before increasing the pressure (from 200 to 40 MPa). In this manner, a set of spectra was recorded at different densities for each solution.

Peak Assignments

The FT-IR spectra of free and bonded D_2O at different TBP concentrations (0-0.16 mol·L^{-1}) and at one fixed D_2O concentration (0.054 mol·L^{-1}) in supercritical CO_2 (40 °C, 20 MPa) is shown on Figure 2.3. The peak assignments for those spectra is based on the one made for the crown ether-water interaction in CO_2 detailed in my published paper "An FT-IR study of crown ether-water complexation in supercritical CO_2," which is reproduced here as appendix F.

The spectrum of pure D_2O (i.e. without any TBP) gives directly the position of the free water peaks; the O-D stretching asymmetric peak is at 2761 cm^{-1} whereas the symmetric one is at 2654 cm^{-1}. Those values are in agreement with the ones found in the literature.[35,55] When TBP was added to the system, an additional peak appeared between 2730 and 2732 cm^{-1}. This peak corresponds to the unbonded O-D stretching vibration marked as (2) in Figure 2.4. Unlike the case in the crown-ether-water spectrum, we cannot observe any peak for the bonded O-D stretching vibration marked as (1) on Figure 2.4; the TBP might have a different effect on this bond than crown ether and its peak might have shifted and became superposed on a stronger peak from which it could not be distinguished.

At higher TBP concentration, an additional peak appears at 2560 cm^{-1}. This

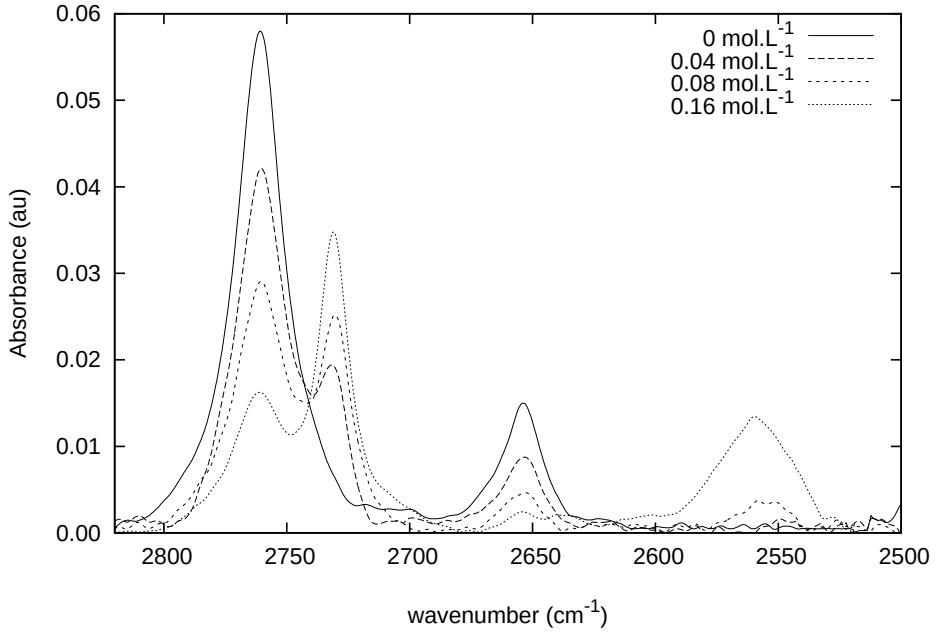

Figure 2.3: FT-IR spectra of free and bonded D_2O at different TBP concentrations (0-0.16 mol·L^{-1}) and at one fixed D_2O concentration (0.054 mol·L^{-1}) in supercritical CO_2 (40 °C, 20 MPa).

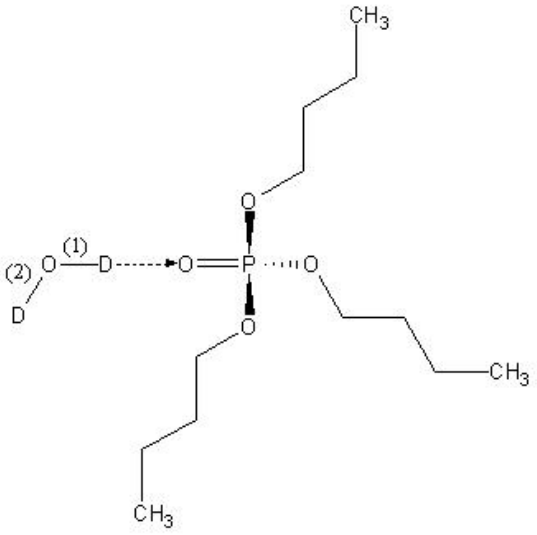

Figure 2.4: Possible configurations of the hydrogen bond between a D_2O and a TBP molecule.

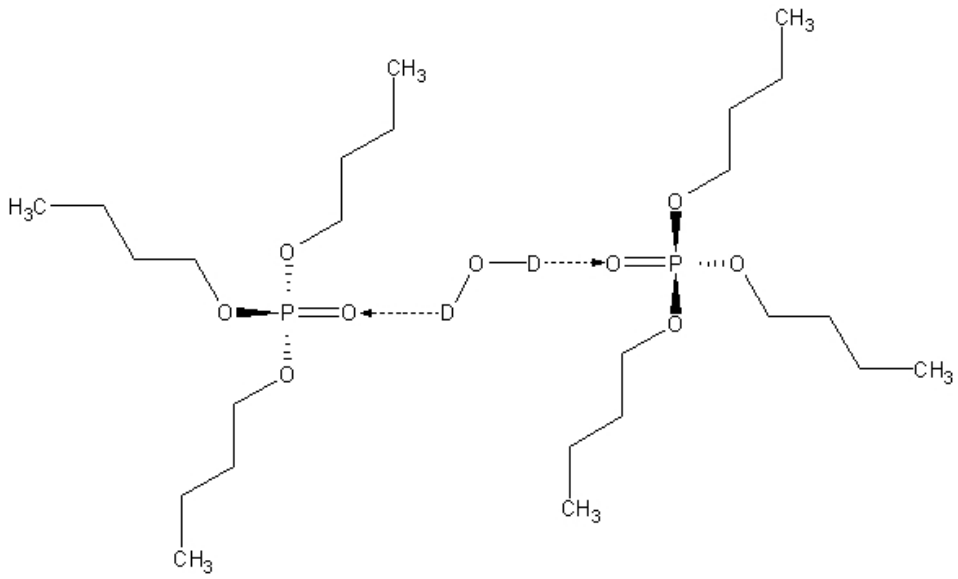

Figure 2.5: Possible configurations of the hydrogen bond between a D_2O and two TBP molecules.

peak is at the same wavenumber as the double hydrogen bond in the crown ether-water study. I therefore believe that it is due to the formation of a complex between 2 TBP molecules and one water molecule as represented in Figure 2.5.

Theoretical Calculations

The equilibrium between water and TBP can be described as the equilibrium between water and crown ether detailed in the paper "An FT-IR study of crown ether-water complexation in supercritical CO_2," reproduced as appendix F page 183. At low TBP concentration, where there is no significant amount of a 2:1 complex between TBP and water, the equilibrium is:

$$\mathrm{TBP} + \mathrm{D_2O} \rightleftharpoons \mathrm{TBP{\cdot}D_2O} \tag{2.1}$$

From this equilibrium, the equilibrium constant K can be defined from

$$K = \frac{[\mathrm{TBP{\cdot}D_2O}]}{[\mathrm{D_2O}][\mathrm{TBP}]}. \tag{2.2}$$

The molar fraction of the TBP complexed to water, k, is defined as:

$$k = \frac{[\mathrm{TBP{\cdot}D_2O}]}{[\mathrm{TBP{\cdot}D_2O}] + [\mathrm{TBP}]}. \tag{2.3}$$

The molar enthalpy of the hydrogen bond (ΔH) can be determined from the measurements of the equilibrium constant at different temperatures and at constant pressure via the well-known thermodynamic relations

$$\left(\frac{\partial \Delta G}{\partial T}\right)_P = -\Delta S = \frac{\Delta G - \Delta H}{T}, \tag{2.4}$$

$$\Delta G^0 = -RT \ln K, \tag{2.5}$$

and

$$\left(\frac{\partial \ln K}{\partial (1/T)}\right)_P = -\frac{\Delta H}{R}. \tag{2.6}$$

T is the absolute temperature in K, ΔS is the entropy in J·mol^{-1}·K^{-1}, ΔG is the Gibbs free energy in J·mol^{-1} and R is the molar gas constant in J·K^{-1}·mol^{-1}.

Equilibrium Parameters

The results of this study are summarized in Table 2.1. These results show that the changes in the values of the equilibrium constant K, the molar fraction of water bonded to the TBP (k), and the amount of free water are small when the temperature and pressure of the CO_2 change. Nevertheless, the changes are sufficient to observe trends, as the different graphs show.

In Figure 2.6, the density effect on the equilibrium constant K at constant temperature and at constant pressure is shown. When the pressure increases from 20 to 40 MPa, K decreases from 12 to 10 L·mol^{-1}. On the other hand when the temperature decreases from 70 to 31 °C, K increases from 9 to 14 L·mol^{-1} and drops to 12 at 25 °C. This unexpected change is certainly due to the change of phase. Indeed, CO_2 is no more supercritical at 25 °C but it is liquid.

In the same way, the dependence of the molar fraction of TBP bonded to water, k, on the density is shown on Figure 2.7. It is evident that k increases with density at

Table 2.1: Equilibrium parameters for water-TBP interaction in supercritical CO_2.

Pressure MPa	temp °C	density g·L^{-1}	K L·mol^{-1}	$[D_2O]_{free}$ mol·L^{-1}	k %
20.0	70	659	9	0.025	18
20.0	60	724	10	0.024	19
20.0	50	784	12	0.022	20
20.0	40	840	12	0.021	21
20.0	35	866	13	0.021	21
20.0	31	886	14	0.020	21
20.0	25	913	12	0.021	21
35.0	40	935	10	0.024	19
40.0	40	956	10	0.024	19
40.0	25	1004	12	0.022	20

Typical statistical errors: Pressure ± 0.1 MPa, Temperature ± 1 °C, K± 5%, $[D_2O]_{free}$± 5% and k± 2%

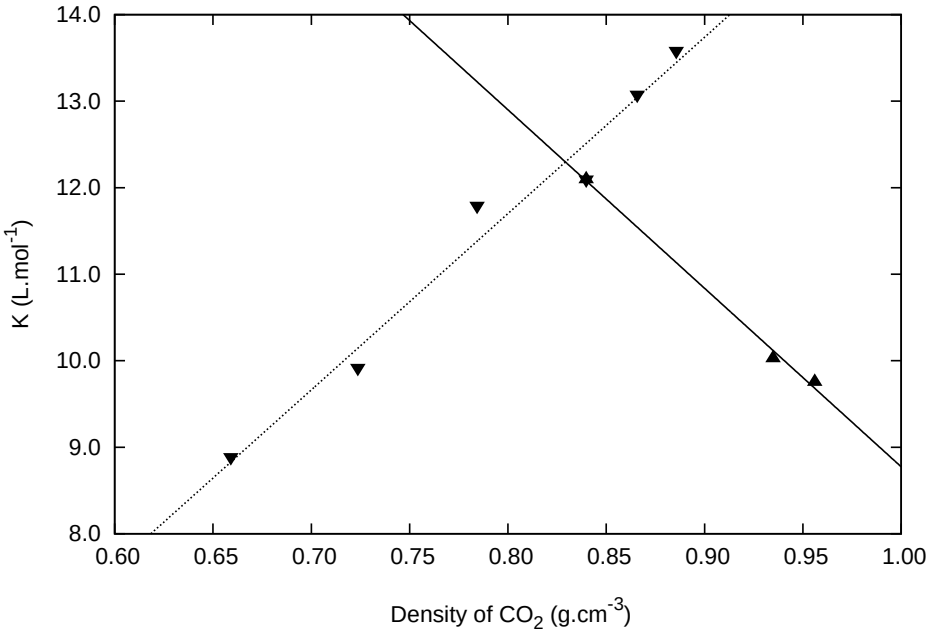

Figure 2.6: Density effect on the equilibrium constant K at constant temperature (▲, 40 °C) and at constant pressure (▼, 20 MPa).

constant pressure (20 MPa) from 18 to 21% and decreases with density at constant temperature (40 °C) from 21 to 19%

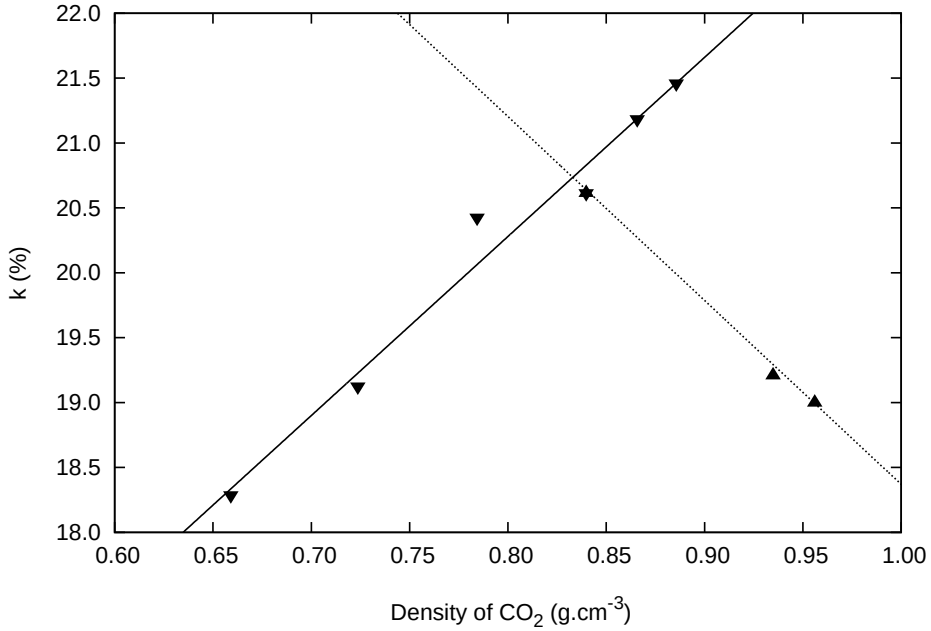

Figure 2.7: Molar fraction of TBP bonded to water k versus density at constant temperature (▲, 40 °C) and at constant pressure (▼, 20 MPa).

Figure 2.8 shows the increase of the free D_2O concentration from 20 to 25 mmol·L^{-1} when the temperature increases from 31 to 70 °C. In the same way, the free D_2O concentration dependence on the density is shown on Figure 2.9. the concentration [D_2O] increases from 21 to 24 mmol·L^{-1} when the density increases at constant temperature and decreases from 25 to 20 mmol·L^{-1} when the density increases at constant pressure.

From this set of data, the molar enthalpy of the hydrogen bond between TBP and water can be determined using equation (2.6) and the linear regression of the plot of $\ln K$ versus the inverse of the temperature in Kelvin (Figure 2.10). The slope is 1.11×10^3 K and ΔH is equal to -9.2 ± 0.6 kJ·mol^{-1} at 20 MPa with R = 8.3144 J·K^{-1}·mol^{-1}. This result implies that the process is exothermic as expected for hydrogen binding. Furthermore, since the species are more entropically ordered,

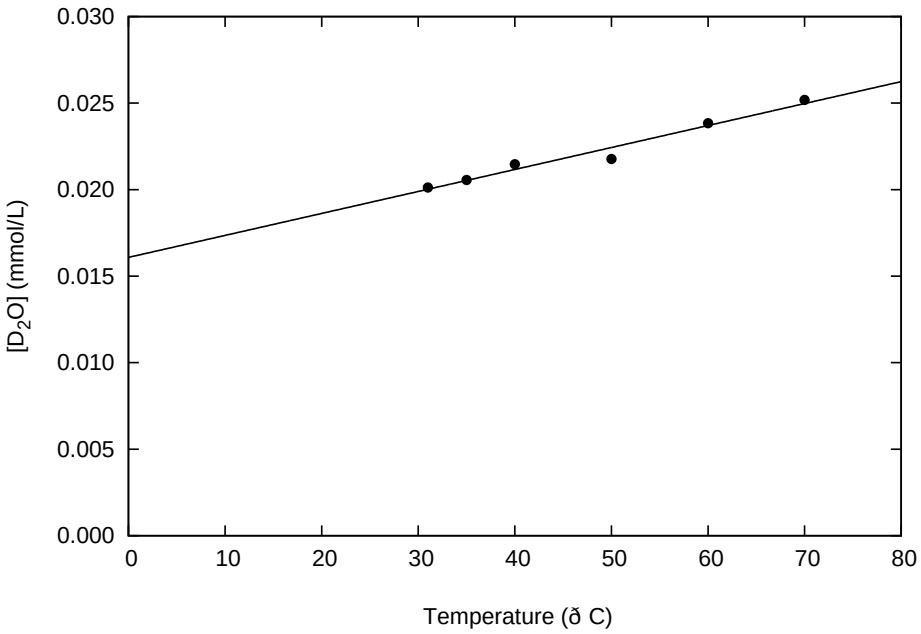

Figure 2.8: Concentration of free D_2O versus temperature at 20 MPa.

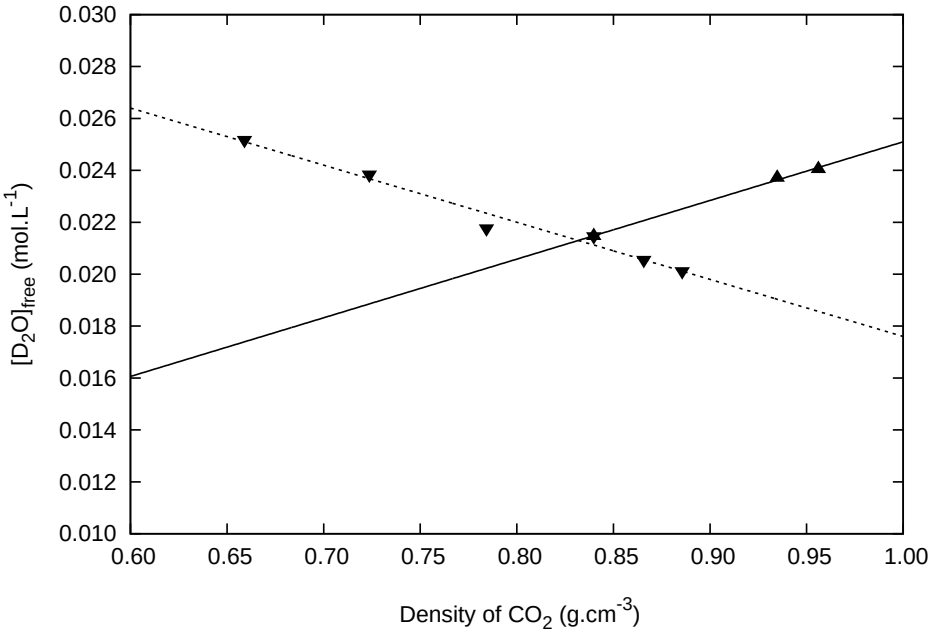

Figure 2.9: Free D_2O concentration versus density for at constant temperature (▲, 40 °C) and at constant pressure (▼, 20 MPa).

it explains the decrease of the K values wi7th the increase of temperature. In other respects, it is important to remember that for this calculation I needed to assume that ΔH is independent of density. This result is in accordance with the enthalpies values for hydrogen bonding in supercritical fluids that are found in the literature.[35,38,57]

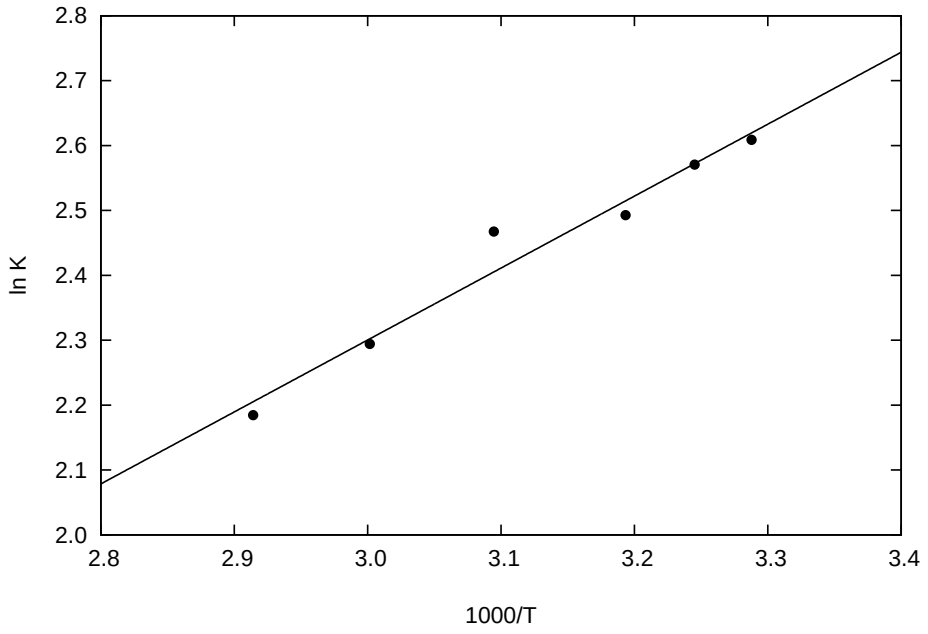

Figure 2.10: Dependence of $\ln K$ on $1000/T$ (T in K) at 20 MPa.

Figure 2.11 shows the dependence of $[D_2O]$ on the equilibrium constant K. The amount of free water in CO_2 decreases when K increases. The dependence appears to be linear, only because the range of the water concentration data is too narrow to see the curvature as predicted by equation (2.2).

The Antisolvent Effect

TBP and water make a one-to-one complex when mixed together with the molar fraction of water bonded to the TBP almost at 100%; it was determined by NMR to be equal to 97 ± 2%. When this 1:1 complex is mixed with an organic solvent (like dodecane, chloroform, kerozene, CO_2 etc.), some micro-droplets of water precipitate out of the organic phase because of the antisolvent effect. When the micro-droplets

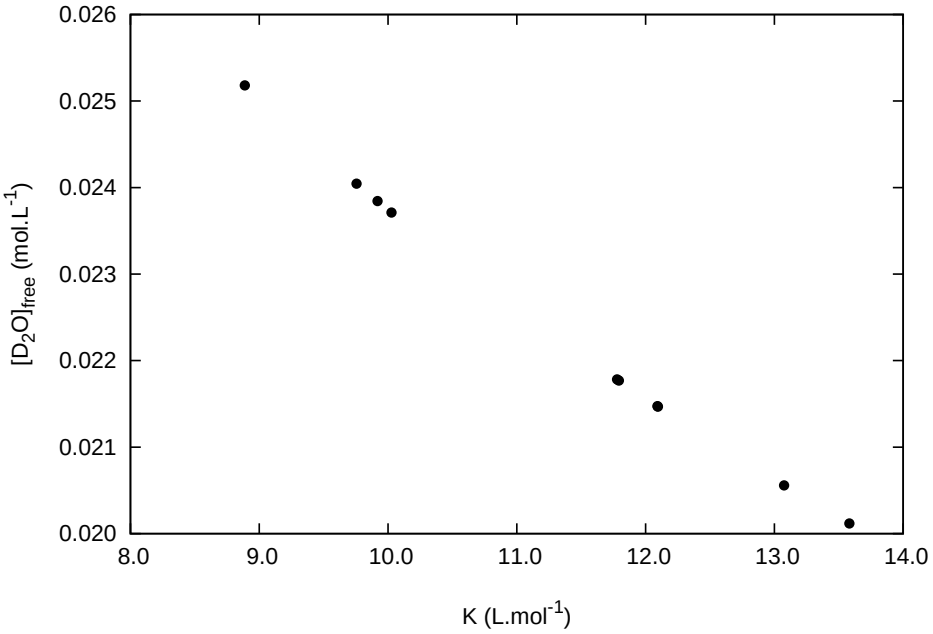

Figure 2.11: Dependence of the free water concentration, $[D_2O]$, on the equilibrium constant K.

are formed, a clouding of the solution is observed. Subsequently, the droplets grow in size and agglomerate on the wall of the container. The volume of these droplets can be quantified knowing the molar fraction of TBP bonded to the water and the solubility of water in the solvent. In the preceding experiments, the molar fraction of water bonded to the TBP dropped from nearly 100% to approximatly 20%. Some of the resulting unbonded water will dissolve in the organic solvent. This amount of free water is equal to the solubility limit of water in the solvent. The remaining water will precipitate out of the organic phase. In this scenario, there is a reservoir of water unlike in the preceding experiments where the amount of water was fixed at a value below the solubility limit of water in the supercritical fluid. Therefore the values of the free water found before are not equal to the solubility limit of the water in the fluid and these values were only used to determined the equilibrium parameters that are the same in both cases.

The solubility of water in CO_2 for different temperatures and pressures is reported

in table 2.2. Some values were found in the literature[6,7] whereas others were extrapolated from the values in the literature according to the linear regression shown in Figure 2.12. The amount of water droplets was determined using the following set of equations: The water and TBP material balance in number of moles is:

$$n_{D_2O_{tot}} = n_{D_2O_{org}} + n_{D_2O_{aq}} + n_{TBP\cdot D_2O_{org}} \tag{2.7}$$

$$n_{TBP_{tot}} = n_{TBP_{org}} + n_{TBP_{aq}} + n_{TBP\cdot D_2O_{org}} \tag{2.8}$$

$$\tag{2.9}$$

The suffixes "*tot*", "*org*" and "*aq*" refer to the total, the organic, and the aqueous phase, respectively. The solubility of TBP in water is very low, therefore, $n_{TBP_{aq}}$ is equal to zero and equation (2.3) can be written as:

$$n_{TBP\cdot D_2O_{org}} = k \cdot n_{TBP_{tot}} \tag{2.10}$$

Knowing the solubility of water in the organic phase ([D_2O]), the value of $n_{D_2O_{org}}$ is found and the volume of the water droplets can finally be found from the number of mole of water in the aqueous phase which is given by

$$n_{D_2O_{aq}} = n_{D_2O_{tot}} - n_{D_2O_{org}} - k \cdot n_{TBP_{tot}}. \tag{2.11}$$

Table 2.2 shows for different pressure and temperatures, the solubility of water, the molar fraction of water bonded to TBP k and the amount of micro-droplets formed when 0.5 mL of the water saturated TBP is mixed with CO_2 in a 10 mL cell. For the two pressure values used (20 and 40 MPa), the amount of droplets was found to increase when the density increases. This is shown in Figure 2.13 for the pressure of 20 MPa. On the other hand, at constant temperature, the amount of droplets decreases when the density increases.

Conclusion

I successfully used the FT-IR technique to determine the equilibrium constant and the molar fraction of water complexed to TBP in CO_2 as function of temperature and the

Table 2.2: Antisolvent effect for a water saturated TBP mixed with CO_2 at different densities.

Pressure MPa	temp °C	density[a] mol.L^{-1}	$[D_2O]^{max}_{free}$ mol·L^{-1}	k %	water droplets[d] μL
20.0	70	16.444	0.152[c]	18	-1[e]
20.0	60	16.444	0.136[c]	19	2
20.0	50	17.821	0.121[b]	20	4
20.0	40	19.082	0.102[c]	21	7
20.0	35	19.671	0.094[c]	21	9
20.0	31	20.123	0.085[b]	21	10
20.0	25	20.773	0.078[b]	21	11
40.0	40	21.724	0.136[c]	19	1
40.0	25	22.818	0.092[b]	20	10

a. values from NIST Chemistry WebBook.[56]
b. values from R. Wiebe[6]
c. values extrapolate from R. Wiebe,[6] cf. Figure 2.12
d. 0.5 mL of water saturated TBP mixed with CO_2 in a 10 mL cell
e. no water droplet formed

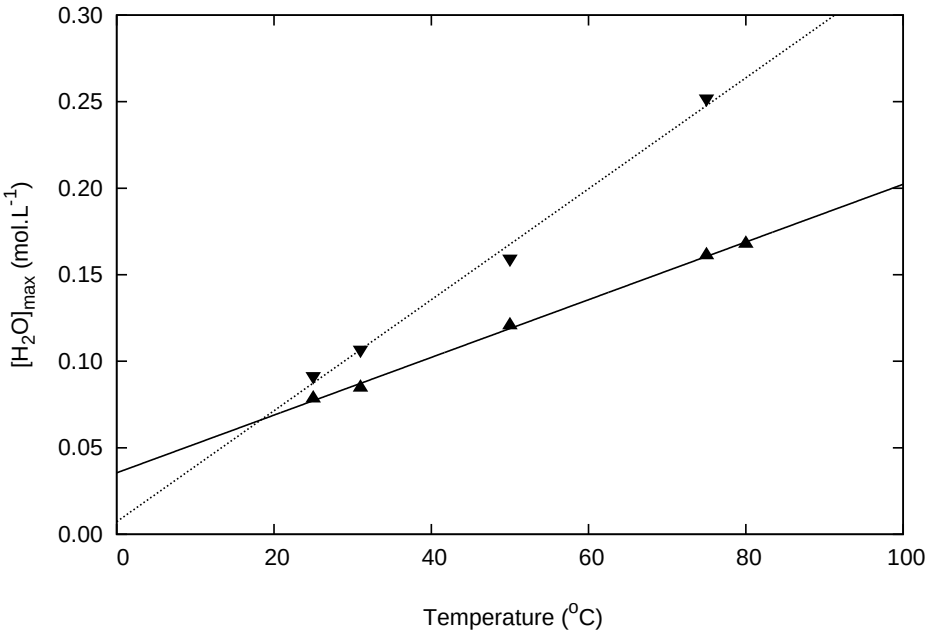

Figure 2.12: linear regression of the molar solubility of water[6,7] in CO_2 versus the temperature at constant pressure (20 (▲) and 40 (▼) MPa).

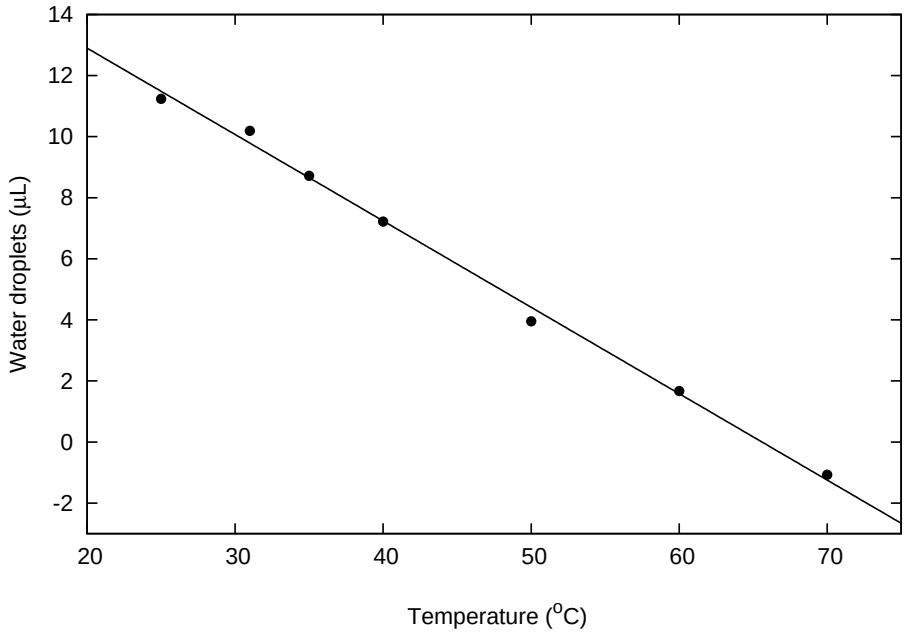

Figure 2.13: Volume of water droplets when 500μL of water saturated TBP is mixed with CO_2 in a 10 mL cell versus the temperature at constant pressure (20 MPa).

pressure of the supercritical fluid. I also found the value of the molar enthalpy for the hydrogen bond between TBP and water (ΔH = -9.2 kJ·mol^{-1}). Most importantly, the FT-IR technique can be used to predict the amount of water droplets produced by the antisolvent effect when the TBP-water complex is mixed with CO_2. This technique should be used to determine the amount of nitric acid droplets when the TBP-water-nitric acid complex is added to a solvent. Unfortunately, nitric acid is very corrosive and I could not achieve this with the equipment available. In order to overcome this problem, the interactions between water, TBP, and nitric acid are studied in chloroform using the NMR spectroscopy. This study will be presented later in section 2.2.

2.1.2 Interaction of Tributyl Phosphate with Water in Solvent Analyzed by Nuclear Magnetic Resonance Spectroscopy

In this section, the TBP-water interaction is detailed using the Nuclear Magnetic Resonance spectroscopy (NMR) in a conventional solvent like chloroform. The results obtained are compared to the one of the previous section, where the same interaction was studied in CO_2 using the Fourier Transform Infra-Red spectroscopy (FT-IR).

Experimental Work

TBP (98% purity) was purchased from Avocado Research Chemicals, Ltd. (ordered through Alpha Aesar Co.) and used with no further purification. Chloroform was used in the deuterated form (99.9 atom % D), and was purchased from Aldrich Chemical Company.

The TBP·H_2O adduct was prepared by mixing TBP with water in a glass tube with a stopper. The mixture of TBP and water was manually shaken vigorously for 4 minutes, followed by centrifuging for an hour. When the remaining organic phase is mixed with a solvent like $CDCl_3$ some water droplets appear. In order to quantify this phenomenon, a study of the interaction between TBP and water in $CDCl_3$ was carried out using different dilutions of TBP in $CDCl_3$. These solutions were mixed with an equal volume of water, shaken for 3 hours and centrifuged for another hour. The remaining organic phase was taken for analysis. Longer mixing and centrifuging times were tried without any significant changes in the data.

Proton NMR (PNMR) measurements were carried out using a 300 and a 500 MHz Bruker spectrometer. The pulse interval was set to 5 sec (acquisition time 3 sec, relaxation delay 2 sec) and 32 scans were taken. Chemical shifts were calibrated by using an insert filled with benzene-d6 (purchased from Aldrich Chemical Company) as an external standard. Benzene-d6 chemical shift was settled to 7.15 ppm. A typical PNMR spectrum of TBP·H_2O dissolved in $CDCl_3$ can be seen in Figures 2.14. The

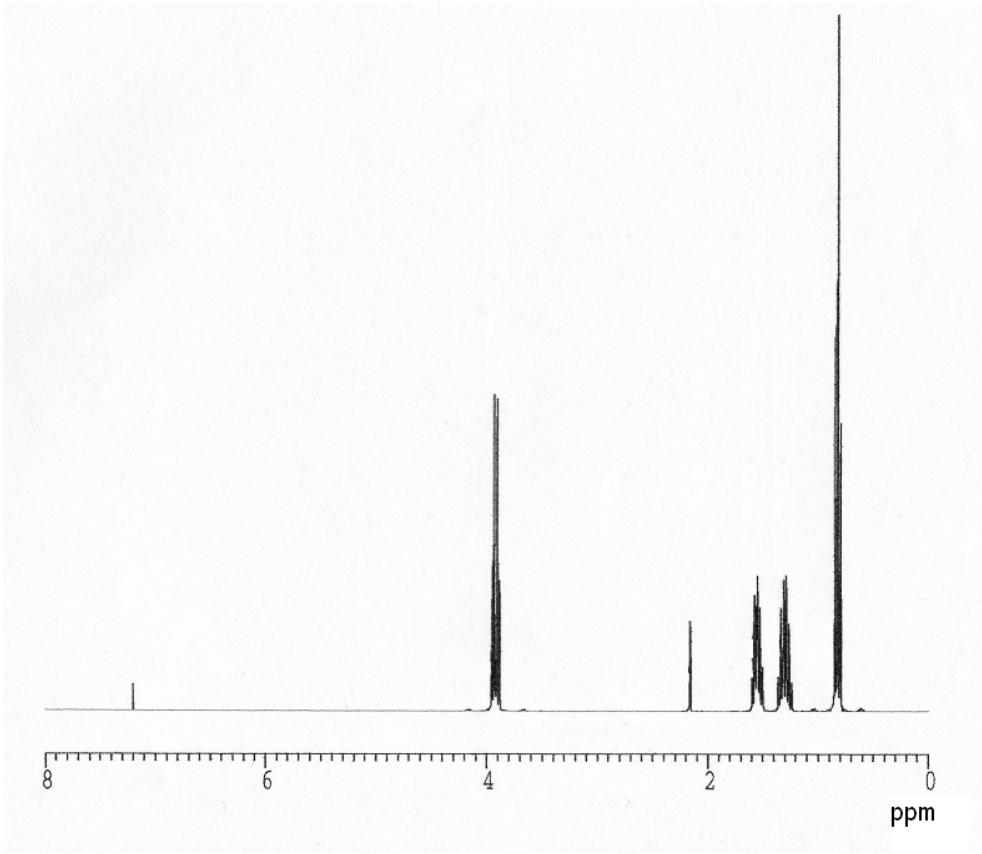

Figure 2.14: 300MHz ^{1}H-NMR spectra of TBP·H_2O in $CDCl_3$.

total water concentration in the organic phase, $[H_2O]^0_{org}$, can be determined directly from the integrated intensity of the water peak observed in these spectra. These intensities are calibrated on the TBP and $CHCl_3$ peaks for which the concentrations are known. The nonlinear regression and curve fitting analysis were performed using the NRLEG (Phillip H. Sherrod) program.

Theoretical Calculations

Chemical Shifts. It is well known that the observed chemical shift, δ_{H_2O}, of a fast exchange between various sites forming n different species is given by:

$$\delta_{H_2O} = \sum_{i=1}^{n} \delta_i \chi_i \tag{2.12}$$

where δ_i is the chemical shift of the specie i and χ_i is its molecular fraction.

TBP/Water Interaction in an Organic Phase. A binary system composed of a ligand (TBP) and water forming an one-to-one hydrate in the organic phase can be modeled by the following chemical equations:

$$H_2O_{aq} \rightleftharpoons H_2O_{org} \tag{2.13}$$

$$TBP_{org} \rightleftharpoons TBP_{aq} \tag{2.14}$$

$$H_2O_{org} + TBP_{org} \rightleftharpoons TBP{\cdot}H_2O_{org} \tag{2.15}$$

where the subscript "org" defines the organic phase that contains water, TBP and $CDCl_3$, and the subscript "aq" defines the aqueous phase. The partition coefficient for TBP can be determined from equation (2.14) by the following relation:

$$D_1 = \frac{[TBP]_{aq}}{[TBP]_{org}} \tag{2.16}$$

The solubility of TBP in water is very low (1.5×10^{-3} mol·L^{-1}) compared to the solubility in $CDCl_3$ (0.24 mol·L^{-1}). For this reason, the D_1 value was considered as

nil in all our experiments. The equilibrium constant K is defined by:

$$K = \frac{[\mathrm{TBP{\cdot}H_2O}]_{\mathrm{org}}}{[\mathrm{TBP}]_{\mathrm{org}}[\mathrm{H_2O}]_{\mathrm{org}}} \tag{2.17}$$

In addition, k, the molar fraction of ligand molecules complexed to water is written as:

$$k = \frac{[\mathrm{TBP{\cdot}H_2O}]_{\mathrm{org}}}{[\mathrm{TBP}]_{\mathrm{org}} + [\mathrm{TBP{\cdot}H_2O}]_{\mathrm{org}}} = \frac{K[\mathrm{H_2O}]_{\mathrm{org}}}{1 + K[\mathrm{H_2O}]_{\mathrm{org}}} \tag{2.18}$$

There are two ways to determine the initial ligand concentration $[\mathrm{TBP}]^0_{\mathrm{ini}}$. First the total amount introduced during the sample preparation can be calculated and second by material balance at equilibrium:

$$[\mathrm{TBP}]^0_{\mathrm{ini}} = [\mathrm{TBP}]_{\mathrm{org}} + [\mathrm{TBP{\cdot}H_2O}]_{\mathrm{org}} + [\mathrm{TBP}]_{\mathrm{aq}} \tag{2.19}$$

The term $[\mathrm{TBP}]_{\mathrm{aq}}$ is negligible considering that the TPB solubility in water is very low. Therefore,

$$[\mathrm{TBP}]^0_{\mathrm{org}} = [\mathrm{TBP}]_{\mathrm{org}} + [\mathrm{TBP{\cdot}H_2O}]_{\mathrm{org}}. \tag{2.20}$$

The water concentration in the organic phase $[\mathrm{H_2O}]^0_{\mathrm{org}}$ can also be defined by material balance at equilibrium:

$$[\mathrm{H_2O}]^0_{\mathrm{org}} = [\mathrm{H_2O}]_{\mathrm{org}} + [\mathrm{TBP{\cdot}H_2O}]_{\mathrm{org}} \tag{2.21}$$

Combining the material balance relations (2.19) and (2.20) with equation (2.17) the linear relation

$$[\mathrm{H_2O}]^0_{\mathrm{org}} = k\,[\mathrm{TBP}]^0_{\mathrm{org}} + [\mathrm{H_2O}]_{\mathrm{org}} \tag{2.22}$$

can be derived. According to equation (2.22), it is easy to determine the free water concentration $[H_2O]_{org}$ and the k value by a plot of $[\mathrm{H_2O}]^0_{\mathrm{org}}$ versus $[\mathrm{TBP}]^0_{\mathrm{org}}$. From these data and equation (2.18), the equilibrium constant K is obtained.

Results and Discussion

Peak Assignment. Different concentrations of TBP (up to 1.8 mol·L^{-1}) in $CDCl_3$ were mixed in equal volume with H_2O and analyzed by NMR. A typical proton

Table 2.3: intensities and coupling constants of the TBP multiplets.

multiplet	δ (ppm)	Intensities						Coupling constants				
quartet	3.97	1.1	2.9	3.0	1.1			6.71	6.71	6.71		
quintet	1.56	1.3	3.8	6.0	4.3	1.2		6.72	7.32	7.33	6.71	
sextet	1.31	1.3	5.4	10.0	9.6	5.2	1.2	7.31	7.32	7.94	7.32	7.33
triplet	0.83	1.2	2.0	1.2				7.32	7.33			

NMR spectrum, taken at 300 MHz, of TBP·H_2O dissolved in $CDCl_3$ can be seen in Figure 2.14. The $CHCl_3$ peak is a singlet that was calibrated at 7.24 ppm. The water droplets should appear at 4.7 ppm because it corresponds to the chemical shift of water in water. Unfortunately, the peak is not visible on this spectrum. The total water in oil peak varies from 1.52 to 3.10 ppm depending on H_2O concentration in the organic phase; in Figure 2.14, it is at 2.16 ppm. Finally, the TBP peaks are at 0.84, 1.32, 1.60 and 3.93 ppm. An enlargement of these TBP peaks taken from a 500MHz spectrum is shown in Figure 2.15 and the intensities and coupling of each multiplet is shown in Table 2.3. The three butyl ether groups are equivalent in the TBP molecule. For this reason and to simplify the peak assignment, I will describe only the branches numbered in Figure 2.16.

The triplet at 0.8 ppm has an intensity environ 50% larger than the other peaks which indicates that it is associated with the hydrogens of the methyl group (carbon 4 in Figure 2.16). The quartet at 4.0 ppm is at higher ppm certainly because it is partially deshielded by the oxygen. However, there is no hydrogen coupled to three other hydrogens in the TBP molecule, and for this reason no quartet should appear. However, the phosphorus (^{31}P) has the same spin quantum number than the hydrogens (1/2) and a heteronuclear coupling is possible between the proton and the phosphorus. This quartet corresponds therefore to the hydrogens of the carbon 1 in Figure 2.16. Finally, there is a quintet and a sextet at 1.6 and 1.3 ppm). The protons associated with the the quintet can "see" four hydrogens, whereas the ones associated

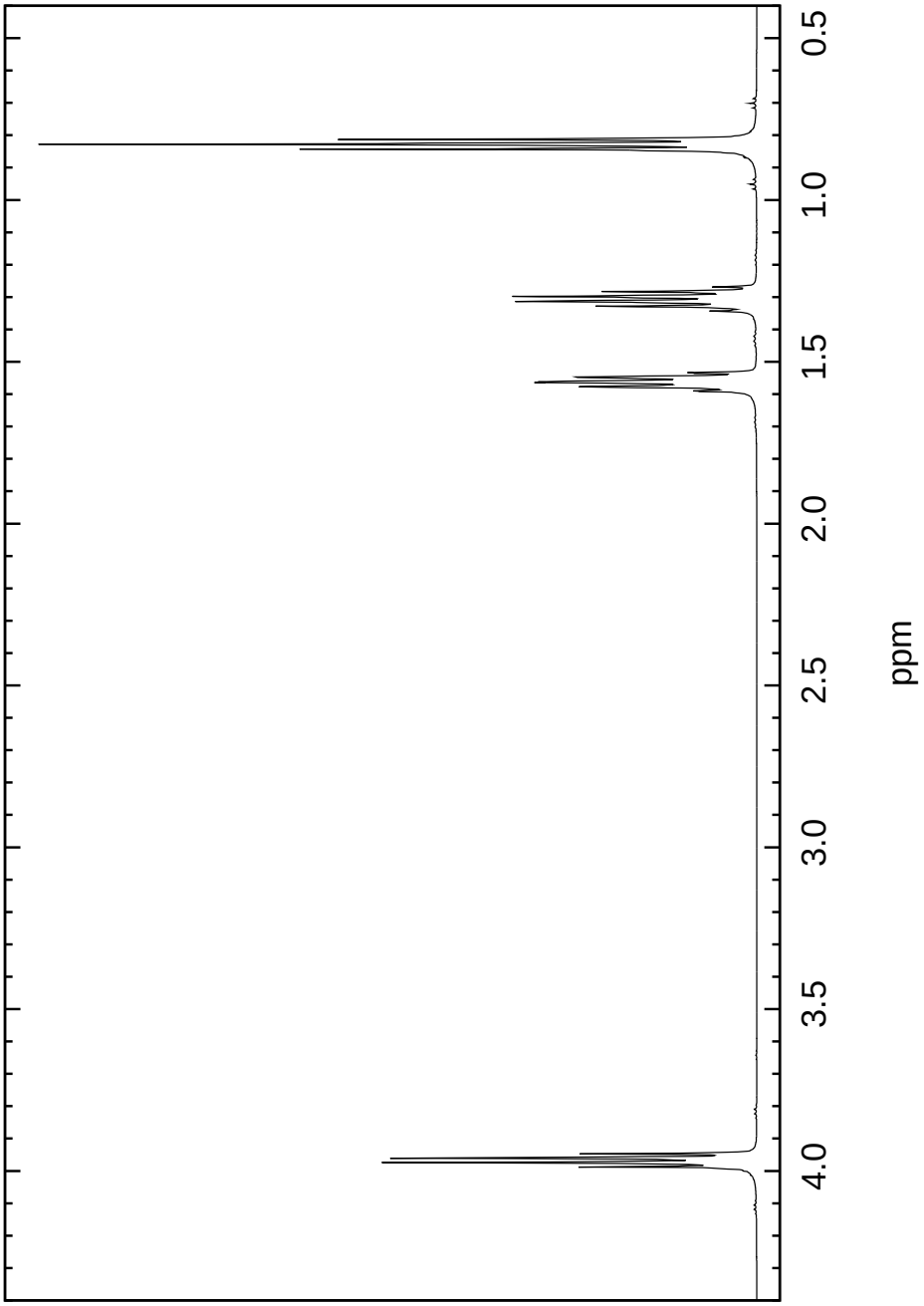

Figure 2.15: Enlargement of a 500MHz ^{1}H-NMR spectra of TBP·HNO_3·H_2O in $CDCl_3$.

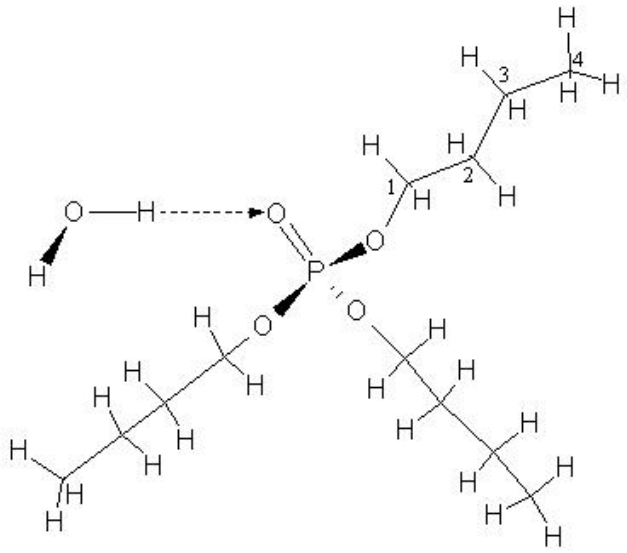

Figure 2.16: Possible configuration for the TBP hydrate.

with the sextet can "see" 5 protons. Consequently, the protons of the quintet belong to the carbon 2 and the ones of the sextet belong to the carbon 3 in Figure 2.16.

Water Chemical Shift. The water in the system studied is in fast exchange between its free state and the state where it is bonded to TBP. Because a NMR spectrum needs several seconds to be recorded, the spectrum shows the average value of the two states instead of each of them separately. Therefore, the H_20 and the TBP·H_2O peaks are combined in one peak and its chemical shift δ_{H_2O} follows the equation

$$\delta_{H_2O} = \delta_0 \chi_{H_2O} + \delta_1 \chi_{TBP \cdot H_2O} \tag{2.23}$$

which is derived from equation (2.12), where δ_{H_2O} is the observed chemical shift for water, and δ_0 and δ_1 are the water chemical shift in 100% $CDCl_3$ and 100% TBP respectively. The molar fractions χ_{H_2O} and $\chi_{TBP \cdot H_2O}$ are defined as follows:

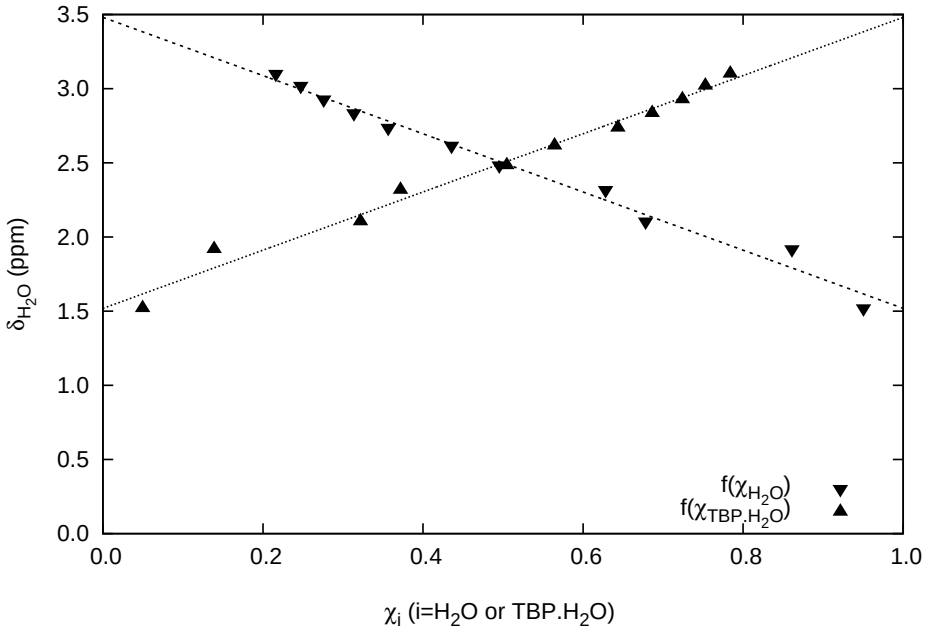

Figure 2.17: Chemical shift observed of water in $CDCl_3$ and in TBP, versus the molecular fractions of free water (▼) and of bonded water (▲). The dashed lines corresponds to their linear regression fits.

$$\chi_{H_2O} = \frac{[\mathrm{H_2O}]_{\mathrm{org}}}{[\mathrm{H_2O}]^0_{\mathrm{org}}} \tag{2.24}$$

and

$$\chi_{TBP\cdot H_2O} = \frac{[\mathrm{H_2O}]^0_{\mathrm{org}} - [\mathrm{H_2O}]_{\mathrm{org}}}{[\mathrm{H_2O}]^0_{\mathrm{org}}} \tag{2.25}$$

In Figure 2.17, the plot of the observed water chemical shift, δ_{H_2O}, versus the molar fraction of free water, χ_{H_2O}, is shown for different water and TBP concentrations in $CDCl_3$. This plot shows that δ_{H_2O} increases linearly when the molar fraction of free water rises. The linear regression on this plot allows the determination of $\delta_0 = 1.51 \pm 0.04$ ppm which corresponds to where the fitted line intersects with the ordinate. In the same figure, the plot of δ_{H_2O} versus the molar fraction of bonded water, $\chi_{TBP\cdot H_2O}$, is shown for the same set of data. Similarly, the fitted line intersects with the ordinate at 3.51 ± 0.04 ppm which corresponds to the value of δ_1.

In Figure 2.18 the observed chemical shift, δ_{H_2O}, is plotted versus the total water

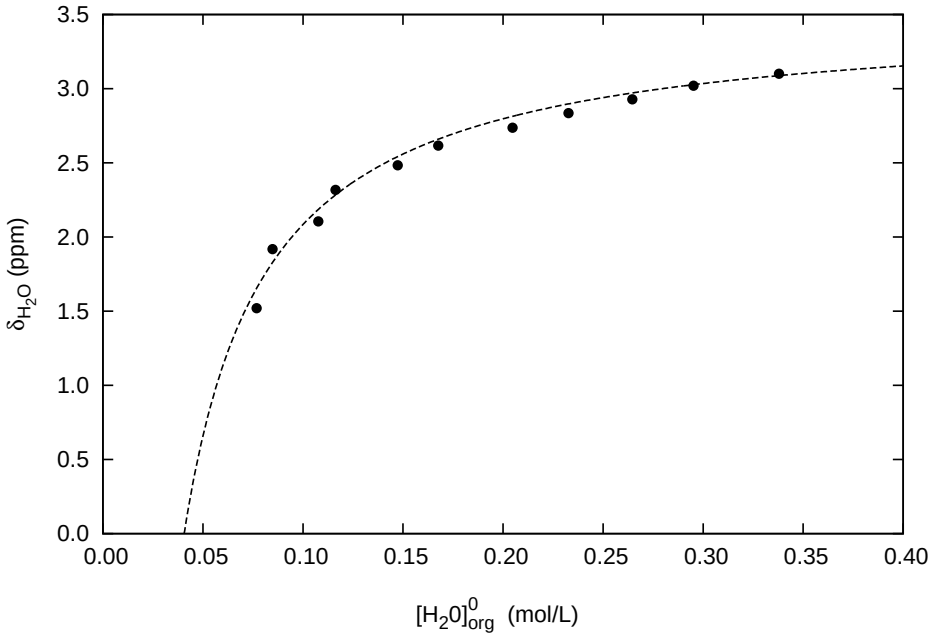

Figure 2.18: Chemical shift observed (black points) and calculated (thin line) of water in $CDCl_3$ and in TBP versus total water concentration in the organic phase.

concentration in the organic phase, $[H_2O]^0_{org}$. The shift δ_{H_2O} increases rapidly until the total water concentration in the organic reaches 0.13 mol·L^{-1}. At higher water concentration, the increase slows down and plateaus to an asymptotic value below 3.6 ppm. The dependency of δ_{H_2O} on $[H_2O]^0_{org}$ can be obtained using equations (2.23), (2.24) and (2.21), which are combined to give the following:

$$\delta_{H_2O} = \frac{\delta_0[H_2O] + \delta_1([H_2O]^0_{org} - [H_2O]_{org})}{[H_2O]^0_{org}}, \tag{2.26}$$

where δ_0 and δ_1 are the constants previously determined and $[H_2O]_{org} = 0.07 \pm 0.02$ mol·L^{-1}as demonstrated in the paragraph describing the chemical equilibrium later in this section (page 128). The plot of the calculated values of δ_{H_2O} versus $[H_2O]^0_{org}$ as given by equation (2.26) is shown in Figure 2.18.

Chloroform Chemical Shift. There is some weak hydrogen bonds between TBP and $CDCl_3$ and for the same reasons as the ones explained previously, the chemical shift between pure chloroform and chloroform mixed with TBP varies slightly de-

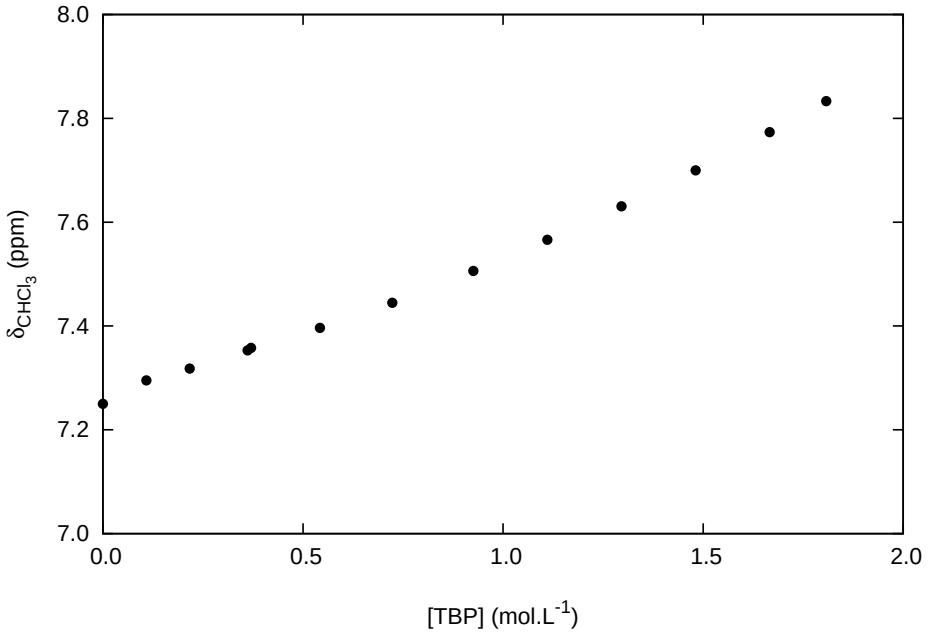

Figure 2.19: Chemical shift observed of $CHCl_3$ in TBP and in $CDCl_3$ versus the TBP concentration in the organic phase.

pending on the TBP concentration.[66] The dependency of the chloroform chemical shift, δ_{CHCl_3}, on the TBP concentration was studied using the same set of spectra as previously. A plot of these results is represented in Figure 2.19. The chemical shift is shown to increase slowly when the TBP concentration in $CDCl_3$ increases.

From this same set of results, the chemical shift of pure chloroform, δ_2, and the one of chloroform dissolved in TBP with 1:1 ratio, δ_3, can be found using the relation:

$$\delta_{CHCl_3} = \delta_2 \chi_{CHCl_3} + \delta_3 \chi_{CHCl_3 \cdot TBP} \tag{2.27}$$

which is derived from equation (2.12). The δ_2 value was calculated at 7.27 $\pm$ 0.03 ppm as expected, because it corresponds to the chemical shift of $CHCl_3$ in $CHCl_3$. On the other hand, δ_3 is equal to 9.20 $\pm$ 0.03 ppm. This is an obvious but important result. Indeed, one can set the $CHCl_3$ chemical shift at its right value depending on TBP concentrations in $CDCl_3$ and use it as a chemical shift reference without having to use any additives like TetraMethylSilane (TMS).

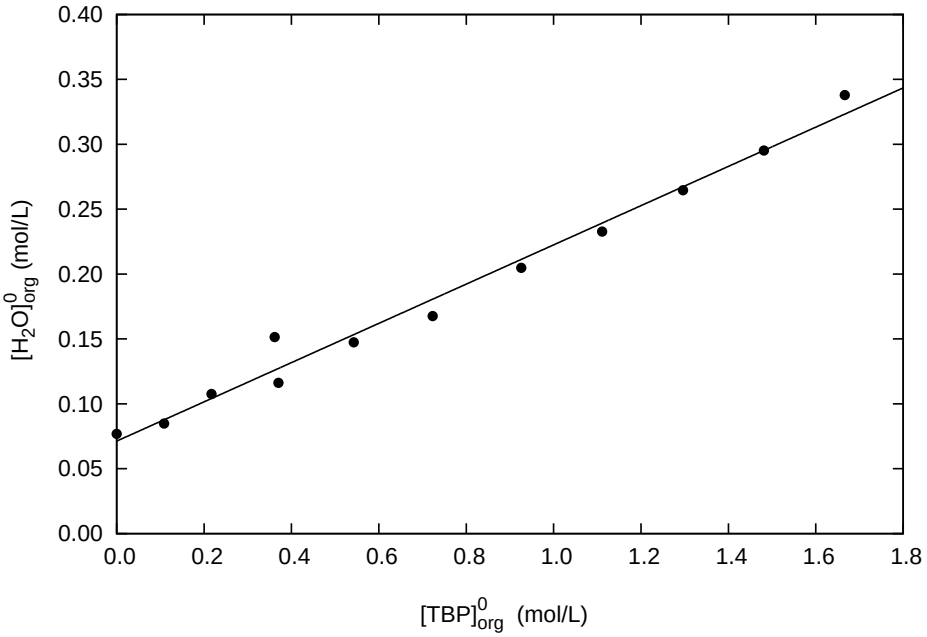

Figure 2.20: Total water ($[H_2O]^0_{org}$) versus total TBP ($[TBP]^0_{org}$) in the organic phase.

Chemical Equilibrium. The plot of total water concentration, $[H_2O]^0_{org}$, versus the total TBP concentration, $[TBP]^0_{org}$, is represented in Figure 2.20. The total water concentration is shown to increase as the total TBP concentration increases. This was expected because TBP forms a strong hydrogen bond with water, therefore increasing the total water solubility in the organic phase when the TBP concentration increases. The free water concentration in $CDCl_3$, $[H_2O]_{org}$, can be determined using equation (2.22). According to this equation, the linear regression of the plot of $[H_2O]_{org}$ versus the total TBP concentration intersects with the ordinate at the value of the free water concentration $[H_2O]_{org} = 0.07 \pm 0.02$ mol·L^{-1}. This result is consistent with the value of the solubility of water in $CHCl_3$ found in the previous study of the crown ether-water interaction in $CDCl_3$ detailed in section 1.2.1, page 75 and section 1.3.3, page 94.

The molar fraction of TBP complexed to water in $CDCl_3$, k, can also be obtained from equation (2.22). It corresponds to the slope of the linear regression of $[H_2O]^0_{org}$

versus the total TBP concentration (Figure 2.20). In this study, k was found equal to 0.15 ± 0.01. The remaining water, which amounts to 85% of the total is released in the form of fine droplets when the water-saturated TBP solution is dissolved in $CDCl_3$. The amount of micro-droplets of water formed because of the antisolvent effect can be calculated from the value of k, knowing that the water solubility in pure $CDCl_3$, $[H_2O]_{org}$, is 0.07 ± 0.02 mol·L^{-1}. For this calculation, equations (2.7) to (2.11) described in section 2.1.1 on page 115 are needed. If 0.5mL of the water saturated TBP is mixed with chloroform in a 10 mL volumetric viol, the volume of micro-droplets will be 14 ± 1 μL.

Last the equilibrium constant (K) can be deduced from the value of k by using equation (2.18). Its value is $K = 2.7 \pm 0.2$ L·mol^{-1}.

Conclusion

This section describes the analysis of the water-TBP equilibrium in supercritical CO_2 using the FT-IR spectroscopy. This equilibrium was also analyzed in chloroform using the NMR spectroscopy. The two analytical methods complement each other to give a complete picture of the equilibrium. Significant results include obtaining the molar fraction of water bonded to TBP, k, and the equilibrium constants in the oil phase. In $CDCl_3$, k was found equal to 0.15 ± 0.01 which is lower than the lowest value obtained in supercritical CO_2 (i.e. 0.18 ± 0.01 at 70 °C and 20 MPa). This result shows that there is more water bonded to TBP in the supercritical fluid at the conditions of my experiments. In pure $CDCl_3$, the amount of free water, $[H_2O]_{org}$, is 0.07 ± 0.02 mol·L^{-1}and the standardized amount of micro-droplets was found equal to 14 ± 1 μL. The amount of micro-droplets formed is at least 3 μL lower in CO_2 considering the experimental conditions used.

NMR also gave information on the chemical shift of water and chloroform in the TBP-water-$CDCl_3$ system. They can both be determined theoretically knowing the TBP concentration.

The analysis of the experiments discussed in this section is not complete without consideration of adding nitric acid, which is essential to the supercritical fluid extraction of uranium. This part will be presented in the next section.

2.2 Interactions with Nitric Acid Analyzed by Nuclear Magnetic Resonance

Introduction

The study of TBP·$(HNO_3)_x$·$(H_2O)_y$ adducts comprise an essential step to the understanding of the supercritical fluid extraction of uranium. Therefore, I will describe first in this section various TBP-water-nitric acid adducts using the Nuclear Magnetic Resonance (NMR) as a spectroscopic tool.

An interesting observation was made when these adducts are mixed with an organic solvent, some micro-droplets of nitric acid immediately appear in the oil due to the so-called antisolvent effect. Throughout this work I came to believe that the acidity and quantity of these micro-droplets enhance the extraction of uranium. To have a better understanding of the formation of these micro-droplets, I will describe later in this section the interactions between TBP·$(HNO_3)_x$·$(H_2O)_y$ adducts and chloroform. Chloroform was selected as a solvent because of its physical properties, which are comparable to supercritical CO_2, and because of its non-interference with the NMR data collection.

2.2.1 Experimental Work

The experimental work for this section is similar to the one in the study of the TBP-water interaction by NMR, section 2.1.2, page 118.

TBP (98% purity) was purchased from Avocado Research Chemicals, Ltd (ordered through Alpha Aesar Co.) and used with no further purification and chloroform was used in the deuterated form (99.9 atom % D), and was purchased from Aldrich Chemical Company. Nitric acid (69.4% (w/w)) was obtained from Fisher Chemical (New Jersey), and was diluted to 15.5 mol·L^{-1} with deionized water.

The TBP·$(HNO_3)_x$·$(H_2O)_y$ complexes were prepared by mixing TBP with a 15.5 mol·L^{-1} solution of nitric acid in a glass tube with a stopper. Different volume ratio of nitric acid and TBP (from 1:10 to 6:1 nitric acid to TBP volume ratio) were

prepared. Thereafter, the mixture was manually shaken vigorously for 4 minutes, followed by centrifuging for an hour. The organic phase was then extracted with a pipette and analyzed. When the remaining organic phase is mixed with a solvent like $CDCl_3$ some water droplets appear. In order to quantify this phenomenon, a study of the interaction between TBP and water in $CDCl_3$ was carried out using different dilutions of TBP in $CDCl_3$. These solutions were mixed with an equal volume of nitric acid (15.5 mol·L^{-1}), shaken for 3 hours and centrifuged for another hour. The remaining organic phase was taken for analysis. Longer mixing and centrifuging times were tried out with no significant change in the data.

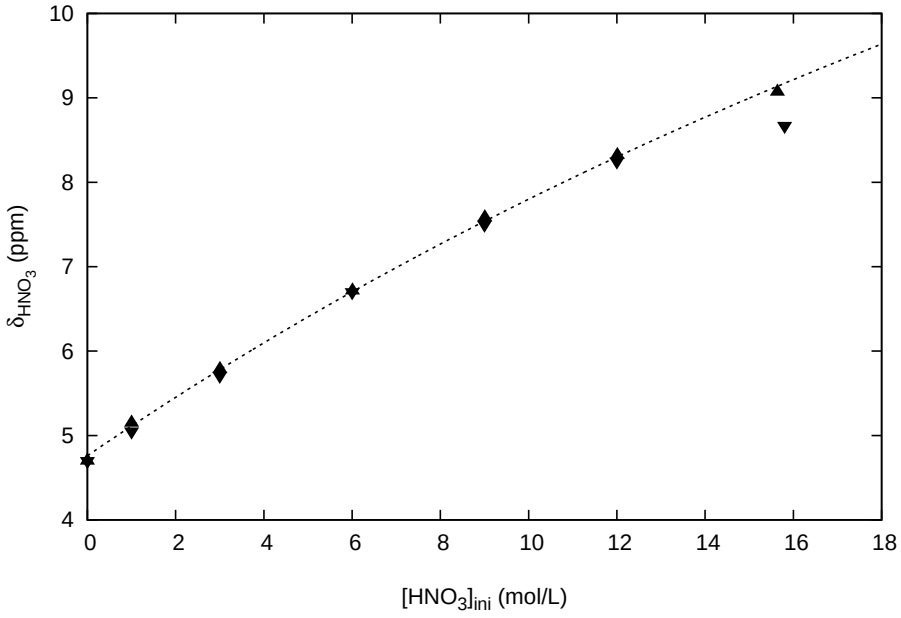

Figure 2.21: Chemical shift of nitric acid observed from the droplets (▼) and from nitric acid solutions in water (▲) and calculated (dashed line) using equation (2.29) versus total nitric acid concentration.

The concentration of H_2O in the organic phase was measured by Karl-Fischer titration (Aquacounter AQ-7, Hiranuma, Japan). The concentration of HNO_3 in the organic phase was measured with an automatic titrator (COM-450, Hiranum, Japan) with 0.1 mol·L^{-1} NaOH solution after adding large excess amount of deionized water. The concentration of HNO_3 in the water droplets was determined by comparison of the

chemical shift of different concentrations of nitric acid in water as shown on Figure (2.21), and confirmed by titration methods. Proton NMR (PNMR) measurements were carried out using a 500 MHz Bruker DX500 spectrometer. The pulse interval was set to 5 sec (acquisition time 3 sec, relaxation delay 2 sec) and 32 scans were taken. Chemical shifts were calibrated by using an insert filled with benzene-d6 (purchased from Aldrich Chemical Company) as an external standard. Benzene-d6 chemical shift was settled to 7.15 ppm. A typical PNMR spectrum of TBP·$(HNO_3)_x$·$(H_2O)_y$ dissolved in $CDCl_3$ can be seen in Figures 2.22. In this spectrum, the four groups of peaks between 1 and 5 ppm belong to the butyl ether groups of the TBP molecule as describe in detail in section 2.1.2, page 121. The peak at 11.80 ppm belong to the nitric acid and the water. These two compounds are bonded in different ways to the TBP and because of the fast equilibrium in between them, only one peak shows as an average of all.

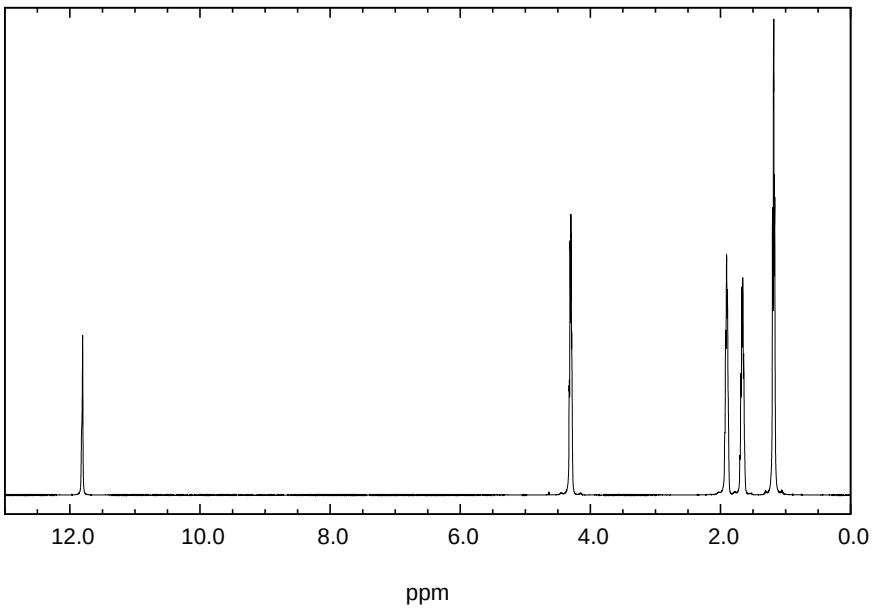

Figure 2.22: A typical proton NMR spectrum of TBP·$(HNO_3)_x$·$(H_2O)_y$ with a benzene-d6 insert. The sample was prepared by mixing 1.0 mL of 15.5M HNO_3 with 4.0 mL of 98% TBP.

Finally, the nonlinear regression and curve fitting analysis were performed using

the NRLEG (© Phillip H. Sherrod) program.

2.2.2 Results and Discussion

In this part, I will describe first the trivial relationship between the chemical shift of nitric acid in water and its concentration. This result allow the determination of the acid concentration in the micro-droplets formed when TBP complexes are mixed with a solvent. Second, I will describe the TBP·$(HNO_3)_x$·$(H_2O)_y$ complex without solvent. In these adducts, the values of x and y represent the number of nitric acid and water molecules per TBP molecule, respectively. Last, I will describe the interaction between TBP, water and nitric acid in chloroform.

Chemical Shift of HNO_3 in Water

Before studying a more complex system, equation (2.12) on page 120 was used to determine the chemical shift of the HNO_3/H_2O peak in water depending on nitric acid concentration. For this system,

$$\delta_{obs} = \delta_4 \chi_{HNO_3} + \delta_5 \chi_{H_2O} \tag{2.28}$$

where δ_4 is the chemical shift for pure H_3O^+ ion and δ_5 is the chemical shift for pure water. The water concentration in water was taken at 55.6 mol·L^{-1}. Equation (2.28) can also be written as:

$$\delta_{obs} = \delta_4 \chi_{HNO_3} + \delta_5 (1 - \chi_{HNO_3}) \quad = \quad (\delta_4 - \delta_5)\chi_{HNO_3} + \delta_5 \tag{2.29}$$

where

$$\chi_{HNO_3} = \frac{[H_3O^+]}{[H_3O^+] + 55.6}. \tag{2.30}$$

According to equation (2.29), the plot of the linear relationship between δ_{obs} and the nitric acid molecular fraction gives directly the values of $\delta_5 = 4.76 \pm 0.03$ ppm and $\delta_4 = 24.6 \pm 0.2$ ppm. Figure 2.21 shows the plot of the chemical shift of nitric acid in water and the calculated fit using equation (2.29) versus the total nitric acid concentration. Combining equations (2.29) and (2.30), with the calculated values of

δ_4 and δ_5, the acid concentration can be expressed in terms of the observed chemical shift, δ_{obs}, using the following equation:

$$[H_3O^+] = 55.6 \times \frac{4.76 - \delta_{obs}}{\delta_{obs} - 24.6}. \tag{2.31}$$

This equation can be used to calculate concentration of the acid droplets resulting of the antisolvent effect, with the simple knowledge of their chemical shift.

TBP·$((HNO_3)_x$·$((H_2O)_y$ System without Solvent

The values of x and y in the TBP·$(HNO_3)_x$·$(H_2O)_y$ adduct represent the number of nitric acid and water molecules per TBP molecule, respectively. The value of x is calculated by dividing the concentration of nitric acid in the organic phase by the concentration of TBP. In the same way, the value of y is calculated by dividing the water concentration by the TBP concentration.

Different concentrations of HNO_3 or water in TBP influence the dissolution of uranium oxides.[29] For this reason, it is important to determine the exact composition of the TBP complex. Figure 2.23 shows the combined chemical shift of H_2O and HNO_3 versus the number of molecules of nitric acid per molecule of TBP, x. The chemical shift increases rapidly from 8.9 to 12.6 ppm when the nitric acid to water mole ratio increases. When this ratio reaches unity, the chemical shift reaches its maximum and starts to decrease slowly to 12.0 ppm, which corresponds to a ratio of 2.4 molecules of nitric acid for each molecule of water.

Table 2.4 summarizes the different experiments performed and gives the corresponding values of the nitric acid and water ratio in TBP. These values were obtained using NMR spectra in both organic and aqueous phases in addition to titration methods.

The number of molecules of HNO_3 per molecule of TBP, x, versus the initial volume ratio of HNO_3 (at 15.5 mol/L in water) to TBP is shown in Figure 2.24. When the initial volume ratio is under unity, the value of x increases rapidly as the volume ratio increases. The curve is shown to level at a maximum of 2.4, corresponding to

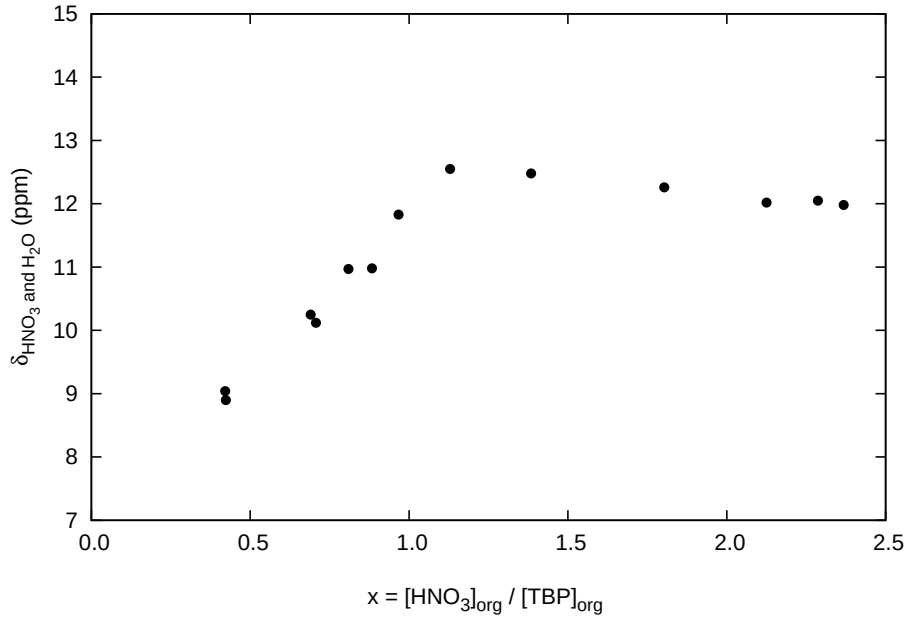

Figure 2.23: Chemical shift observed of nitric acid and water in TBP versus the mole ratio of nitric acid on TBP in the organic phase.

a concentration of 6.2 mol·L^{-1}in nitric acid. This concentration correspond to the maximum solubility of HNO_3 in TBP. These results indicate that TBP, as a Lewis base, can carry acids in an organic phase. This property can be used to perform chemical reactions with acids in sub- or supercritical CO_2, because acids are generally not very soluble in CO_2.

From the same set of data, the partition coefficient of HNO_3 between the aqueous phase and the TBP phase (D_{HNO_3}) can be found by plotting $[HNO_3]_{aq}$ versus $[HNO_3]_{org}$ according to the following equation:

$$D_{HNO_3} = \frac{[HNO_3]_{aq}}{[HNO_3]_{org}}. \tag{2.32}$$

The linear regression analysis performed on the data of the nitric acid concentrations in the aqueous and in the organic phase gives $D_{HNO_3} = 2.4 \pm 0.8$. This result implies that there is nearly 2.4 times more nitric acid in the aqueous phase than in the organic phase when the equilibrium is achieved for an initial concentration of 15.5 mol·L^{-1} in nitric acid.

Table 2.4: Composition of TBP·$(HNO_3)_x$·$(H_2O)_y$ complexes.

Vol* HNO_3	Vol* TBP	x = $[HNO_3]/[TBP]_{org}$	y = $[H_2O]/[TBP]_{org}$	Molecular ratio for TBP:HNO_3:H_2O
0	5	0	1.06	1 : 0 : 1.1
0.5	5	0.42	0.83	1 : 0.4 : 0.8
1	10	0.42	0.74	1 : 0.4 : 0.7
1	6	0.71	0.73	1 : 0.7 : 0.7
1	5	0.81	0.42	1 : 0.8 : 0.4
1	4.5	0.88	0.46	1 : 0.9 : 0.5
1	4	0.97	0.41	1 : 1.0 : 0.4
1	3	1.13	0.36	1 : 1.1 : 0.4
1	2	1.38	0.40	1 : 1.4 : 0.4
1	1	1.80	0.44	1 : 1.8 : 0.4
2	1	2.13	0.54	1 : 2.1 : 0.5
3	1	2.29	0.48	1 : 2.3 : 0.5
6	1	2.37	0.53	1 : 2.4 : 0.7

* Initial volume (mL) used for complex preparation with TBP at 98% and HNO_3 at 15.5 mol·L^{-1}.

Figure 2.25 shows the mole ratio of HNO_3/H_2O, x/y, in the TBP phase at equilibrium versus the initial volume ratio of HNO_3 to TBP. First, the x/y ratio increases rapidly when the amount of nitric acid in the organic phase increases, then it flattens out under 5. In the condition of my experiment, the mole ratio of nitric acid to water can not exceed 5 in the TBP phase. This maximum ratio is reached rapidly when the volume ratio of HNO_3/TBP exceeds unity.

When the TBP·$(HNO_3)_x$·$(H_2O)_y$ complex is diluted in an organic solvent, the excess water and nitric acid precipitate out of the organic phase as micro-droplets, due to the antisolvent effect. The acidity of these micro-droplets is important because it is related to the efficiency of extraction of uranium, as an example. I will therefore describe next the properties of the TBP complex when it is mixed with chloroform.

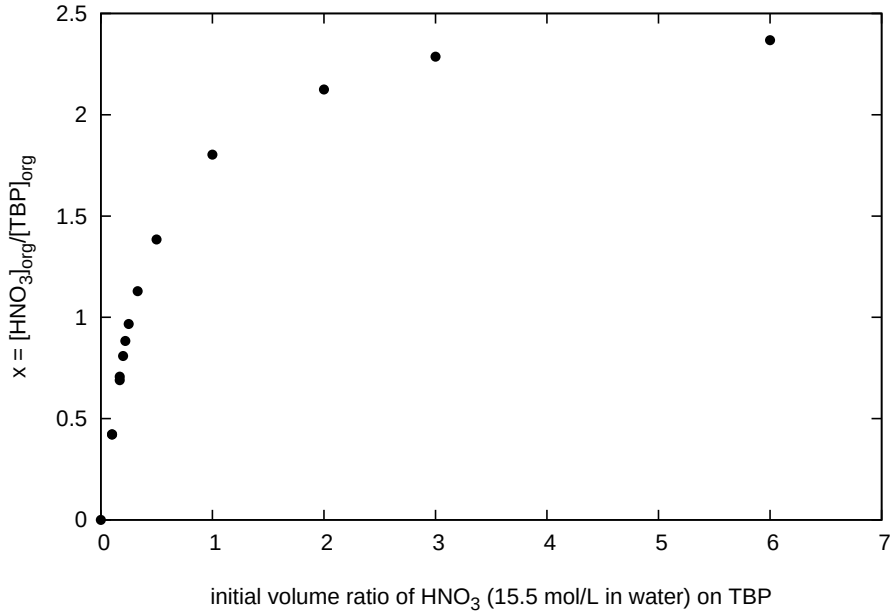

Figure 2.24: Number of moles of HNO_3 in the TBP phase at equilibrium (or x) versus the initial volume ratio of HNO_3 (at 15.5 mol·L^{-1} in water) on TBP.

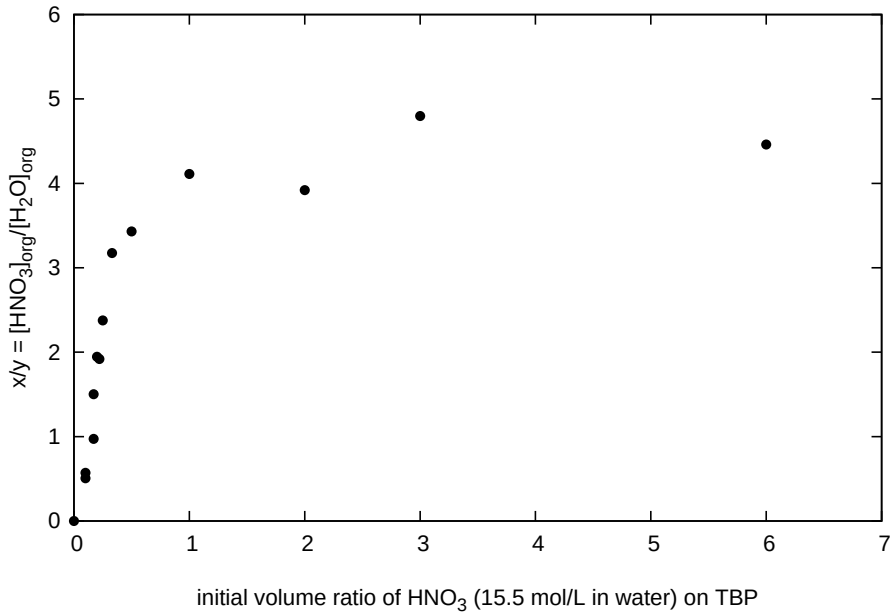

Figure 2.25: Mole ratio of HNO_3/H2O in the TBP phase at equilibrium (or x/y) versus the initial volume ratio of HNO_3 (at 15.5 mol·L^{-1} in water) on TBP.

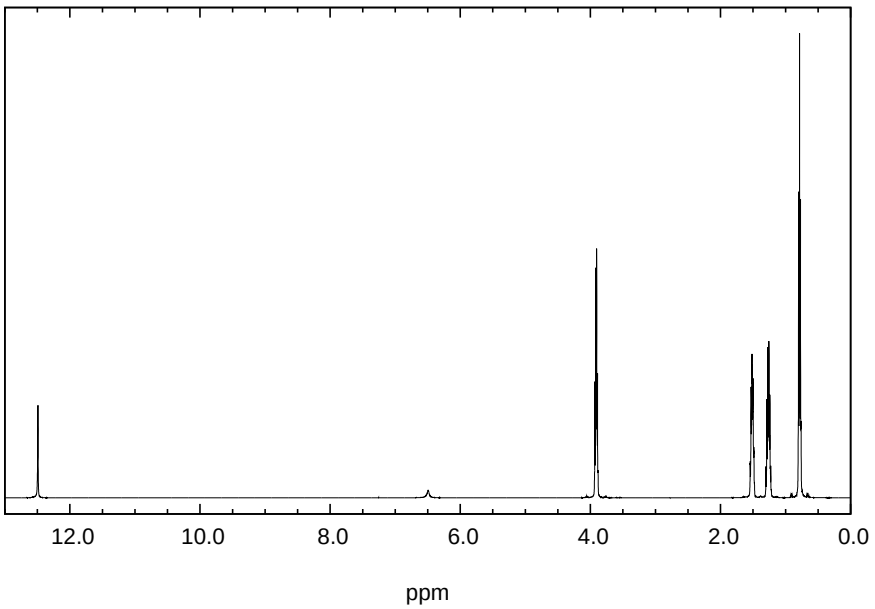

Figure 2.26: Proton NMR spectrum of TBP·$(HNO_3)_x$·$(H_2O)_y$ in $CDCl_3$. The complex was prepared by mixing 4 mL of TBP and 1 mL of 15.5 mol·L^{-1} HNO_3; volume ratio of TBP·$(HNO_3)_x$·$(H_2O)_y$ to $CDCl_3$ = 1:1.

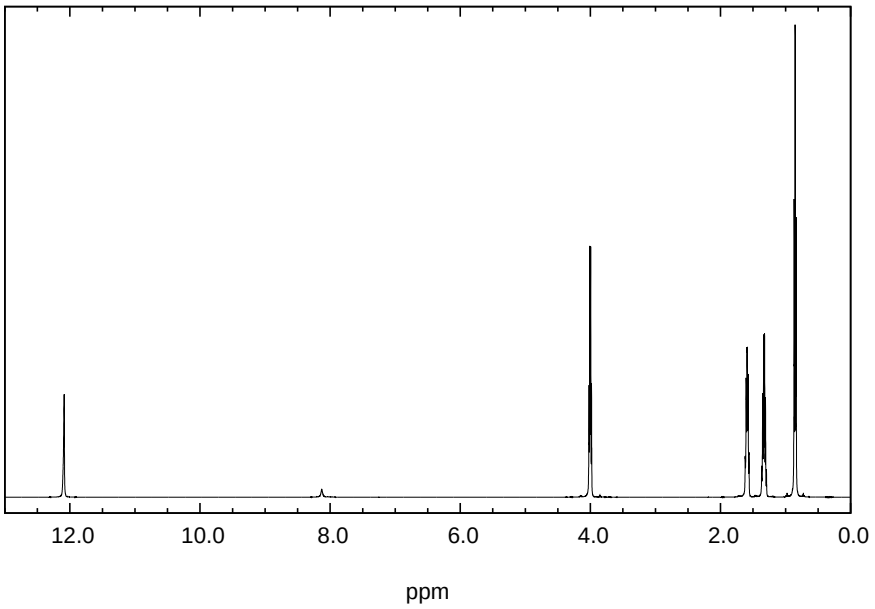

Figure 2.27: Proton NMR spectrum of TBP·$(HNO_3)_x$·$(H_2O)_y$ in $CDCl_3$. The complex was prepared by mixing 2 mL of TBP and 2 mL of 15.5 mol·L^{-1} HNO_3; volume ratio of TBP·$(HNO_3)_x$·$(H_2O)_y$ to $CDCl_3$ = 1:1.

TBP·$(HNO_3)_x$·$(H_2O)_y$ System in a Solvent

Figures 2.26 and 2.27 are two proton NMR spectra of TBP·$(HNO_3)_x$·$(H_2O)_y$ in $CDCl_3$. The first one, shown in Figure 2.26, was recorded after mixing the 1:1.0:0.4 complex at equal volume with $CDCl_3$. The complex (1:1.0:0.4) was formed by adding 4 mL of TBP to 1 mL of nitric acid following the experimental procedure explained in detail in section 2.2.1 (page 131). The second spectrum, shown in Figure 2.27, was made after mixing the 1:1.8:0.4 complex at equal volume with $CDCl_3$. Using the same procedure as previously, the 1:1.8:0.4 complex was formed by adding 2 mL of TBP to 2 mL of nitric acid.

In both spectra, the peaks of the butyl ether groups belonging to the TBP molecule are shown between 0 and 5 ppm. The singlet peak of nitric acid and water in the organic phase is the average resonance of bonded to TBP water, free water, and nitric acid. This peak is observed at 12.48 ppm as shown in Figure 2.26. In Figure 2.27, the same peak is observed at 12.08 ppm. This result demonstrates that the chemical shift of nitric acid and water is shifted upfield when the total concentration in nitric acid increases in the organic phase.

In both spectra, two other singlet peaks appear at 6.48 ppm in Figure 2.26 and at 8.12 ppm in Figure 2.27. These peaks are due to the micro-droplets of nitric acid in water that are formed when the TBP complex is mixed with chloroform. The concentration in acid of these droplets can be determined using equation (2.31). For the 1:1.0:0.4 complex, the concentration $[HNO_3]_{aq} = 5.2$ mol·L^{-1} whereas for the 1:1.8:0.4 complex, the concentration $[HNO_3]_{aq} = 11.3$ mol·L^{-1}. These results show that the concentration of the nitric acid in the droplets increases when the ratio of nitric acid to water increases in the TBP complex.

Another experiment was performed to study the micro-droplet formation phenomenon in more details. For this experiment, solutions of TBP at different concentrations in chloroform where mixed at equal volume with nitric acid (15.5 mol·L^{-1}). NMR spectra of the remaining organic phase were taken and the pH of the aqueous

phase was determined using titration methods.

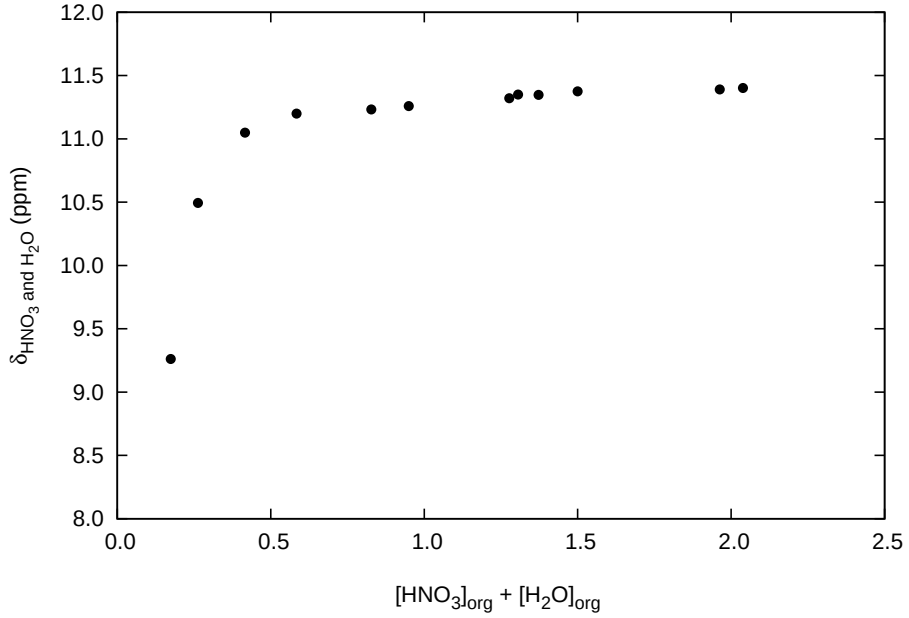

Figure 2.28: Chemical shift of the nitric acid and the water versus total water and nitric acid concentration in the organic phase.

In Figure 2.28, the chemical shift of the nitric acid and the water is plotted versus the total water and nitric acid concentration in $CDCl_3$. The chemical shift is shown to increase rapidly until the total concentration reaches 0.5 mol·L^{-1}. When the total concentration in acid and water exceeds 0.5 mol·L^{-1}, the chemical shift increase flattens out and approaches a plateau at 11.5 ppm.

The plot of the concentration of nitric acid in the aqueous phase, $[HNO_3]_{aq}$, versus initial TBP concentration in the organic phase, $[TBP]_{ini}$, is shown in Figure 2.29. The overall trend is for the nitric acid concentration in water to decrease as $[TBP]_{ini}$ increases. However, this trend is not monotonic as three stages can be recognized. First, $[HNO_3]_{aq}$ decrease fast until $[TBP_{ini}$ reaches approximately 0.5 mol·L^{-1}. Second, the nitric acid concentration in the water stays constant (or increases slightly) as the TBP concentration increases up to ∼1 mol·L^{-1}. Last, the $[HNO_3]_{aq}$ starts to decrease again for TBP concentrations higher than unity.

The total water and nitric acid concentration in the organic phase is shown to

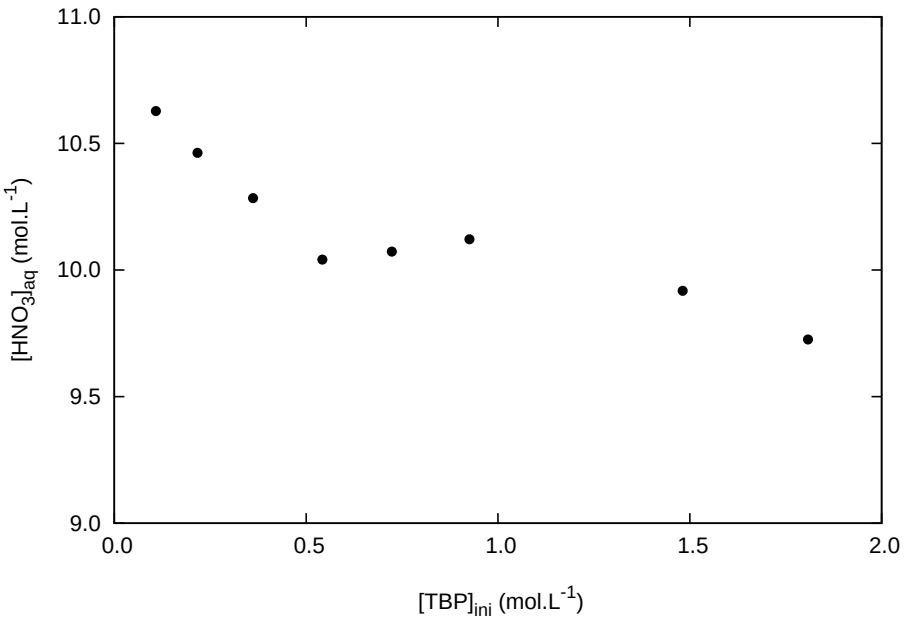

Figure 2.29: Concentration of nitric acid in the aqueous phase versus initial TBP concentration in the organic phase.

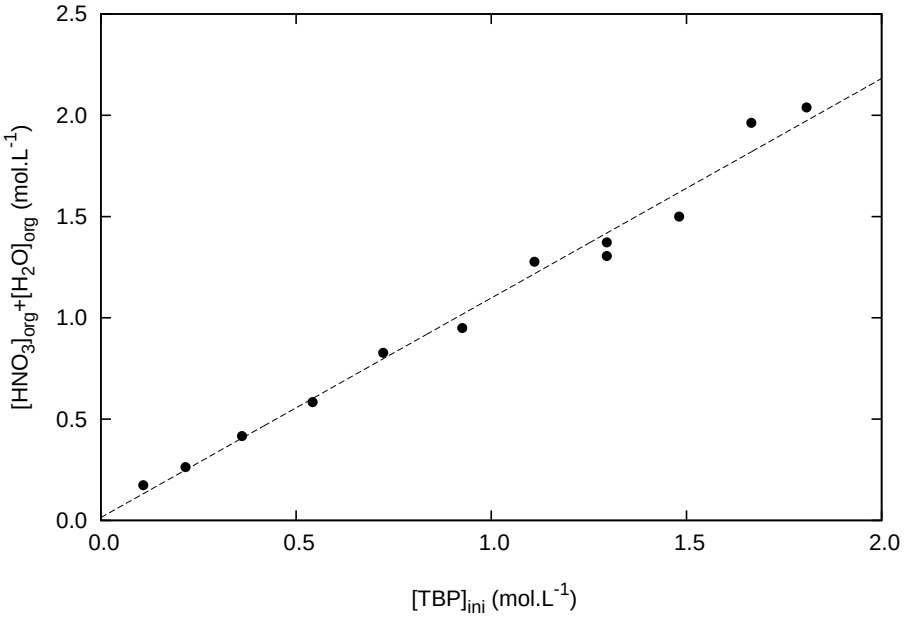

Figure 2.30: Total water and nitric acid concentration in $CDCl_3$ versus initial TBP concentration.

increase linearly with the initial concentration of TBP according to the plot in Figure 2.30. This kind of linear plot was obtained before where the two values were not linear. An example of it has been given in section 2.1.1, page 113, where the dependence of $[D_2O]$ on the equilibrium constant K is plotted. In this example, the data range was too narrow to see the curvature predicted by the theoretical equations. Therefore, I can not be sure of the linearity of the plot in Figure 2.30.

In the absence of TBP, the concentration of water and nitric acid in the organic phase is the one of free water and nitric acid. This free concentration corresponds to the solubility limit of nitric acid and water in chloroform. This value is given by the y-axis intercept of the plot of the total water and nitric acid in the organic phase versus the initial concentration of TBP. If the relationship in between this two variables is properly represented as linear, the regression of the data shown in Figure 2.30 gives $[HNO_3]_{\text{free}} + [H_2O]_{\text{free}} = 0.01 \pm 0.08$ mol·L^{-1}.

Conclusion

In this section, the different TBP·$(HNO_3)_x$·$(H_2O)_y$ complexes were first studied without solvent. Their composition was determined depending on the initial volume ratio of TBP and nitric acid at 15.5 mol·L^{-1} in water. Later, the complexes were studied in chloroform as solvent. The formation of micro-droplets of acid due to the antisolvent effect was demonstrated using NMR when the TBP complexes were mixed with chloroform. The utility of these complexes will be shown by means of spectroscopy in the next section (section 2.3, page 144), for which TBP-water-nitric acid complexes were used to extract uranium in supercritical CO_2.

2.3 Practical Application: Uranium Extraction from Solid Matrices

Introduction

This section describes a practical extension of the present experimental and theoretical achievements. The objectives of this applied research cover not only demonstrating but also optimizing uranium extraction from ash using supercritical CO_2. The different uranium-containing ash types that were used originated from the incineration of byproducts generated in the course of nuclear fuel pellet manufacturing at AREVA (Framatome-ANP) facilities in Richland and Lynchburg, USA. My work to develop and optimize the extraction process was successful to prove the feasibility of a pilot plant in Richland, which is currently under construction.

The TBP-nitric acid-water complexes described in detail in the previous sections were used to oxidize the uranium and as chelating agent. The apparatus I constructed and the different conditions tested to optimize the extraction process will be described in detail along with the gamma spectroscopy used to quantify the extraction efficiency.

The gamma spectroscopy was the main spectroscopic tool used for the experiments described in this section. Gamma rays come from the radiation of nucleus when they transit from a high energy state to a lower one.

A gamma spectrometer is generally composed of a scintillation counter probe connected to a computer. The scintillation probe has a phosphor (generally a sodium iodide crystal for gamma detection) that emits a flash of light when struck by a radiation. The emitted light is directed to a photo-cathode that produce electrons by photoelectric effect. The electronic signal is then amplified and send to a computer for analysis. The resulting spectrum gives the number of count, i.e. the number of radiations that hits the probe window, versus the energy of the transition that is responsible for the radiation. The energy and magnitude of peaks provide the means for identifying the presence of certain isotopes and and a measure of their quantity.

Numerous experiments have been done to inquire whether Supercritical Fluid Extraction (SFE) of uranium with CO_2 using a PUREX-like process is possible.[27–30,67] However, published research reported no significant progress beyond simple theoretical treatment or discussion of idealized conditions. Some experiments were reported, but these were performed with lab-synthesized matrices containing uranium.[68,69]

It appears that unpublished work in Japan points to more progress in this area as suggested by a pilot project under construction utilizing the so-called Super-DIREX process. This project appears to deal with similar issues as treated in this thesis research, however there are no detailed results available in the open literature that can be used as a starting point.

The next section is devoted to demonstrating that it is possible to recover uranium from real matrices including incineration ash generated as byproduct of nuclear fuel manufacturing.

2.3.1 Experimental Work

Chemicals

Tributyl phosphate (97% pure) was purchased from Sigma-Aldrich Chemical Co. and used without further purification. Utra pure water was obtained using the Milli-Q water purification system from millipore Company. Nitric acid (63-64% w/w) was purchased from VWR international and was diluted to 15.5 mol·L^{-1} with ultra pure water. Carbon dioxide (purity $\geq$99.99%, Coleman grade) was obtained from Polar cryogenics. AREVA provided 3 different matrices from where the uranium was to be extracted. The composition of those matrices is shown in table 2.5. L and R are inceniration ashes from the Lynchburg and Richland sites and Y is a yellow residu from classical purex extraction. For the titration, Sodium hydroxide was purchased from Fisher chemicals and was diluted with ultra pure water to 0.1 mol·L^{-1} or lower. Potassium oxalate was purchased from Fisher chemical and was dissolved in water up to saturation and neutralized to a pH 7 with nitric acid. Phenolphthalein was added

Table 2.5: Composition of the different matrices used for extraction determined by mass spectroscopy.

Name	Symbol	L(mg/g)	R(mg/g)	Y(mg/g)
Antimony	Sb	1630	988	60.9
Barium	Ba	825	1020	913
Calcium	Ca	10500	9500	5900
Chromium	Cr	1790	2690	130
Copper	Cu	2380	9920	461
Gadolinium	Gd	8.9	154	11.5
Iron	Fe	86100	103000	132000
Lead	Pb	66.5	2180	109
Manganese	Mn	1040	768	88.6
Molybdenum	Mo	687	1090	10500
Nickel	Ni	5120	1550	74.8
Phosphorous	P	17900	32800	14100
Tin	Sn	1560	1050	769
Titanium	Ti	73200	44600	223000
Uranium	U	55700	126000	563000
Zinc	Zn	9810	31100	350
Zirconium	Zr	6370	5630	38400
Enrichment	$\%^{235}U$	3.69	3.27	2.94

to the potassium oxalate solution to be used as a titration indicator.

Experimental Setup

The TBP·$(HNO_3)_x$·$(H_2O)_y$ complexes were prepared by mixing TBP with a 15.5 mol·L^{-1} solution of nitric acid in a glass tube with a stopper. Different volume ratios of TBP to nitric acid were prepared according to table 2.4 on page 137. Thereafter, the mixture was manually shaken vigorously for 5 minutes, followed by centrifuging for an hour. The organic phase was then extracted with a pipette and stored.

The experimental setup is shown in Figure (2.31). It consists of a syringe pump (ISCO, model 260D) that pressurizes, regulates and delivers CO_2 to the system. The entire setup is rated up to 30 MPa. The mixing cell (MC) is a 3 mL cylinder with an entry and an exit for the fluid at each end. The two high pressure extraction cells

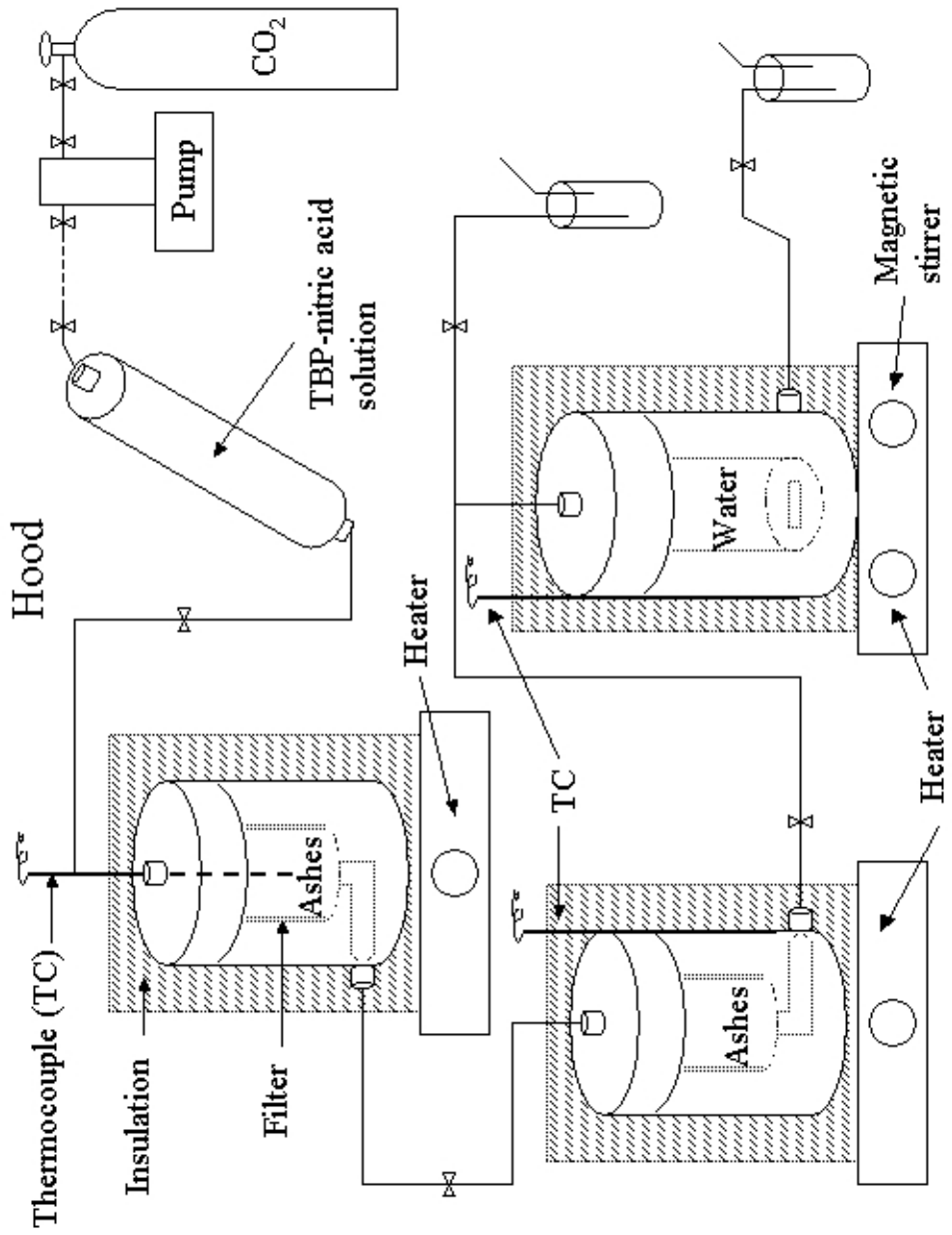

Figure 2.31: UO_2 extraction: experimental setup.

(EC1 and EC2) were especially designed for these experiments. They are composed of a filter that is shaped like a beaker and fits inside the cells. The flow goes into the cell from the top through the filter and goes out under the filter on the lower side of the cell. The internal volume of each extraction cell is 9 mL. The stripping cell (SC) has a 15 mL internal volume. The fluid goes in from the top. The outputs are at the top or at the bottom of the cell to retrieve the CO_2 phase or the water phase, respectively. All cells are insulated and heated by a hot plate. Thermocouples were used to monitor the temperature with a tolerance of $\pm$ 1 °C. For practical reasons, the thermocouples were installed inside the cell for EC1 or between the cell and the insulation for EC2 and SC. A magnetic stirrer was used to mechanically stir the solutions in SC. Several valves were used to control the flow at the entrance and exits of each cell.

Before the first extraction, 0.5 to 3 mL of the TBP/HNO_3 solution was injected into the mixing cell and 0.2 to 2 g of ashes were introduced in each filter before placing them in the extraction cells. The stripping cell was filled with 2 to 5 mL of water. The system and all the valves were then closed and the pump was turned on. The heaters were turned on for each cell. The mixing cell was then pressurized and the TBP/HNO_3 complex was left with CO_2 to be dissolved for $\sim$30 min or until the other cells reached an equilibrium temperature. The valve between the mixing cell and the first extraction cell was then open. The system was left for a static extraction for 1 hour or more. After the static extraction period, the valve between EC1 and EC2 was slightly open to allow a dynamic extraction from EC1 to EC2. The flowrate was set at 5 mL/min or lower. After EC2 was filled, the same protocol as the one used for EC1 was followed.

After the extraction was finished, the organic phase was directed into SC by opening slightly the valve between them. When SC become full, the magnet stirrer was turned one and the two phases were mixed for at least one hour. The valve between EC2 and SC was then closed and the water phase was extracted from the

lower part, and the TBP phase was extracted along with CO_2 from the upper part of the stripping cell. The remaining ash and both solutions were then analyzed.

To improve the stripping efficiency, known amount of uranium nitrate and nitric acid were dissolved in water and extracted with TBP in CO_2 under various conditions. Most experiments were done at 20 MPa and 50 °C with a TBP to water volume ratio of 1:1.9. The water and the TBP solutions were thereafter analyzed with gamma spectroscopy and the nitric acid content was determined by titration.

Some stripping experiments were performed at ambient pressure (without CO_2) were also experimented. The organic phase was composed of TBP with a concentration of 535 $g{\cdot}L^{-1}$ of uranium and 5 $mol{\cdot}L^{-1}$ of nitric acid. For these experiments, the organic phase was stripped with an equal volume of warm water (50 °C). The two phases were then separated. The aqueous phase was analyzed and the remaining organic phase was stripped again with an equal volume of warm water. This process was repeated several times.

Analysis

The analysis of the samples was performed using different techniques. The content in uranium was determine using the gamma spectroscopy and important results were confirmed using Inductively Coupled Plasma Mass Spectroscopy (ICP-MS). The ICP-MS analysis was performed by an external lab facility, which was arranged by AREVA. The pH of the different solutions was measured using titration methods.

Gamma Spectroscopy. The gamma spectrometer used (Canberra Industries) was composed of a scintillation counter (NaI phosphor) connected to a computer running the Genie 2000 software, which manages data collection and performed spectral analysis. The gamma probe was protected from the outside radiations with a cylindrical lead shield with a lead cover. A specially designed plastic tray was placed over the gamma probe. The tray restrained the sample glass tube to be sure it is in the exact same position relative to the probe for all measurements.

Before the acquisition, the sample glass tubes were filled with 0.5 mL of the liquid sample or 0.5 g of solid sample and placed over the probe. The lead cover was put over the sample and the probe to shield them. The gamma radiations were counted for 2000 seconds. The gamma spectrum (count versus energy) was then plotted. After each spectrum acquisition, the sample was rotated. Five spectral measurements were taken and averaged out.

Typical gamma spectra are shown in Figure 2.32 for the background radiation and for the UO_2^{2+} ion radiations in an aqueous solution and in a TBP solution. The background spectrum is flat demonstrating that the sample is well shielded. For both uranyl solutions, four major peaks can be seen at 63.3, 92.6, 143.8, and 185.7 keV. The peaks at 63.3 and 92.6, keV correspond to the energy of radiation emitted by thorium-234. The peaks at 143.8 and 185.7 keV correspond to the gamma radiations emitted by uranium-235. Thorium-234 comes from the alpha decay of uranium-238. In appendix B, the disintegrations of ^{235}U and ^{238}U are detailed in two tables.

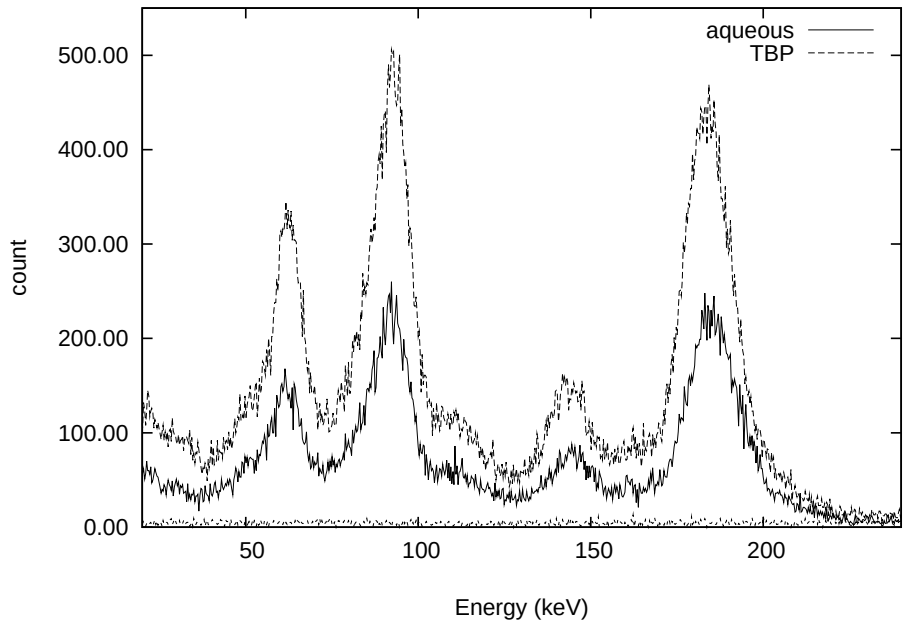

Figure 2.32: Gamma spectra of the background, and of uranyl ion enriched at 3.1% in ^{235}U and at 8.7 g·L^{-1} of uranium in water, and of the UO_2^{2+} ion (2.9% ^{235}U) at 24 g·L^{-1} in TBP.

The gamma energies were calibrated using a solution at high concentration of uranium nitrate in water. For each energy (peak position), the number of counts is proportional to the concentration of the isotope that emits the gamma radiation at that energy. The ratio between the number of counts and the concentration was calculated by using standard solutions in TBP and water or by using a standard amount of ash before extraction. For a better accuracy, the area of the peak was used to determine the concentrations. Figure 2.33 shows the calibration curves for the uranyl ion in TBP and water. For both calibration and measurements, only the ^{235}U peak at 185.7 keV was used because it has the highest abundance (53%). The other ^{235}U peak, at 143.8 keV, is to small and if chosen (abundance of 10%), the area measurements would have been less accurate. The thorium peaks are overlapping with peaks from other decay isotopes and can therefore not be used for analysis. The dectection limit, with maintained accuracy, of this experimental setup was 0.03 g·L^{-1} of ^{235}U, which corresponds to 1.5 gU·L^{-1} or to 750 μg of total uranium.

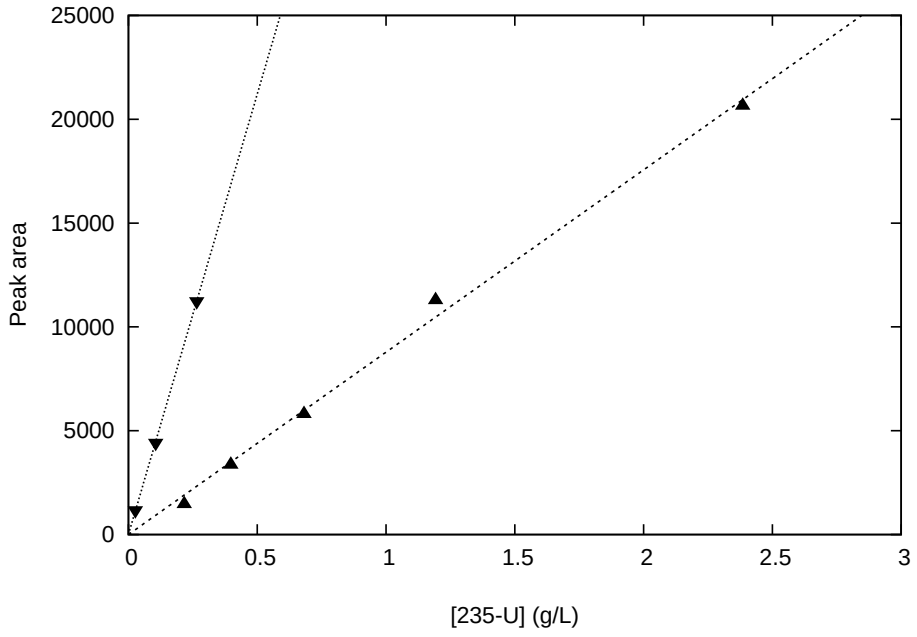

Figure 2.33: Calibration curves for UO_2^{2+} ion in water (▼, 3.1% ^{235}U) and in TBP (▲, 2.9% in ^{235}U).

pH Analysis. Uranyl nitrate (also called uranium nitrate, $UO_2(NO_3)_2$) can react with hydroxide ions to form uranyl hydroxide according to the following chemical equation:

$$UO_2(NO_3)_2 + 2NaOH \rightarrow UO_2(OH)_2 + 2NaNO_3 \tag{2.33}$$

To avoid the formation of uranyl hydroxide, 5 mL of a potassium oxalate solution at pH 7 was added to 0.2 mL of the aqueous solutions prior to titration. The potassium oxalate is added in excess to react with the uranium nitrate and therefore it makes it impossible for the uranium nitrate to react with sodium hydroxide. This procedure allows the determination of the free acid concentration. The pH indicator used was phenolphthaleine and it was dissolved in the potassium oxalate solution before its neutralization. The solutions were thereafter titrated with sodium hydroxide at 0.1 $mol{\cdot}L^{-1}$ or lower, depending on the acid concentration.

To titrate the organic phase, the acid was first stripped out from the organic phase using a large quantity of water. This water was thereafter titrated with the same protocol as the one used to directly titrate the aqueous phase with the exception that the sodium hydroxide concentration was lower.

2.3.2 Extraction of UO_2 from Different Matrices

During the extraction, the uranium(IV) dioxide (UO_2) is oxidized into uranium(IV) nitrate with the help of nitric acid, which is the oxidizing agent. This oxidation follows the chemical reaction:

$$3\ UO_2 + 8\ HNO_3 \rightarrow 3\ UO_2(NO_3)_2 + 2\ NO + 4\ H_2O \tag{2.34}$$

When TBP is used, one uranium nitrate bonds to two TBP molecules according to this chemical equation:

$$UO_2(NO_3)_2 + 2\ TBP + 2\ H_2O \rightarrow UO_2(NO_3)_2{\cdot}2TBP{\cdot}2H_2O \tag{2.35}$$

The supercritical fluid extraction of uranium for any $TBP{\cdot}(HNO_3)_x{\cdot}(H_2O)_y$ complexes can be described using two equations, Equations (2.36) and (2.37). When the

molecular ratio of nitric acid to TBP, x, is greater than or equal to 4/3, and the molecular ratio of water to TBP, y, is greater than or equal to 1/3, the extraction follows the chemical reaction of equation (2.36).

$$UO_2 + 2\ TBP{\cdot}(HNO_3)_x{\cdot}(H_2O)_y \rightarrow$$

$$UO_2(NO_3)_2{\cdot}2TBP{\cdot}2H_2O + \frac{2}{3}\ NO + \frac{6y-2}{3}\ H_2O + \frac{6x-8}{3}\ HNO_3 \qquad (2.36)$$

Independently of the value of x, equation 2.37 describes in a general way the extraction of uranium.

$$3\ UO_2\ +\ (6+z)\ TBP{\cdot}(HNO_3)_x{\cdot}(H_2O)_y \rightarrow$$

$$3\ UO_2(NO_3)_2 \cdot 2TBP{\cdot}2H_2O + 2\ NO + (6y-2+z)\ H_2O + (6x-8+z)\ HNO_3 \quad (2.37)$$

where z is equal of greater than $6x-8$.

In the following part, I will first describe the different parameters that can influence the extraction efficiency and then I will summarize the optimized parameters obtained for the system studied.

Extraction Efficiency Improvement

Different parameters were adjusted to obtain the best extraction efficiency with an acceptable protocol. Such protocol needed to be conservative regarding safety and should be cost and energy efficient.

The gamma spectroscopy was used to determine the yield of the extraction by analyzing the matrices before and after extraction. These results were confirmed by the analyze of the amount of uranium extracted in the TBP phase using gamma spectroscopy. Mass Spectroscopy was also used to confirm the gamma data. In Figure 2.34 the gamma spectrum of the three types of matrices used for uranium extraction are shown.

The different parameters that were adjusted are the TBP complex composition, the temperature and pressure, the TBP/matrix ratio, the static extraction time and the flowrate, and the number of successive extractions.

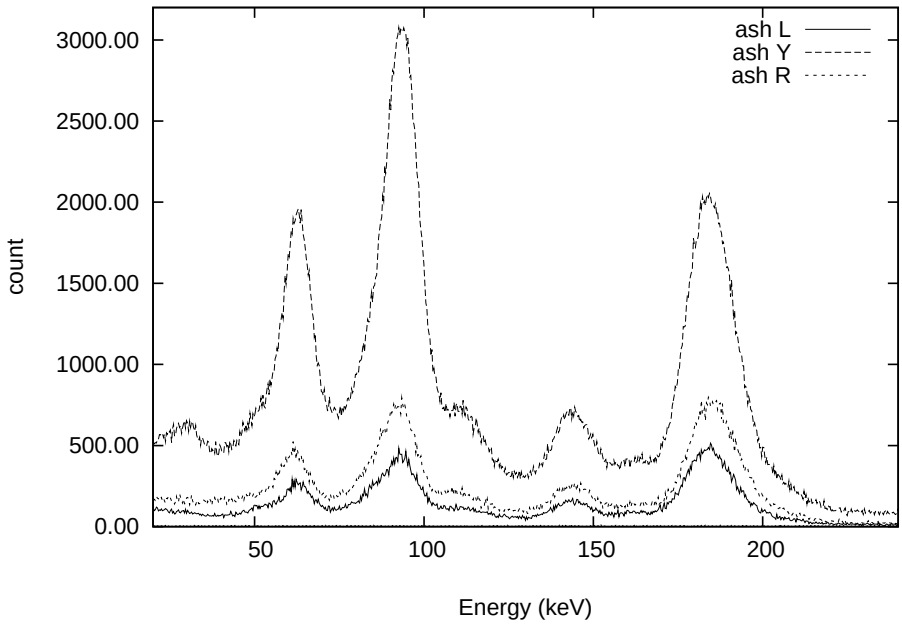

Figure 2.34: gamma spectra of the background and of the three kind of matrices (R, L and Y) used for extraction.

TBP Complex Composition. Different TBP complexes can be prepared by mixing TBP with nitric acid at different volume ratios, as detailed in section 2.2.2, page 135. The ideal composition is the one that has a sufficient amount of nitric acid to oxidize uranium dioxide into uranium nitrate ($UO_2(NO_3)_2$) at a reasonable rate. The quantity of TBP should also be enough to carry the uranium nitrate into the CO_2 phase.

Theoretically, $TBP{\cdot}(HNO_3)_{1.8}{\cdot}(H_2O)_{0.4}$ is the best composition. Indeed, it has the highest nitric acid to water molecular ratio with a sufficient amount of TBP according to Table 2.4 on page 137. Furthermore, Wai et al.[29] have shown that this complex is the most efficient to dissolve UO_2. For these reasons, the $TBP{\cdot}(HNO_3)_{1.8}{\cdot}(H_2O)_{0.4}$ complex was chosen for the extraction of uranium.

Several other complexes were briefly tried out. The one with a lower nitric acid to water molecular ratio lowered the amount of uranium extracted from the ash, which is not acceptable. On the other hand, the one with higher nitric acid to TBP

molecular ratio did not improve the extraction efficiency significantly and would make the stripping of the uranium from TBP into water more difficult.

Temperature and Pressure. Higher temperatures generally improve the rate of any reaction, but in supercritical CO_2 it also lower the density of the supercritical fluid. At lower density, CO_2 is less able to dissolve species such as the TBP-water-nitric acid or the TBP-uranium nitrate complexes. To counteract the effect of the higher temperature on the density, the pressure can be increased. Unfortunately, for safety reasons the pressure needed to be kept at a reasonable level (i.e. under 40 MPa).

It is known that the dissolution of UO_2 in supercritical CO_2 depends on the density of the fluid. Samsonov et al.[28] have shown that the best condition for the dissolution of UO_2 is 65 °C and 250 atm, which correspond to a density of 765.6 $g.L^{-1}$. This was therefore the starting condition that I used. Higher pressures and temperatures (up to 125 °C and 40 MPa) were tried out without a significant improvement in the extraction. On the other hand, by lowering the pressure and temperature to 20 MPa and 60 °C , for a density of 723.7 $g.L^{-1}$, the recovery yield was unchanged. Further lowering in the temperature and pressure were tried out, but the efficiency was greatly affected. Therefore a temperature and pressure of 60 °C and 20 MPa were selected for the extraction as optimum values.

TBP/Matrix Ratio. For a good extraction efficiency, an excess of nitric acid and therefore an excess of TBP-water-nitric acid complex is needed. On the other hand, a large excess will lower the concentration of uranium nitrate and increase the concentration of nitric acid. Both of these consequences decrease the stripping efficiency. The best yield was obtained with 2 mL of $TBP{\cdot}(HNO_3)_{1.8}{\cdot}(H_2O)_{0.4}$ per gram of ash.

Static Extraction Time and Flowrate. The static extraction time allows the reaction between nitric acid and UO_2 to be completed. No change in the extraction efficiency was observed after one hour of static extraction, therefore the extraction time was set to one hour.

After the static extraction is finished, the dynamic extraction is initiated and the fluid goes first to the second extraction cell and then goes to the stripping cell. The flowrate of the dynamic extraction had to be adjusted to be as fast as possible without compromising the extraction. High flowrates result in depressurizing CO_2 and thus reducing its density, and consequently reducing its ability to is to dissolve the uranium nitrate-TBP complex that needs to be extracted. No changes were observed in the amount of uranium recovered when the flowrate was kept under 0.5 mL per minute.

Number of Extractions. After the optimization of the other parameters (i.e. temperature, pressure, complex composition, static extraction time, flowrate and TBP/matrix ratio), the number of successive extractions did not improve the extraction efficiency any further. I believe that the remaining uranium is strongly bonded to the matrix and is not removable with supercritical fluid extraction process used in these experiments.

Nevertheless, two extraction vessels were used in series (Figure 2.31) to improve the concentration of uranium in the TBP phase and therefore enhance the stripping of uranium into water.

Optimal Parameters for the Extraction

The optimized parameters used are shown in Table 2.6. Table 2.7 summarized the optimum recovery efficiencies, which I obtained for the three types of matrices used in the experiments.

The efficiency of supercritical fluid extraction is well beyond the one of the traditional Purex process. For this application, the supercritical fluid extraction has another advantage over the Purex process, the ashes are dry after extraction and the

Table 2.6: Optimal parameters for the supercritical CO_2 extraction.

Parameters	unit	Optimal Values
Pressure	MPa	20.0
Temperature	°C	60
Density	$g{\cdot}L^{-1}$	723.7
$TBP{\cdot}NO_3)_x{\cdot}(H_2O)_y$ complex	molecular ratio	1:1.8:0.4
TBP complex:matrix ratio	mL:g	2:1
Static extraction time	hour	1
flowrate	mL/min	≤ 0.5
Number of extractions		1

Table 2.7: Optimum uranium recovery efficiencies.

Matrix	% extracted	%U before	%U after	optimized
R	85	10.4	1.6	yes
L	90	6.2	0.6	yes
Y	25	35	26	no

extra water and nitric acid do not need to be evaporated.

2.3.3 Stripping of the Uranium from TBP Media to Water

After the extraction, the cell had to be slowly depressurized inside a sample glass tube in which the CO_2 deposits the $TBP{\cdot}UO_2{\cdot}(NO_3)_2$ complex with excess of nitric acid and TBP. It is important to recover the uranium from the TBP solution into water because it will allow the recycling of the TBP and an easy reprocessing of the enriched UO_2. This is called stripping and it was carried out with water at atmospheric pressure or with CO_2 and water, continuously with the extraction as shown on Figure 2.31.

After the stripping, gamma analysis of the water and TBP phases were carried out to determine the efficiency of the stripping. In Figure 2.35, an example of the spectrum of the TBP stripped solution and the aqueous solution is shown.

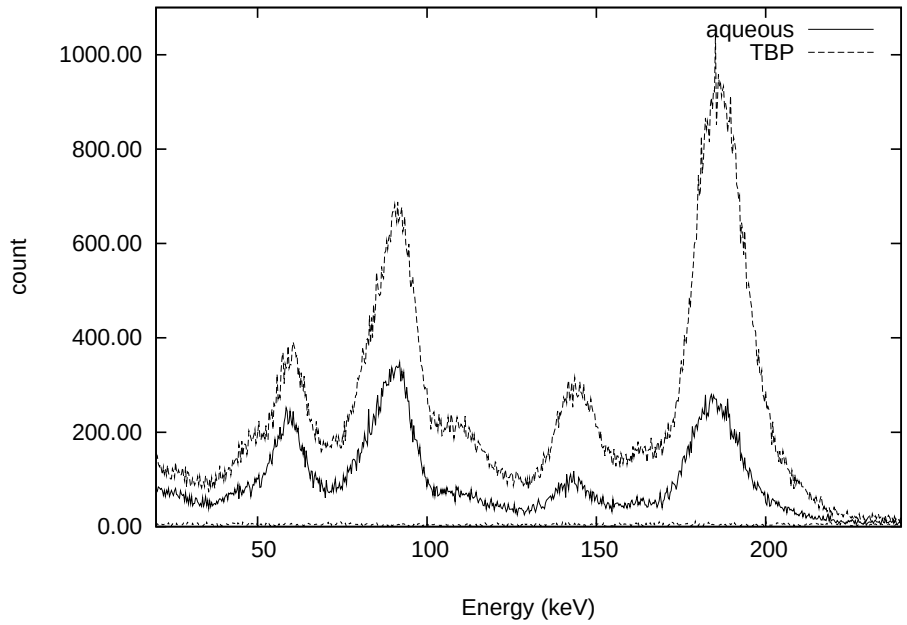

Figure 2.35: gamma spectra of the background and of the uranyl ion (2.9% U) in the TBP stripped solution at and in the aqueous solution.

Stripping at Atmospheric Pressure

In this section the efficiency of the stripping with water at atmospheric pressure was evaluated. The conditions were optimized to maximize the stripping efficiency, i.e. the concentration in the organic phase was high in uranium and low in acid and the water temperature was elevated to 50 °C. Figure 2.36 is shows the results of this experiment. The total mass of uranium stripped is plotted versus the total amount of water used. A total of 15 ± 1% of uranium was stripped from the TBP phase with a 5:1 volume ratio of the aqueous phase to the organic phase. The total uranium concentration in the organic phase was 14 ± 1 g·L^{-1}.

Stripping under Pressure, Continuous with the Extraction

Some experiments were performed to improve the stripping efficiency of uranium from the TBP phase to the aqueous phase. Standard solutions of uranium nitrate and nitric acid in water were extracted with TBP and CO_2. The remaining phases

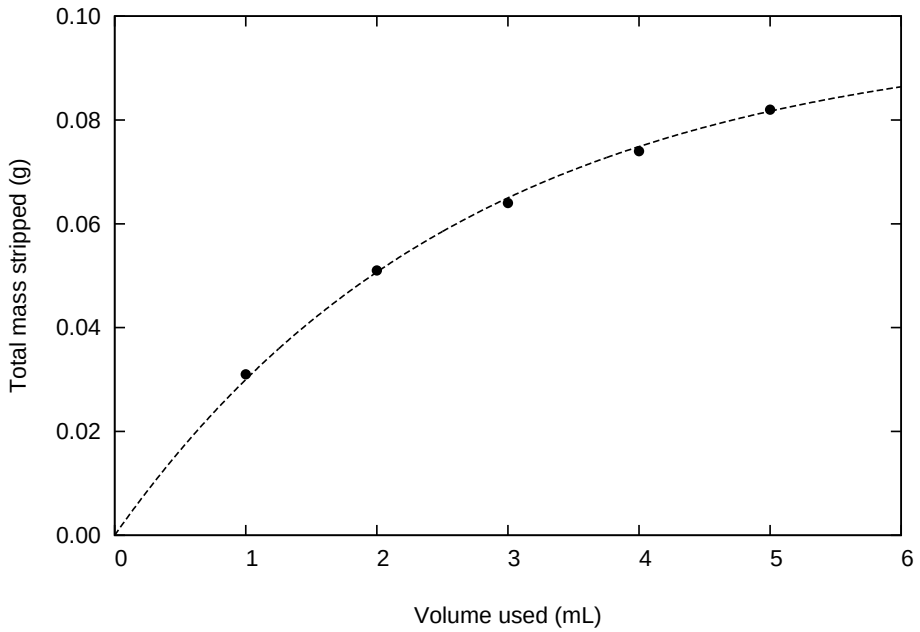

Figure 2.36: Total mass of uranium stripped versus total volume of water used. The line is a guide for the eyes and does not have any theoretical or analytical value.

were titrated and analyzed with gamma spectroscopy.

Figure 2.37 shows the partition of the nitric acid between the two phases. The initial amount of acid or uranium in the aqueous phase does not influence the acid partition. The partition coefficient, D, is obtained from equation (2.38) and Figure 2.37.

$$D = [HNO_3]_{aq}/[HNO_3]_{org} \tag{2.38}$$

D was found equal to 1.4 ± 0.4 when the extraction occurred at 50 °C and 20 MPa, and with a volume ratio of 1:1.9 between the organic and the aqueous phases. This result implies that 60% of the acid is in the aqueous phase whereas 40% goes in the organic phase.

In Figure 2.38, the partition of uranium between the organic and the aqueous phases is shown for three initial nitric acid concentrations (1.6, 3.3, and 7 mol·L^{-1}) with the same conditions as above. It is shown that the continuous stripping of uranium into the aqueous phase is less efficient when the initial amount of nitric acid

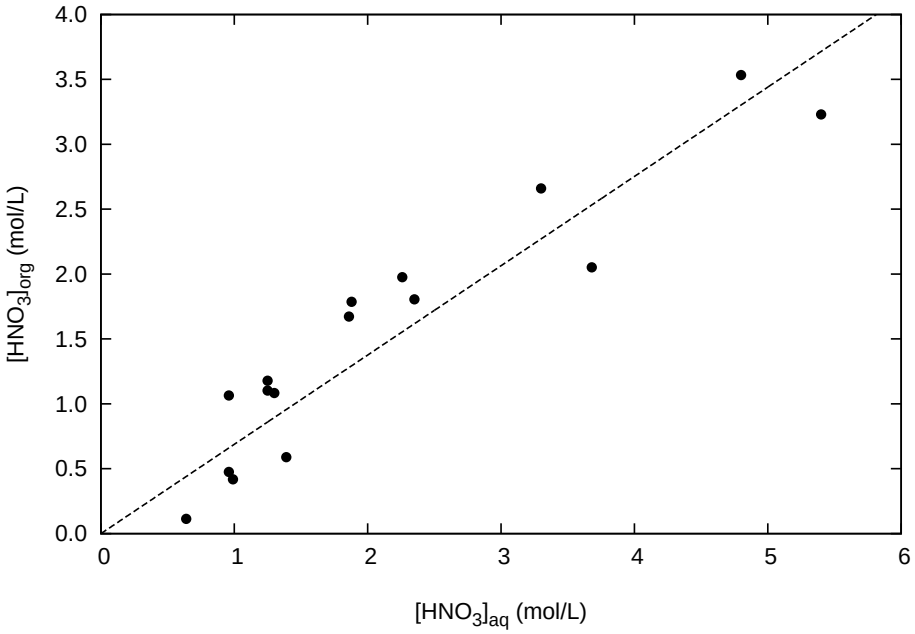

Figure 2.37: Partition of HNO_3 between the organic and the aqueous phases at 50 °C, 20 MPa and with a TBP:water volume ratio of 1:1.9.

is greater.

Table 2.8 provides detailed results of the stripping experiments. It shows the efficiency of the uranium stripping at 50°C, 20 MPa, and with a 1:1.9 TBP to water volume ratio. As shown in Figure 2.38, an increase in the initial acidic concentration lowers the stripping efficiency. On the other hand, at higher concentrations of nitric acid, the initial uranium concentration greatly influence the efficiency. Indeed, the percentage of uranium in the aqueous phase drops from 39 to 5% when the initial uranium concentration decreases from 219 to 58 g·L. This phenomenum is not observed at lower acidic concentration where the efficiency is the same regardless of the initial uranium concentration and considering the experimental errors.

The preceding data were all collected at the same conditions, i.e. 50 °C, 20 MPa and a volume ratio of 1:1.9 of the organic to the aqueous phase. Next I will show the changes when other conditions were used. In Figure 2.39, the percentage loss of extraction efficiency is plotted versus the initial nitric acid concentration. The loss of

Table 2.8: Results of the stripping experiments at 50°C, 20 MPa, and with a 1:1.9 TBP to water volume ratio.[a]

$[U]_{ini}$ ($g \cdot L^{-1}$)	$[HNO_3]_{ini}$ ($mol \cdot L^{-1}$)	stripping efficiency (%)	$[U]_{org}$ ($g \cdot L^{-1}$)	$[U]_{aq}$ ($g \cdot L^{-1}$)	$[HNO_3]_{aq}$ ($mol \cdot L^{-1}$)	$[HNO_3]_{org}$ ($mol \cdot L^{-1}$)
219	8.3	39	133	86	5.0	6.3
162	6.7	31	112	50	4.8	3.6
108	7.1	18	88	19	5.4	3.2
59	7.4	5	56	3	5.9	2.8
174	4.8	31	120	54	3.7	2.1
110	4.7	28	79	31	3.3	2.7
34	4.3	23	26	8	2.4	3.5
182	3.3	47	97	85	2.4	1.8
130	3.3	40	77	52	2.3	2.0
91	3.3	31	63	28	2.1	2.3
187	2.7	35	121	66	1.9	1.7
65	2.8	32	44	21	1.9	1.8
205	1.9	56	90	115	1.3	1.1
147	1.5	53	69	78	1.0	1.1
112	1.9	49	58	54	1.3	1.2
106	1.7	57	46	60	1.4	0.6
75	1.8	54	35	41	1.3	1.1
205	1.2	62	79	126	1.0	0.5
205	1.2	61	81	124	1.0	0.4
103	0.7	91	9	94	0.6	0.1

a. Typical statistic errors are less than 5% for the uranium concentrations and are less than 10% for the nitric acid concentrations and the stripping efficiency.

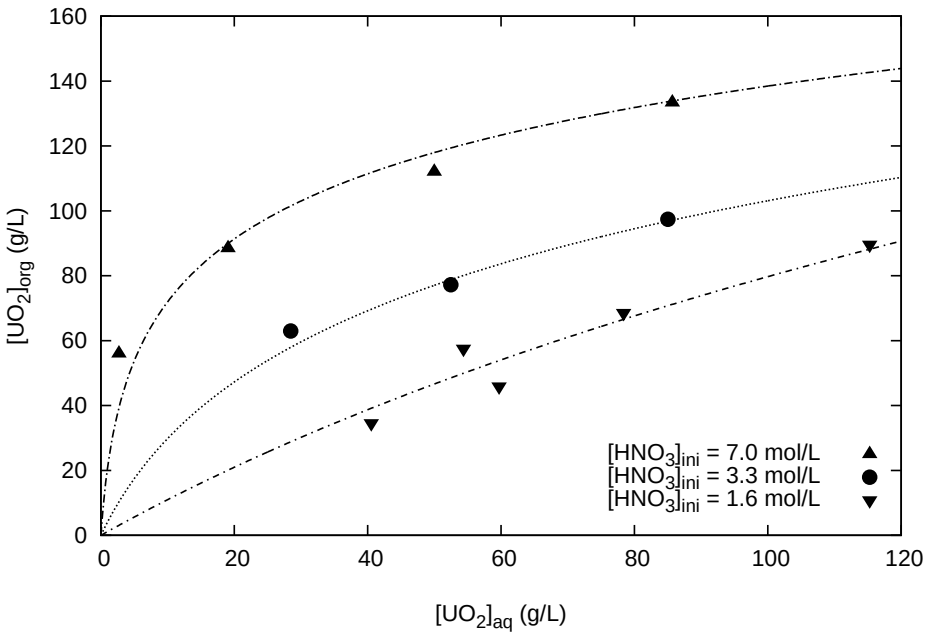

Figure 2.38: Partition of uranium between the organic and the aqueous phases for different initial nitric acid concentrations. The experiment was performed at 50 °C, 20 MPa and with a TBP:water volume ratio of 1:1.9. Lines are guides for the eyes and do not have any theoretical or analytical value.

efficiency is the most important (up to 68%) when the volume of the aqueous phase is reduced. The decrease in the stripping temperature to 24 °C has a lesser impact on the efficiency ($\leq$ 32%). However, a general tendency is observed independently of the condition changed. At high acidic concentration, the loss of efficiency is more important than at low nitric acid concentration. An increase in the efficiency is even shown at 24 °C, for initial concentrations in nitric acid below 2 mol·L^{-1}.

Conclusion

During this research work, the extraction of uranium from ash and other matrices has been proven possible with a very good yield. The stripping stage performed continuously with the extraction has also been shown to be feasible. Continuous stripping was shown to be more efficient than the separate process at atmospheric pressure. Supercritical fluid extraction allows the recovery of dry processed ashes

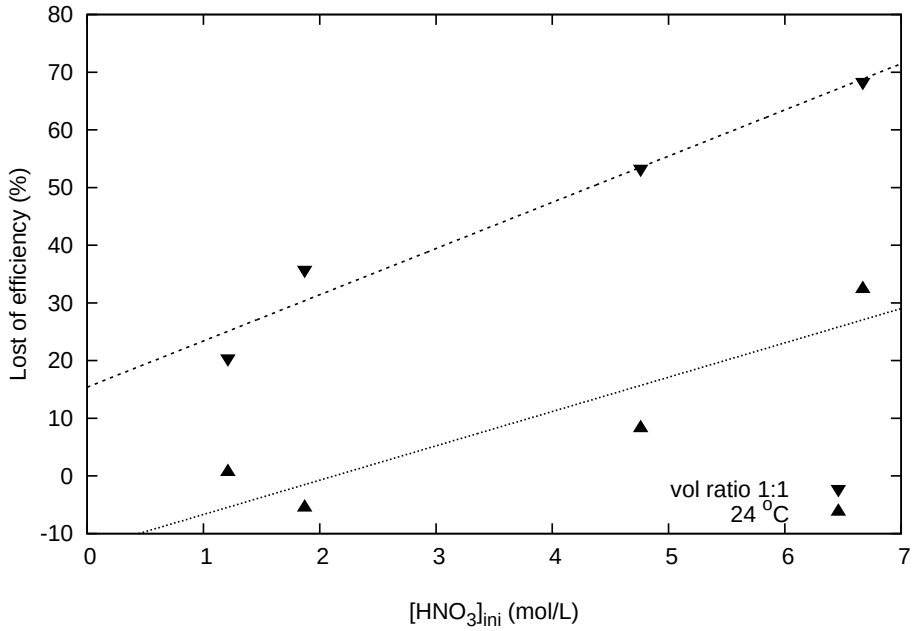

Figure 2.39: Lost of efficiency when the volume ratio is 1:1 between the two phases (▼) and when the temperature is 24 °C (▲).

with a low radioactive content. These two advantages are very important, because the ashes can be disposed of as low-level waste without further cleaning or processing.

Nevertheless, there is still room for further improvement before using this process in a large-scale plant, which is outside the scope of this work. For example, the extraction efficiency could be potentially enhanced with the use of an ultra-sonic bath. Other suggestions to improve the stripping efficiency include the use of pulse columns, electrolysis, and osmosis.

Conclusion

This chapter was dedicated to the study of the supercritical fluid extraction of uranium from different matrices such as incineration ash coming from the byproducts of nuclear fuel production. For this project, I used a mixture of the TriButyl Phosphate (TPB), as a complexing agent, and nitric acid, as an oxidizing agent. As part of this research, the interaction TBP and water was studied in supercritical CO_2 and in chloroform using the Fourier Transform Infra-Red (FT-IR) and the Nuclear Magnetic Resonance (NMR) spectroscopies. It was found that TBP and water make a one–to–one complex when mixed with an excess of water. When this complex is mixed with another solvent such as chloroform, or supercritical CO_2, some microdroplets of water appear in the oil due to the antisolvent effect. The amount of these droplets was calculated for a ∼1:19 volume ratio of TBP complex to solvent. When chloroform was chosen as a solvent, $14 \pm 1\mu$L of microdroplets of water were formed. In sub- and supercritical CO_2, the amount of microdroplets varies between none to ∼11 μL when the temperature decreases from 70 to 25 °C at a constant pressure of 200 bar. This amount decreases from ∼7 to ∼1 μL when the pressure increases from 200 to 400 bar at 40 °C. Chloroform is therefore comparable to CO_2 at low temperature and pressure, regarding the amount of microdroplets formed.

Next, the composition of different TBP–water–nitric acid complexes was determined without a solvent using the NMR spectroscopy. In the condition of my experiments, the maximum number of nitric acid molecules per water molecule in the $TBP{\cdot}(HNO_3)_x{\cdot}(H_2O)_y$ adducts does not exceed five. Thereafter I studied the formation of microdroplets when these TBP adducts are mixed with a solvent (chloroform). The acidic concentration in the droplets depends on the composition of the TBP–water–nitric acid complex. The amount of nitric acid in the microdroplets increases greatly when the molecular ratio of nitric acid to water increases.

To bring the topic of this chapter to closure, the feasibility of extracting UO_2

from different matrices was demonstrated. Some of these matrices are incineration ash coming from the byproducts of the nuclear fuel pellet fabrication. The conditions of the extraction, i.e. temperature, pressure, TBP–water–nitric acid complex used, extraction time, flow-rate, etc. were optimized. At least 85% of the enriched uranium was recovered from the ash at these optimized conditions. After the extraction, CO_2 can be released in the air and the extracted uranium is recovered as a TBP complex with an excess of TBP and nitric acid. Uranium can not be recycled in the fuel fabrication proces in this form. It needs to be stripped into an aqueous phase. The simple stripping at atmospheric pressure with warm water is not efficient enough. This stripping would need a great amount of water that would have to be evaporated. A better way of stripping the uranium out of the organic phase is to do it continuously with the extraction. The efficiency of this stripping method was optimized using standard solutions. A smaler amount of water was needed for the continuous stripping compared to the normal stripping at atmospheric pressure. Based on this research work, a pilot plant is now operational at the AREVA (Framatome-ANP) facility in Richland, Washington.

Some improvements are suggested for the experimental setup to make the extraction and the stripping more efficient. For example, the extraction cells can be put in an ultra-sonic bath. This technique might enhance the extraction efficiency by liberating the uranium strongly bonded to the matrix. On the other hand, the stripping can also be enhanced by using a pulse column or replaced for electrolysis, which could be used to precipitate out UO_2. Osmosis can be also a good alternative, where the process has been already optimized on large scale for desalting sea water.

General Conclusions

This research work was devoted to the understanding of the supercritical fluid extraction of cesium and uranium. These two elements were especially chosen because of their abundance in various types of nuclear waste and because of their importance in the reprocessing and recycling of such waste. Original contributions were made to the understanding of the phenomena and interactions involved, which further the advance of the extraction chemistry and technology.

In the following paragraphs, I will give a synopsis of the different parts of my work and mention the findings and contributions from each part.

Supercritical fluid extraction of metal ions requires the use of a chelating agent. Crown ethers have been chosen as ligand in the extraction of cesium where often water plays a important role. Therefore, the interaction between crown ethers and water was first described in chapter 1. This interaction was studied in sub- and supercritical CO_2 using FT-IR. The differentiation between three water–crown ether configurations (i.e. the bridge, the single, and the sandwich forms) was made with the help of this analytical technique. The sandwich configuration in the organic phase between two crown ethers and a water molecule was first discovered through this work. The equilibrium parameters (i.e. the equilibrium constant, the molar fraction of crown ether bonded to water, and the amount of free water) were determined for the bridge and single configurations at different pressures and temperatures. The value of these parameters were also determined for the global study that lumps together the equilibria of the bridge and the single configuration in one equilibrium. This last set of results was compared with the one in organic solvent found using NMR as a

method of analysis.

The study of the water–crown ether interaction in organic solvents shows that the interaction depends strongly on the crown ether used and on the nature of solvents. The main factor of this dependence is the polarity of the solvent. As the polarity increases, the molar fraction (k) of crown ether complexed with water increases from 61 to 97% for 18-crown-6. These values can be compared to the ones in supercritical fluids, where k varied from 33 to 54% as the temperature decreases at constant pressure ($\sim$20 MPa). These results show that at least 46% of the water is free in CO_2, where less than 39% is free in $CDCl_3$ and CCl_4 mixtures.

The role of water in the cesium extraction equilibrium was discussed at the closure of Chapter 1. The cesium extraction was described using four equilibrium reactions. The calculation of the equilibrium constants leads to three conclusions.

1. The sandwich configuration between two crown ethers and one cesium picrate is not possible if water is part of it.

2. The one-to-one complex of the cesium picrate with the crown ether is preferred with water than without water.

3. The "sandwich" configuration is preferred to the one-to-one complex when water is involved.

It was also observed that the amount of water in oil decreases with the increase of the cesium picrate concentration. It seems that the water is competing with crown ether to be carried out of the water phase. The efficiency of the extraction might be enhanced in a "water-free" extraction.

The second chapter of this thesis work is focused on the supercritical fluid extraction of uranium. TBP-nitric acid-water complexes were used as chelating agent. When TBP-water or TBP-nitric acid-water complexes are mixed with a solvent characterized with a low dielectric constant, some micro-droplets appear due to the anti-solvent effect. Therefore the first part of the chapter was devoted to the understand-

ing of the TBP-water and the TBP-nitric acid-water interactions in various solvents. FT-IR technique was successfully used to describe the TBP-water complex in sub- and supercritical CO_2. The equilibrium constant and the molar fraction of water complexed to TBP in CO_2 as function of temperature and pressure were determined. Most importantly, the FT-IR technique was used to predict the amount of water droplets produced by the antisolvent effect when the TBP-water complex is mixed with CO_2. These results where compared with the measurement obtained in chloroform using NMR as an analytical tool. These two analytical methods complement each other to give a complete picture of the equilibrium. The analysis of the molar fraction of TBP bonded to water shows that there is more water bonded to TBP in the supercritical fluid. Consequently, the amount of free water is larger in the organic phase when $CDCl_3$ is chosen as a solvent. In pure $CDCl_3$ the standardized amount of micro-droplets was found equal to 14 ± 1 μL. This is 3 μL more than the highest volume obtain in CO_2 , where the pressure and temperature were at the lowest setting studied (i.e. 20 MPa and 25 °C).

A further understanding of the interactions was acquired when the TBP-water equilibrium was studied with the addition of nitric acid, which is essential to the supercritical fluid extraction of uranium. Different $TBP(HNO_3)_x(H_2O)_y$ complexes were studied without solvent to determine their composition depending on the initial volume ratio of TBP and nitric acid. The formation of micro-droplets of acid due to the antisolvent effect was demonstrated using NMR when the TBP complexes were mixed with chloroform. It was found that the pH of these micro-droplets decreases when the nitric acid to water molecular ratio increases in the TBP complex.

Finally, a practical application for the TBP-nitric acid-water adducts was demonstrated when they were used to extract uranium from nuclear fuel manufacturing incineration ash and other solid matrices into supercritical CO_2. The extraction of uranium has been proven possible with a very good yield. The stripping stage performed continuously with the extraction has also been shown to be feasible and more

efficient than the separate process at atmospheric pressure. The uranium extraction process developed and optimized through this work has been received well in the nuclear industry, where a pilot plant applying this new process has been recently commissioned at the AREVA Framatome-ANP fuel manufacturing facility in Richland USA.

To sum up, this research work has successfully demonstrated that supercritical fluid extraction could be used to recover uranium and cesium. These and other elements can be extracted from high level radioactive waste on a large scale. Gradually and in a controlled manner, each element could be removed from the main waste allowing a specific waste management solution for each element. In particular, extracted plutonium and uranium could be reused as fuel for power-plants. Other isotopes could be used for research or medical purposes, whereas low level waste could be easily forgotten underground. Even if no practical use were found for certain isotopes, their recycling and/or storage would be much easier when separated from the bulk. The remaining high level waste could be processed as traditionally envisioned, i.e. using short term storage, long term storage, and neutron transmutation, that is of course when such technology matures eventually. It would be necessary to monitor the water and hydrogen level in such plant. Indeed, due to radiolysis effects, potentially explosive hydrogen gas is generated from water in these materials.

For future consideration and extension of my work, I suggest that other important elements that were not included in this experimental work such as plutonium, neptunium, and americium should be also studied. If shown to be successful, the benefits of a supercritical fluid extraction plant would be greatly expanded.

Appendix A

Mass Yield of the Fission Element

Table A.1: Mass (g) and radioactivity (Ci) of elements (150 days after discharge from a PWR) per ton (Mg) of uranium (freshly loaded in the reactor) for all elements.

Element	Symbol	Atomic number	Mass (g/Mg)	Radioactivity (Ci/Mg)
Uranium	U	92	9.54E+05	4.05E+00
Neptunium	Np	93	7.49E+02	1.81E+01
Plutonium	Pu	94	9.03E+03	1.08E+05
Americium	Am	95	1.40E+02	1.88E+02
Curium	Cm	96	4.70E+01	1.89E+04
Selenium	Se	34	4.87E+01	3.96E-01
Bromine	Br	35	1.38E+01	0.00E+00
Krypton	Kr	36	3.60E+02	1.10E+04
Rubidium	Rb	37	3.23E+02	1.90E+02
Strontium	Sr	38	8.68E+02	1.74E+05
Yttrium	Y	39	4.53E+02	2.38E+05
Zirconium	Zr	40	3.42E+03	2.77E+05
Niobium	Nb	41	1.16E+01	5.21E+05
Molybdenum	Mo	42	3.09E+03	0.00E+00
Technetium	Tc	43	7.52E+02	1.43E+01
Ruthenium	Ru	44	1.90E+03	4.99E+05
Rhodium	Rh	45	3.19E+02	4.99E+05
Palladium	Pd	46	8.49E+02	0.00E+00
Silver	Ag	47	4.21E+01	2.75E+03
Cadmium	Cd	48	4.75E+01	5.95E+01
Indium	In	49	1.09E+00	3.57E-01
Tin	Sn	50	3.28E+01	3.85E+04
Antimony	Sb	51	1.36E+01	7.96E+03
Tellurium	Te	52	4.85E+02	1.34E+04
Iodine	I	53	2.12E+02	2.22E+00
Xenon	Xe	54	4.87E+03	3.12E+00
Cesium	Cs	55	2.40E+03	3.21E+05
Barium	Ba	56	1.20E+03	1.00E+05
Lanthanum	La	57	1.14E+03	4.92E+02
Cerium	Ce	58	2.47E+03	8.27E+05
Praseodymium	Pr	59	1.09E+03	7.71E+05
Neodymium	Nd	60	3.51E+03	9.47E+01
Promethium	Pm	61	1.10E+02	1.00E+05
Samarium	Sm	62	6.96E+02	1.25E+03
Europium	Eu	63	1.26E+02	1.35E+04
Gadolinium	Gd	64	6.29E+01	2.32E+01
Terbium	Tb	65	1.25E+00	3.02E+02
Dysprosium	Dy	66	6.28E-01	0.00E+00

Appendix B

Decay Series

Table B.1: Main decay energies for 238-Uranium.

Isotope	Atomic Mass	Half-life*	Decay Mode**	Decay Energy (MeV)	Gamma Energy*** (keV)	Gamma Ray Intensity (%)
$^{238}_{92}$U	238.0508	4.46x10^9 y	α		49.55	0.07
$^{234}_{90}$Th	234.0436	24.10 d	β^{-1}	0.270	63.29	3.8
					92.35	2.7
					92.78	2.7
					112.80	0.24
$^{234m}_{91}$Pa		1.17 min	99.9% β^{-1}	2.29	766.41	.21
			0.13% I.T.		1001.00	.65
$^{234}_{91}$Pa	234.0433	6.70 h	β^{-1}	2.199	131.2	20
					569.5	11
					883.24	12
$^{234}_{92}$U	234.0409	2.45x10^5 y	α	4.856	53.23	.12
$^{230}_{90}$Th	230.0331	7.54x10^4 y	α	4.771		
$^{226}_{88}$Ra	226.0254	1600 y	α	4.870	186.1	3.30
$^{222}_{86}$Rn	222.0176	3.82 d	α	5.590	510	0.07
$^{218}_{84}$Po		3.11 min	α	6.114		
$^{214}_{82}$Pb	213.9998	26.8 min	β^{-1}	1.032	241.92	7.5
					295.09	19.2
					351.87	37
					785.82	1.1
$^{214}_{83}$Bi	213.9987	19.9 min	β^{-1}	3.27	609.31	46.1
					768.35	4.9
					1120.27	15
					1238.10	5.96
					1764.49	15.9
$^{214}_{84}$Po	213.9952	164 μsec	α	7.833		
$^{210}_{82}$Pb	209.9842	22.3 y	β^{-1}	.063		
$^{210}_{83}$Bi	209.4841	5.01 d	β^{-1}	1.16		
$^{210}_{84}$Po	209.9828	138.4 d	α	5.407	803.13	0.001
$^{206}_{82}$Pb	205.9744	stable				

* y = year(s); d = day(s); h = hour(s); min = minute(s); s = second(s)
** α = alpha particle emission; β^{-1} = negative beta emission; I.T. Isomeric transition
*** uncertainties $\leq$ 0.4 %

Table B.2: Main decay energies for 235-Uranium.

Isotope	Atomic Mass	Half-life*	Decay Mode**	Decay Energy (MeV)	Gamma Energy*** (keV)	Gamma Ray Intensity (%)
$^{235}_{92}$U	235.0439	7.04x10^8 y	α	4.6793	109.17	1.5
					143.78	10.5
					163.38	4.7
					185.74	53
					202.13	1.5
					205.33	4.7
$^{231}_{90}$Th	231.0363	25.2 d	β^{-1}	0.389	25.64	15
					84.203	6.6
$^{231}_{91}$Pa	231.0359	3.27x10^4 y	α	5.148	27.396	9.3
					300.07	2.4
$^{227}_{89}$Ac	227.0278	21.6 y	98.6% β^{-1}	0.041		
			1.4% α	5.148		
$^{227}_{90}$Th	227.0277	18.72 d	α	6.146	50.14	8.5
					235.97	11.2
					256.24	6.7
$^{223}_{87}$Fr	223.0197	21.8 min	β^{-1}	1.147	50.14	33
					79.72	8.9
$^{223}_{88}$Ra	223.0185	11.43 d	α	5.979	154.18	5.6
					269.39	14
$^{219}_{86}$Rn	219.0095	3.96 sec	α	6.946	271.13	9.9
					401.70	6.6
$^{215}_{84}$Po	214.9994	1.78 msec	α	7.526		
$^{211}_{82}$Pb	210.9887	36.1 min	β^{-1}	1.379	404.86	3.8
					427.00	1.7
					83.06	3.8
$^{211}_{83}$Bi	210.9873	2.14 min	0.3% β^{-1}	0.584	350.1	12.8
			99.7% α			
$^{211}_{84}$Po	210.9866	0.52 sec	α	7.594	569.5	
					897.23	0.52
$^{207}_{82}$Tl	206.9774	4.77 min	β^{-1}	1.427	897.23	0.24
$^{207}_{82}$Pb	206.9759	stable				

* y = year(s); d = day(s); h = hour(s); min = minute(s); s = second(s)
** α = alpha particle emission; β^{-1} = negative beta emission; I.T. Isomeric transition
*** uncertainties $\leq$ 0.1 %

Appendix C

Acronyms

ATW Accelerator Transmutation of Waste

DOE Department Of Energy

FID Free Induction Decay

FT-IR Fourrier Transform Infra Red

HLW High level Waste

IASR Industrial Accident Safety Rate

ICP-MS Inductively Coupled Plasma Mass Spectroscopy

ILW Intermediate level Waste

INSC International Nuclear Safety Center

LLW Low level Waste

LMFBR Liquid Metal Fast Breeder Reactors

MCT Mercury-Cadmium-Telluride

MRI Magnetic Resonance Imaging

MS Mass Spectroscopy

NIST National Institute of standards and Technology

NMR Nuclear Magnetic Resonance

NRC Nuclear Regulatory Commission

PNMR Proton Nuclear Magnetic Resonance

PUREX Plutonium Uranium Recovery by Extraction

PWR Pressurized Water Reactors

RF Radio Frequency

SFC Supercritical Fluid Chromatography

SF-CO_2 Supercritical Fluid Extraction using CO_2

SFE Supercritical Fluid Extraction

SNF Spent Nuclear Fuel

TBP Tri-nButyl Phosphate

TMS TetraMethylSilane

UV Ultra Violet

Appendix D

Curriculum Vitae

Address

France :	41grand'rue 68280 ANDOLSHEIM
USA:	106 Edgewood Drive Richland WA 99352
phone:	+1 509 628 3030
e-mail:	Anne_Farawila@hotmail.com

Academic History

1994 - 1998 Louis Pasteur University, Strasbourg (France)
- Diploma of general undergraduate studies (DEUG) of chemistry
- Bachelor (Licence) of chemistry and physics

The American equivalence of this diploma is a bachelor degree, with an academic major in chemistry and an academic minor in physics and mathematics.

1998 - 2000 Louis Pasteur University, Strasbourg (France)
- Maîtrise of chemistry and physics
- Diploma of thorough studies (DEA) of chemistry and physics.

The American equivalence of this diploma is a master degree, with an academic major in chemistry and an academic minor in physics.

2000 - 2005 Louis Pasteur University, Strasbourg (France)
and University of Idaho, Moscow (Idaho, USA)
- Ph.D. of physical chemistry, June 2005 (thesis herein presented)

Master Publications and Conference Presentations

1. Fluorescence spectroscopy of U(VI) in the presence of perchlorate ions. Rustenholtz, A.; Billard, I.; Duplâtre, G.; Lützenkirchen, K.; Sémon, L.; *Radiochim. Acta*; **2001**; *89*; 83–89.

2. Fluorescence of UO_2^{2+} in a non-complexing medium: $HClO_4/NaClO_4$ up to 10 M. Billard, I.; Rustenholtz, A.; Sémon, L.; Lützenkirchen, K.; *Chem. Phys.*; **2001**; *270*; 345–354.

3. Anne Rustenholtz, Isabelle Billard. Fluorescence spectroscopy of U(VI) in the presence of perchlorate ions. *Poster presented in the 7èmes Journées Nationales de Radiochimie et de Chimie Nucléaire, Saint Rémy les Chevreuses, France*, **Septembre 27–29 2000**.

Ph.D. Publications and Conference Presentations

1. Characterization of a Tri-n-butyl Phosphate-Nitric Acid Complex: a CO_2 - Soluble Extractant for Dissolution of Uranium Dioxide. Enokida, Y.; Tomioka, O.; Lee, S.-C.; Rustenholtz, A.; Wai, C. M.; *Ind. Eng. Chem. Res.*; **2003**; *42(21)*; 5037–5041.

2. Partition Coefficients and Equilibrium Constants of Crown Ethers between Water and Organic Solvents Determined by Proton Nuclear Magnetic Resonance. Cheng, H.-W.; Rustenholtz, A.; Porter, R. A.; Ye, X. R.; Wai, C. M.; *J. Chem. Eng. Data*; **2004**; *49(3)*; 594–598.

3. An FT-IR Study of Crown Ether-Water Complexation in Supercritical CO_2. Rustenholtz, A.; Fulton, J. L.; Wai, C. M.; *J. Phys. Chem. A.*; **2003**; *107(50)*; 11239–11244.

4. A. F. Rustenholtz. An FT-IR Study of crown ether complexation with water in liquid and supercritical CO_2. *Poster presented in the 225th ACS National meeting, New Orleans*, **March 23–27 2003**.

Appendix E

Abstract

Supercritical Fluid Extraction: Spectroscopic Study of Interactions Comparison to Solvent Extraction

Supercritical fluid carbon dioxide (SF-CO_2) was chosen to study Supercritical Fluid Extraction (SFE) of cesium and uranium. At first, crown ethers were considered as chelating agents for the SFE of cesium. The role of water and its interaction with crown ethers were especially studied using Fourier-Transform Infra-Red (FT-IR) spectroscopy in SF-CO_2. A sandwich configuration between two crown ethers and a water molecule was observed in the SF-CO_2 phase for the first time. The equilibrium between the single and the bridge configurations was defined. The enthalpy of the hydrogen bond formation was also calculated. These results were then compared to the one in different mixtures of chloroform and carbon tetrachloride using Nuclear Magnetic Resonance (NMR). To conclude this first part and in order to understand the whole picture of the recovery of cesium, I studied the role of water in the equilibrium between the cesium and the dicyclohexano18-crown-6.

In a second part, the supercritical fluid extraction of uranium was studied in SF-CO_2. For this purpose, different complexes of TriButyl Phosphate (TBP), nitric acid and water were used as chelating and oxidizing agents. I first used FT-IR to study the TBP-water interaction in SF-CO_2. These results were then compared to the one obtained with NMR in chloroform. NMR spectroscopy was also used to understand the TBP-nitric acid-water interaction first alone and then in chloroform. To conclude

my research work, I succeeded to improve the efficiency of uranium extraction and stripping into water for a pilot-plant where enriched uranium is extracted from incinerated waste coming from nuclear fuel fabrication. TBP-nitric acid complexes were used in SF-CO_2 for the extraction of uranium from ash.

KEYWORDS: Reprocessing – Nuclear waste – NMR – FT-IR – Extraction – SFE – Supercritical fluids – Solvents – Water – Uranium – Cesium – Crown ethers – Carbon dioxide – CO_2 – TBP – TriButyl Phosphate – Nitric acid – Antisolvent effect – Uranyl – Hydrogen bond

Appendix F

An FT-IR Study of Crown Ether-Water Complexation in Supercritical CO_2

Appendix G

Partition Coefficients and Equilibrium Constants of Crown Ethers between Water and Organic Solvents Determined by Proton Nuclear Magnetic Resonance

Appendix H

Characterization of a Tri-n-butyl Phosphate-Nitric Acid Complex: a CO_2-Soluble Extractant for Dissolution of Uranium Dioxide

Youichi Enokida, Osamu Tomioka, Su-Chen Lee, **Anne Rustenholtz**, and Chien M. Wai

Characterization of a tri-n-butyl phosphate-nitric acid complex : a CO2-soluble extractant for dissolution of uranium dioxide.

Ind. Eng. Chem. Res. 42, 5037-5041 (2003)

Pages 5037-5041 :

References

1. "http://www.insc.anl.gov/pwrmaps/map/world_map.php", .

2. "http://sci2k.net/chernobylradiation.html", .

3. Benedict, M.; Pigford, T. H.; Levi, H. W. *Nuclear Chemical Engineering 2nd ed.;* McGraw-Hill: New York, 1981, p. 388.

4. Roberts, J. D. *Nuclear Magnetic Resonance;* McGraw-Hill: 1959, p. 14.

5. "http://www.sigmaaldrich.com", .

6. Wiebe, R. *Chem. Rev.* **1941,** *29,* 475–481.

7. Charastil, J. *J. Phys. Chem.* **1982,** *86,* 3016.

8. Benedict, M.; Pigford, T. H.; Levi, H. W. *Nuclear Chemical Engineering 2nd ed.;* McGraw-Hill: New York, 1981, p. 565.

9. "http://www.ocrwm.doe.gov/", .

10. Benedict, M.; Pigford, T. H.; Levi, H. W. *Nuclear Chemical Engineering 2nd ed.;* McGraw-Hill: New York, 1981, p. 458–459.

11. Sailor, W. C.; Beard, C. A.; Venneri, F.; Davidson, J. W. *Progress in Nuclear Energy* **1994,** *July 7,*.

12. "http://www.pnl.gov/atw/", .

13. Benedict, M.; Pigford, T. H.; Levi, H. W. *Nuclear Chemical Engineering 2nd ed.;* McGraw-Hill: New York, 1981, p. 467.

14. Smart, N. G.; Carleson, T.; Kast, T.; Clifford, A. A.; Burford, M. D.; Wai, C. M. *Talanta* **1997,** *44,* 137.

15. Lin, Y.; Smart, N. G.; Wai, C. M. *Trends Anal. Chem.* **1995,** *14,* 123.

16. Wai, C. M.; Lin, Y.; Brauer, R. D.; Wang, S.; Beckert, W. F. *Talanta* **1993,** *40,* 1325.

17. Laintz, K. E.; Wai, C. M.; Yonker, C. R.; Smith, R. D. *Anal. Chem.* **1992,** *64,* 2875.

18. Dietz, M. L.; Horwitz, E. P.; Rhoads, S.; Bartsch, R. A.; Krzykawski, J. *J. Solvent Extr. Ion Exch.* **1996,** *14,* 1–12.

19. Iwacho, T.; Sadakane, A.; Tei, K. *Bul. Chem. Soc. Japan* **1978,** *51,* 629.

20. Kolthoff, I. M. *Can. J. Chem.* **1981,** *59,* 1548–1551.

21. Shamsipur, M.; Popov, A. I. *J. Phys. Chem.* **1987,** *91,* 447.

22. Kolthoff, I. M.; Chantooni, M. K. *J. Chem. Eng. Data* **1997,** *42,* 49.

23. Talanova, G. G.; Elkarim, N. S. A.; Jr, V. S. T. R. E. H.; Hwang, H.; Bartsch, R. A.; Rogers, R. D. *J. Am. Chem. Soc.* **1999,** *121,* 11281.

24. Mochizuki, S.; Wada, N.; Jr., R. L. S.; Inomata, H. *Anal. Commun.* **1999,** *36,* 51–52.

25. Wai, C. M.; Kulyako, Y. M.; Myasoedov, B. F. *Mendeleev Commun.* **1999,** 180–181.

26. Meguro, Y.; Sasaki, T.; Yoshida, Z. *Anal. Chem.* **1998,** *70,* 774.

27. Tomioka, O.; Meguro, Y.; Enokida, Y.; Yoshida, Z.; Yamamoto, I. *J. Nucl. Sci. Technol* **2001,** *38,* 1097–1102.

28. Samsonov, M. D.; Wai, C. M.; Lee, S.-C.; Kulyako, Y.; Smart, N. G. *Chem. Commun.* **2001,** 1868–1869.

29. Enokida, Y.; El-Fatah, S. A.; Wai, C. M. *Ind. Eng. Chem. Res.* **2002,** *41,* 2282–2286.

30. Carrott, M. J.; Waller, B. E.; Smart, N. G.; Wai, C. M. *Chem. Commun.* **1998,** 373–374.

31. Carrott, M. J.; Wai, C. M. *Anal. Chem.* **1998,** *70,* 2421–2425.

32. de Jong, F.; Reinhoudt, D. N.; Smit, C. J. *Tetrahedron Lett.* **1976,** *17,* 1371–1374.

33. Golovkova, L. P.; Telyatnik, A. I.; Bidzilya, V. A. *Theor. Exp. Chem. (Eng. Transl.)* **1984,** *20,* 219–222 Teor. Eksp. Khim. 1984, 20, 231-234.

34. Wallen, S. L.; Schoenbachler, L. K.; Dawson, E. D.; Blatchford, M. A. *Anal. Chem.* **2000,** *72(17),* 4230–4234.

35. Rustenholtz, A.; Fulton, J. L.; Wai, C. M. *J. Phys. Chem. A* **2003,** *107,* 11239–11244.

36. Bryan, S. A.; Willis, R. R.; Moyer, B. A. *J. Phys. Chem.* **1990,** *94,* 5230–5233.

37. Fulton, J. L.; Yee, G. G.; Smith, R. D. *J. Am. Chem. Soc.* **1991,** *113,* 8327.

38. Gupta, R. B.; Combes, J. R.; Johnston, K. P. *J. Phys. Chem.* **1993,** *97,* 707.

39. Yamamoto,; Iwai, Y.; Nakajima, T.; Arai, Y. *J. Phys. Chem. A* **1999,** *103,* 3525.

40. Xu, Q.; Han, B.; Yan, H. *J. Phys. Chem. A* **1999,** *103,* 5240.

41. Izatt, R. M.; Pawlak, K.; Bradshaw, J. S. *Chem. Rev.* **1991,** *91,* 1721–2085.

42. Dietz, M. L.; Bond, A. H.; Hay, B. P.; Chiarizia, R.; Huber, V. J.; Herlinger, A. W. *Chem. Commun.* **1999,** *13,* 1177–1178.

43. Phelps, C. L.; Smart, N. G.; Wai, C. M. *J. Chem. Educ.* **1996,** *12,* 1163–1168.

44. Steed, J. W.; Junk, P. *J. Chem. Soc., Dalton Trans.* **1999,** *13,* 2141–2146.

45. Horwitz, E. P.; Schulz, W. W. *Metal-Ion Separation and Preconcentration;* A. H. Bond and M. L. Dietz and R. D. Rogers: ACS Symp. Ser. 716 ed.; Chap. 2, p. 20–50.

46. Yakshin, V. V.; Vilkova, O. M. *Russ. J. Inorg. Chem. (Eng. Transl.)* **1998,** *43,* 1629–1632 Zh. Neorg. Khim. 1998, 43(10), 1753-1755.

47. Muzet, N.; Engler, E.; Wipff, G. *J. Phys. Chem. B* **1998,** *102,* 10772–10788.

48. Barakat, N.; Burgard, M.; Asfari, Z.; Vicens, J.; Montavon, G.; Duplatre, G. *Polyhedron* **1998,** *17,* 3649–3656.

49. Mei, E.; Dye, J. L.; Popov, A. L. *J. Am. Chem. Soc.* **19760,** *98,* 1619–1620.

50. Mei, E.; Popov, A. L.; Dye, J. L. *J. Am. Chem. Soc.* **1977,** *99,* 6532–6536.

51. Thury, M. N.; Bryan, J. C.; Lamare, V.; Dozol, J. F.; Asfari, Z.; Vicens, J. *J. Chem. Soc., Dalton Trans.* **1997,** *22,* 4191–4202.

52. de Namor, A. F. D.; Yelarde, F. J. S.; Casal, A. R.; Pugliese, A.; Goitia, M. T.; Montero, M.; Lopez, F. F. *J. Chem. Soc., Faraday Trans.* **1997,** *93,* 3955–3959.

53. Rhangino, G.; Romano, S.; Lehn, J. M.; Wipff, G. *J. Am. Chem. Soc.* **1985,** *103,* 7873.

54. Vayssière, P.; Wipff, G. *Phys. Chem. Chem. Phys.* **2003,** *5,* 127.

55. Herzberg, G. *Molecular spectra & molecular structure. Infrared and Raman Spectra of polyatomic molecules;* Van Norstrand Reinhold LTD Company: 1945, p. 282.

56. "http://webbook.nist.gov", .

57. OShea, K. E.; Kirmse, K. M.; Fox, M. A.; Johnston, K. P. *J. Phys. Chem.* **1991,** *95,* 7863.

58. Weast, R. C., Ed.; *Handbook of chemistry and physics;* CRC press, Inc.: Boca Raton, Florida, first student ed.; 1988, E–44 and E–52.

59. Jackson, K.; Bowman, L. E.; Fulton, J. L. *Anal. Chem.* **1995,** *67(14),* 2368–2372.

60. Penninger, J. M. L. *Supercritical fluid technology;* Elsevier Science: Amsterdam, 1985, p. 191.

61. Chen, M. J. private communication on NMR experiments done in Argonne National Laboratory, 2001.

62. Woelk, K.; Rathke, J. W.; Klinger, R. J. *J. magn. reson. A* **1994,** *109,* 137–146.

63. Baaden, M.; Schurhammer, R.; Wipff, G. *J. Phys. Chem. B* **2002,** *106,* 434–441.

64. Schurhammer, R.; Wipff, G. *New J. Chem.* **2002,** *26,* 229–233.

65. Weast, R. C., Ed.; *Handbook of chemistry and physics;* CRC press, Inc.: Boca Raton, Florida, first student ed.; 1988, C-428.

66. Choi, K.; Tedder, D. W. *Spectrochim. acta A* **1995,** *51,* 2301–2305.

67. Meguro, Y.; Iso, S.; Takeishi, H.; Yoshida, Z. *Radiochim. acta* **1996,** *75,* 185.

68. Tomioka, O.; Meguro, Y.; ISO, S.; Yoshida, Z.; Enokida, Y.; Yamamoto, I. *J. Nucl. Sci. Technol* **2001,** *38,* 461–462.

69. Shimada, T.; Ogumo, S.; Ishihara, N.; Kosaka, Y.; Mori, Y. *J. Nucl. Sci. Technol* **2002,** *3,* 757–760.

Extraction en Milieu Supercritique : Etude Spectroscopic des Interactions – Comparaison avec des Solvants Classiques

par

Anne RUSTENHOLTZ FARAWILA[1]

Sous la direction de

Dr Isabelle BILLARD KLEIN[2] et Prof. Chien M. WAI[3]

Le dioxyde de carbone supercritique (SF-CO_2) a été choisi afin d'étudier l'extraction en milieu supercritique d'ions métalliques tels que le césium et l'uranium. Un intérêt particulier a été porté au rôle de l'eau lors de ces extractions ainsi qu'à son interaction avec des agents chélateurs (AC). En première partie, les éthers couronne ont été choisis comme AC du césium et leur interaction avec l'eau a été étudiée dans le SF-CO_2 en utilisant la spectroscopie InfraRouge à Transformée de Fourier (IR-TF). Une configuration sandwich entre deux éthers couronne et une molécule d'eau a été observée dans le SF-CO_2. Pour les configurations simple et pontée, l'équilibre a été défini et l'enthalpie de formation de la liaison hydrogène a été calculée. Ces résultats ont ensuite été comparés à ceux obtenus dans des mélanges de $CHCl_3$ et de CCl_4 en utilisant la spectroscopie à Résonance Magnétique Nucléaire (RMN). Pour conclure cette première partie, le rôle de l'eau a été étudié lors de l'extraction du picrate de césium par le DCH18C6 et les constantes d'équilibre ont été déterminées.

Dans une deuxième partie, l'extraction de l'uranium a été étudiée dans le SF-CO_2. Des complexes de Phosphate de TriButyle (TBP), d'eau et d'acide nitrique ont été utilisés comme AC et oxydants. L'IR-TF a été utilisée pour étudier l'interaction entre le TBP et l'eau dans le SF-CO_2. Ces résultats ont été comparés à ceux trouvés dans le $CHCl_3$ en utilisant la RMN. Cette même spectroscopie a été utilisée pour comprendre les interactions entre l'acide nitrique, le TBP et l'eau, seuls puis dissous dans du $CHCl_3$. La formation de microgouttelettes d'acide et d'eau dues à l'effet anti-solvant a été observée et quantifiée. Pour conclure ce travail de thèse j'ai réussi à optimiser l'extraction et la récupération d'uranium enrichi provenant de cendres d'incinération de déchets de fabrication de combustible nucléaire. Un complexe de TBP, d'eau et d'acide nitrique dissous dans du SF-CO_2 a été utilisé à cette fin.

Mots clefs : Retraitement – Déchets nucléaires – RMN – IR – Extraction – Fluides supercritiques – CO_2 – Dioxyde de carbone – Solvants – Acide nitrique – Uranium – Césium – Eau – Ethers couronne – TBP – Uranyle – Liaison hydrogène – Effet anti-solvant

[1]Anne_Farawila@hotmail.com

[2]IReS UMR7500, CNRS/IN2P3 - ULP, Chimie Nucleaire – Bat. 35 – 23, rue de Loess – BP 28 – 67037 Strasbourg cedex 2 – France

[3]University of Idaho – Department of Chemistry – Moscow, ID 83844-2344 – USA